Development of the Dipole Flow and Reactive Tracer Test (DFRTT) for Aquifer Parameter Estimation

by

Gillian Nicole Roos

A thesis
presented to the University of Waterloo
in fulfillment of the
thesis requirement for the degree of
Master of Applied Science
in
Civil Engineering

Waterloo, Ontario, Canada, 2009

Author's Declaration

I hereby declare that I am the sole author of this thesis. This is a true copy of the thesis, including any required final revisions, as accepted by my examiners.

I understand that my thesis may be made electronically available to the public.

Abstract

The effective and efficient remediation of contaminated groundwater sites requires site specific information regarding the physical, chemical and biological properties of the aquifer (e.g., hydraulic conductivity, porosity, ion exchange capacity, redox capacity, and biodegradation potential). Hydrogeological parameters are known to vary both laterally and vertically; therefore to support the design of a remedial treatment system, aquifer parameter estimates specific to the site must be obtained. *Ex situ* parameter estimation methods for biological or chemical properties may not provide estimates representative of field conditions; however, recent work with partitioning inter-well tracer tests (PITTs) and push-pull tests indicate that *in situ* approaches present a potential opportunity to identify aquifer parameters. Building on the dipole flow test (DFT) and the dipole flow and tracer test (DFTT), the dipole flow and reactive tracer test (DFRTT) has been proposed as *in situ* aquifer parameter estimation method. The test setup consists of three inflatable packers isolating two chambers in a cased well. A pump moves water at a constant flow rate from the aquifer into one chamber and transfers the water to the other chamber where it returns to the aquifer. Once steady-state flow conditions have been reached, a suite of reactive tracers are released into the injection stream and the tracer concentrations are monitored in the extraction chamber to create the breakthrough curves (BTCs). It is envisioned that tracer BTCs generated in the field can be analyzed with a suitable simulation model to estimate the required aquifer parameters (e.g., distribution coefficient, intrinsic degradation rate coefficient). The overall goal of this thesis was to demonstrate the ability of a prototype dipole system to produce tracer BTCs in conventional wells installed in an unconfined sandy aquifer.

The Waterloo dipole probe was constructed with characteristic dimensions L = 0.22 m and Δ = 0.08 m and field tested in 6 conventional monitoring wells (with and without filter packs) installed at CFB Borden. DFTs conducted at 0.10 m increments along the length of the screen of non-filter packed monitoring wells provided similar estimates of radial hydraulic conductivity

(K_r) to slug tests and literature values. In general, good agreement was found between the K_r profiles obtained from the individual chamber pressure drawup and drawdown which provide more representative estimate of K_r than the use of the combined chamber (K_r^C) profile. This result was also supported by the results of numerical simulations which indicated the drawdown and drawup measurements are functions not only of the K field across the chamber but also of the K field in the vicinity of the chamber. The geometric mean K_r^C estimated in the filter packed wells was approximately an order of magnitude greater than the mean K_r^C estimate for the non-filter packed wells. In addition, less variability observed in the K_r estimates in the filter packed monitoring wells compared to the K_r estimates in the non-filter packed wells. This indicates short-circuiting through the skin zone (hydraulic conductivity K_s) is more pronounced in the DFTs completed with the prototype dipole probe in the filter packed monitoring wells than the non-filter packed wells.

A total of 46 DFTTs were completed in the monitoring wells at CFB Borden to investigate the properties of the BTCs. The shape of the BTC for a conservative tracer is affected by test set up parameters, well construction, and aquifer formation properties. The BTCs from the DFTTs completed in the non-filter pack monitoring wells were categorized into four "type curves" based on the curve properties (time to peak, peak concentration, etc.). The differences between the type curves were largely defined by the ratio of K between the skin zone and the aquifer (K_s/K_r).

In order for aquifer parameters to be estimated from the BTC of a DFTT, one must have confidence the BTC is representative of the aquifer conditions. The series of DFTTs completed to assess the repeatability of the BTCs demonstrate portions of the DFTT BTCs are repeatable and that Type 1 and Type 2 BTCs showed similar times to peak concentration between DFTTs. The BTCs from DFTTs completed at the same locations but at different flow rates can be scaled to produce similar BTCs. The peak of the field BTCs was largely defined by the aquifer properties and not affected by tracer recirculation; however, tracer recirculation was important

for controlling the shape of the tail of the BTC. Longer durations of tracer injection were found to increase and delay the peak concentration of the BTC consistent with theory.

The differences between the BTCs of DFTTs completed in filter packed wells and non-filter pack wells emphasize the importance of well construction on the interpretation of DFTT BTCs. The importance of trace recirculation on the shape of the BTCs for DFTTs in filter packed wells was demonstrated by DFTTs completed with and without tracer recirculation. Successive peaks on the recirculatory BTC were not visible on the non-recirculation BTC indicating the initial concentration peak was recirculated through the filter pack. The DFTTs completed in the filter packed wells may or may not include tracer movement through the aquifer in addition to tracer movement through the filter pack.

The dipole flow and reactive tracer test (DFRTT) has been proposed as a method to obtain site specific *in situ* estimates of aquifer parameters to aid in the design of a remedial system for a contaminated site. Now that a series of DFTT BTCs have been generated, the DFRTT model will be used to estimate the aquifer parameters. To continue the work outlined in this thesis, DFRTTs are planned for well-documented contaminated sites. A field trial has also been proposed for the use of the dipole apparatus to deliver chemical oxidants at a source zone of a contaminated site.

Acknowledgements

First and foremost, I would like to acknowledge Neil Thomson for accepting me into his research program. It has been an amazing and educational experience.

The coop students who spent long days in the field with me deserve special acknowledgement: Charmaine Baxter, David Thompson, and Daniel Princz. Thank you for all your hard work and your patience.

Many people at the University of Waterloo were instrumental in getting the project off the drawing board. Paul Johnson and Bob Ingleton constructed the prototype dipole probe. Claudia Naas helped prepare the environmental approval application and was always available to answer field questions. Terry Ridgway and Ken Bowman helped with equipment sourcing and construction options and never left me stranded with broken field equipment. Mark Sobon provided invaluable lab assistance and Bruce Stickney assisted with the original aboveground equipment selection and setup. The other students who worked at CFB Borden were great for sharing ideas, inspiration, and equipment while they were working on their own projects. This would not have been possible without all of you.

Our project collaborators from the University of Sheffield, Ryan Wilson, Steve Thornton, and Ben Eagle, provided an excellent introduction to conducting dipole flow and tracer tests and always had ideas for improvement.

Finally, thank you to my friends and family for all your support over the last two years.

This collaborative research project was supported by funding provided by the Ontario Centres of Excellence, Ontario Ministry of the Environment, Terrapex Environmental Ltd, and a Natural Sciences and Engineering Research Council of Canada (NSERC) Canada Graduate Scholarship (CGS).

Table of Contents

Appendices

List of Figures

List of Figures (continued)

Appendix Figures

Appendix Figures (continued)

Appendix Figures (continued)

List of Tables

Appendix Tables

Chapter 1 Introduction

The effective and efficient remediation of contaminated groundwater sites requires site specific information regarding the physical, chemical and biological properties of the aquifer (e.g., hydraulic conductivity, porosity, ion exchange capacity, redox capacity, and biodegradation potential). Hydraulic conductivity, which governs the rate at which a fluid can move through a medium, is known to vary both laterally and vertically (e.g., Molz et al., 1994; Butler, 2005; Zemansky et al., 2005; Dietrich et al., 2008), while biodegradation rates can vary due to differences in sediment texture, pH, temperature, microbial populations, carbon, oxygen and other nutrient availability (Schroth et al., 1998; Sandrin et al., 2004). To support the design of a remedial treatment system, aquifer parameter estimates specific to the site must be obtained. The use of literature values results in uncertain and potentially overly conservative predictions of remediation performance and may lead to unnecessarily cautious risk assessment and costly remediation strategies (Thomson et al., 2005).

Current methods for the direction measurement of aquifer parameters are typically divided into *ex situ* and *in situ* techniques. *Ex situ* measurement techniques involve the removal of aquifer material from the impacted site for laboratory analysis. Although the materials can be tested to determine aquifer properties such as hydraulic conductivity, porosity, ion exchange capacity and biodegradation potential, *ex situ* techniques may provide parameter estimates not representative of the aquifer material due to the reduction of sample integrity during collection, transport, and laboratory setup and testing. Numerous *in situ* techniques are available for estimating aquifer physical and geologic characteristics (e.g., hydraulic conductivity, storativity, porosity, and fracture zones); however, few *in situ* methods are available to estimate biological or chemical properties. The main advantage to choosing an *in situ* technique over an *ex situ* technique is the opportunity to collect information over multiple depths and locations across an impacted site while minimizing disturbance to the aquifer material sample. Further advantages of *in situ* techniques are assessment at the relevant scale of the parameter variation and real-time analysis of collected data. Recent work with partitioning inter-well tracer tests (PITTs) and push-pull tests indicate that *in situ* approaches present a potential opportunity to identify additional aquifer parameters.

A PITT consists of the simultaneous injection of several tracers with different partitioning coefficients at one or more injection wells and the subsequent measurement of tracer concentrations at one or more monitoring wells to estimate the presence of non-aqueous phase liquids (NAPLs) (Jin et al., 1995). Typically, PITTs are conducted prior to and post source zone treatment to quantify the effectiveness of the remediation activities (e.g., Cain et al., 2000; Meinardus et al., 2002). The logistical and cost constraints tend to restrict the use of PITTs despite significant advances in their design and post-test analysis methods. Push-pull tests have been used to quantify microbial metabolic activities (Istok et al., 1997) and *in situ* reaction rate parameters (Haggerty et al., 1998) in petroleum contaminated aquifers. Push-pull tests have also recently been used to estimate the natural oxidant demand of an aquifer (Mumford et al., 2004) and TCE degradation rates and permanganate consumption rates (Ko et al., 2007). One of the major disadvantages to using the push-pull test to estimate aquifer properties is the need to determine groundwater velocity direction and magnitude during the test as they are responsible for transporting the injected solution down-gradient of the monitoring well during the reaction phase.

Butler (2005) summarizes existing methods to estimate hydraulic conductivity (K) using *in situ* hydraulic tests (slug tests, borehole flowmeter tests, and dipole flow tests) and describes the ongoing development of direct push methods to rapidly estimate the vertical variations in K. The slug test is a simple field method which provides a K estimate which is the thickness weighted average of the materials along the well screen (Butler et al., 1994). Packers can be used to isolate sections of the well screen for slug testing in order to determine a vertical profile of K. K estimates from another hydraulic test, the borehole flowmeter test (BFT), may not be representative of the formation due to flow bypassing the flowmeter through short circuiting through the skin zone (Boman et al., 1997). The dipole flow test (DFT) is a single-well hydraulic test consisting of three inflatable packers isolating two chambers in a cased well (Figure 1.1) and is used to estimate the vertical distribution of the radial hydraulic conductivity (K_r) in the vicinity of a test borehole. A submersible pump located in the central packer moves water at a constant flow rate from the aquifer into one chamber and transfers the water to the other chamber where it returns to the aquifer (Kabala, 1993). Pressure transducers located in each chamber monitor pressure changes (drawup and drawdown) which are used in conjunction

with a simple analytical model to estimate K_r. Numerous DFTs have been conducted in various diameter wells with different dipole configurations and flow rates and estimated K_r profiles generated from DFTs have shown similar trends and values to K estimates obtained through grain size analysis, permeameters, sieve analyses, flowmeters, and pump tests (Zlotnik et al., 1998; Zlotnik et al., 2001; Zlotnik et al., 2003).

Sutton et al. (2000) proposed an extension to the DFT by adding a conservative tracer; thus creating a dipole flow and tracer test (DFTT). The DFTT works in a similar fashion to the DFT except when a steady-state flow field has been established, a conservative tracer is released into the injection chamber and the tracer concentration is monitored in the extraction chamber. The tracer is re-circulated since the extracted tracer solution is re-injected into injection chamber. Sutton et al. (2000) suggested that a combination of the chamber pressure changes and key properties of the tracer breakthrough curve (BTC) could be used to estimate the K_r and the longitudinal dispersivity (α_L) along the DFT flowpaths.

Recently, the dipole flow and reactive tracer test (DFRTT) has been proposed as *in situ* aquifer parameter estimation method (Thomson et al., 2005) and has a similar setup to the DFTT except that in addition to conservative tracer a suite of reactive tracers (i.e., sorbing, degrading, biodegrading, etc.) are injected either as a spike or for an extended period of time. The concentrations of the tracers and their breakdown products are monitored in the extraction chamber to produce a number of tracer BTCs. It is envisioned that these BTCs can then be analyzed with a suitable simulation model to estimate the required aquifer parameters (Thomson et al., 2005; Reiha, 2006). The difference between a conservative tracer BTC and a reactive tracer BTC will depend on the nature of the reactive tracer injected. For example a sorbing tracer such as trichlorofluoromethane will result in a retarded BTC relative to the conservative tracer, while a biodegrading tracer is expected to produce a BTC that shows signs of degradation relative to the conservative tracer BTC. These BTCs can be interpreted using simulation models in conjunction with optimization tools to estimate the value of controlling parameter(s) such as the distribution coefficient for the sorption process or the intrinsic degradation rate coefficient for the biodegradation process.

1.1 Thesis objectives

The objectives of this thesis are to:

1. Design, construct, and field test a prototype dipole probe to perform DFTs and DFRTTs;

2. Demonstrate the use of the developed prototype dipole probe as a site characterization tool to provide detailed vertical profiles of K_r in conventional monitoring wells; and

3. Investigate the ability of the developed prototype dipole probe and DFTT to produce conservative BTCs and investigate the sensitivity of the BTCs to changes in operational parameters.

The results from this research effort will be used as the framework for ongoing research exploring the utility of reactive tracers to characterize key aquifer properties *in situ*.

1.2 Thesis scope

To satisfy the thesis objectives stated above, a dipole probe prototype was constructed and tested, and then used in a series of both DFT and DFTT experiments performed at Canadian Forces Base (CFB) Borden. The relevant background, methods, and results and discussion follow in Chapter 2 and Chapter 3. Chapter 2 focuses on the use of the prototype dipole system with DFTs as a site characterization tool for estimating the vertical variations in K_r while Chapter 3 deals with work on the DFTTs. Both Chapter 2 and Chapter 3 are structured as initial manuscript drafts and as such are relatively stand-alone; hence some information is repeated throughout this thesis. Finally, Chapter 4 presents major findings and outlines recommendations for future research. DFT results not discussed in Chapter 2 are presented in Appendix A. Results of all tracer tests are presented in Appendix B, and preliminary work with DFRTTs is summarized in Appendix C.

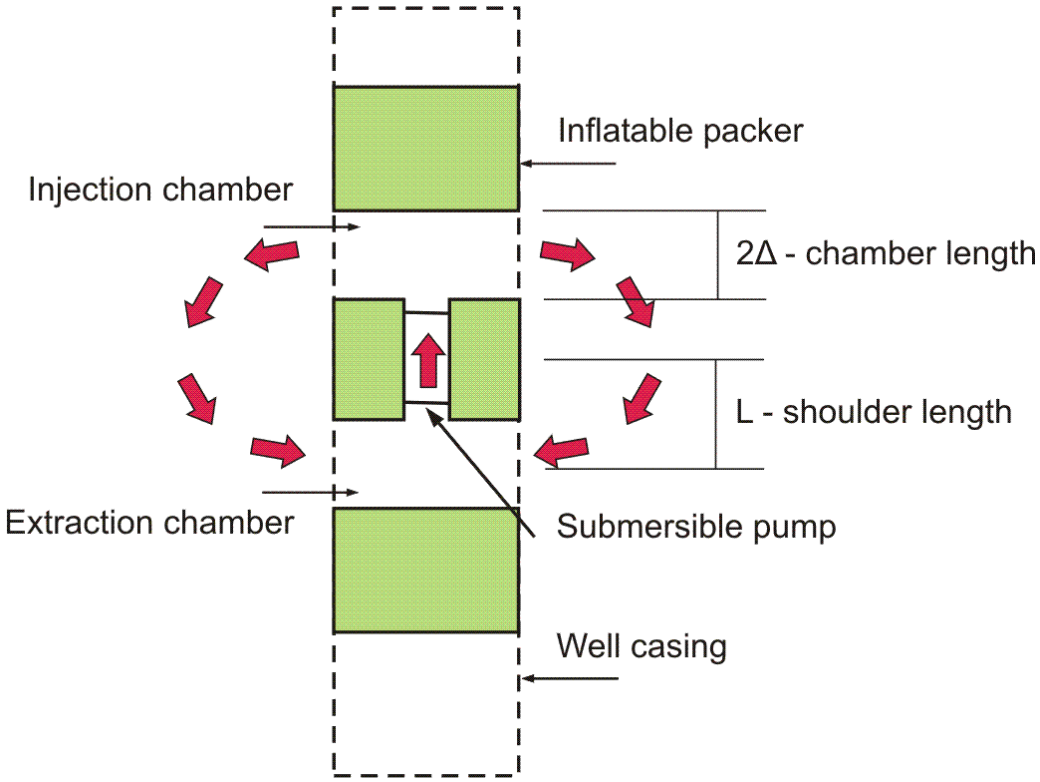

Figure 1.1 The dipole flow test (DFT) as originally proposed by Kabala (1993).

Chapter 2 Dipole Flow Tests (DFTs)

2.1 Introduction

Hydraulic conductivity (K) governs the rate at which a fluid can move through a porous medium and is a function of the properties of both the fluid and the medium. K is known to vary both laterally and vertically (e.g., Molz et al., 1994; Butler, 2005; Zemansky et al., 2005; Dietrich et al., 2008) and therefore the spatial variations in K across a site govern the advective transport of a contaminant. Appropriate site characterization to determine site-specific hydraulic features (e.g., high or low K zones) is required to understand contaminant transport at a given site and develop a remedial approach.

The K of an aquifer can be estimated in the laboratory as well as the field. Laboratory methods, including permeameters and grain size analysis (e.g., Hazen, 1911), may not provide K estimates representative of field conditions (e.g., Taylor et al., 1990; Butler, 2005). Pumping tests can be used to estimate K for the zone of influence but provide limited insight into the small-scale variations of K. Butler (2005) summarizes existing methods to estimate K (slug tests, borehole flowmeter tests, and dipole flow tests) and describes the ongoing development of direct push methods to rapidly estimate the vertical variations in K.

The slug test, which monitors the recovery of a water column in a well after a rapid change in head, is a simple field method for estimating K near a well. The rapid change in head can be caused by the addition or displacement of a known volume of water and changes in head are monitored with a pressure transducer. Conventional slug test analyses include the Hvroselv analysis (1951), the Bouwer and Rice analysis (Bouwer et al., 1976; Bouwer, 1989) and the Cooper, Bredehoeft and Papadopulos analysis (Cooper et al., 1967), while more recent developments (e.g., Hyder et al., 1994) incorporate the effects of partial well penetration, anisotropy and a finite radius well skin. Butler et al. (1996) provides numerous suggestions to improve the quality of slug test K estimates including appropriate well construction and development procedures. The K estimate provided by a slug test is a thickness weighted average of the materials along the well screen (Butler et al., 1994). Packers can be used to isolate sections of the well screen for slug testing (e.g., Zemansky et al., 2005; Ross et al., 2007) in

order to determine a vertical profile of K (termed multi-level slug tests (MLSTs), straddle-packer tests or double-packer tests).

The borehole flowmeter test (BFT) involves pumping a well at a constant rate and measuring the vertical velocity profile. The K at a given location is estimated from the difference in flow between measurement points. This analysis relies on the assumption of horizontal flow towards the well (Butler, 2005). Boman et al. (1997) note the difficulties in conducting BFTs in filter packed wells due to significant vertical flow in the filter pack and flow bypassing the flowmeter due to short circuiting through the filter pack.

Direct-push techniques for K estimation have the advantage that monitoring wells are not required. The direct-push injection logger (DPIL) consists of a small diameter rod with a screen near the tip. To perform a DPIL K test, tool advancement stops and the resistance to water injection is measured by an aboveground pressure transducer. The DPIL is a rapid method for the estimation of K however it can provide only semi-quantitative K estimates through regressions with K estimates provided by other methods (Dietrich et al., 2008). The direct push permeameter (DPP) uses a similar tool to the DPIL however the pressure transducers are mounted on the tool near the screen. The delicate nature of the pressure transducers limits the DPP to stratigraphy where the tool can be pushed by a direct push rig (Butler et al., 2007).

The dipole flow test (DFT) is a single-well hydraulic test consisting of three inflatable packers isolating two chambers in a cased well and is used to estimate the vertical distribution of the radial (K_r) and vertical (K_z) hydraulic conductivity, and the specific storativity (S_s) in the vicinity of a test borehole. A submersible pump located in the central packer moves water at a constant flow rate from the aquifer into one chamber and transfers the water to the other chamber where it returns to the aquifer (Figure 2.1). Pressure transducers located in each chamber monitor pressure changes (drawup and drawdown). To estimate the hydraulic aquifer parameters (K_r, K_z and S_s) the transient chamber pressure changes are matched to type curves generated from an analytical solution (Kabala, 1993). Zlotnik et al. (1996) observed that the chamber pressures during a DFT reached steady-state quickly and suggested that the following could be used to estimate K_r

$$K_r = \frac{Q}{2\pi(s_I + s_E)\Delta} \ln\left(\frac{4a\Phi(\lambda)\Delta}{er_w}\right), \quad (1)$$

$$\text{with } \Phi(\lambda) = \left(\frac{\lambda^2}{\lambda^2 - 1}\right)^{\lambda/2} \left(\frac{\lambda - 1}{\lambda + 1}\right)^{1/2}, \; a = \left(\frac{K_r}{K_z}\right)^{0.5} \text{ and } \lambda = \frac{L}{\Delta}, \quad (2)$$

where s_I and s_E are the steady-state absolute pressure head difference in the injection and extraction chamber respectively, r_w is the internal well radius, e = 2.718…, 2Δ is the chamber length, 2L is the dipole shoulder defined as the distance between chamber centers ($L = D + \Delta$), and 2D is the dipole chamber separation. The function Φ(λ) increases from 0.5 to 1.0 as λ increases and the anisotropy ratio a must either be assumed or known prior to the test.

Numerous field studies of the DFT have been conducted in various diameter wells with different dipole configurations and flow rates (Table 2.1). Estimated K_r profiles generated from DFTs have shown similar trends and values to K estimates obtained through grain size analysis, permeameters, sieve analyses, flowmeters, and pump tests (Zlotnik et al., 1998; Zlotnik et al., 2001). Analysis of the individual chamber pressure changes (s_I or s_E) can provide estimates of K_r in the immediate vicinity of the chamber (K_r^I or K_r^E). Zlotnik et al. (2003) also conducted DFTs, MLSTs and BFTs in order to compare estimates of K_r. The DFT K_r^I and K_r^E estimates were found to be closely correlated ($0.97 < r^2 < 0.99$) when compared at the same depth (comparison of two DFTs). The DFT K_r^E estimates were also closely correlated to the MLSTs ($0.96 < r^2 < 0.98$) conducted at the same depth and with the same screen length; however, the DFT results were less well correlated to the BFT results either due the BFT not being able to physically isolate the test interval, the difference in support volume between the hydraulic tests or violations of the assumptions inherent in the BFT analysis. Most recently, Zlotnik et al. (2007) reported the use of the DFT in a laboratory setting to investigate the effects of entrapped air on the K estimate.

One potential problem with the DFT is the short-circuiting of flow through the disturbed zone or well skin (hydraulic conductivity K_s). Since the DFT induces a predominantly vertical flow field, the well skin may be more pronounced in the DFT than in other single-borehole tests (Kabala, 1993; Zlotnik et al., 1998). In a series of DFTs performed in filter-packed wells in a

heterogeneous highly permeable aquifer Zlotnik et al. (2001) observed a slight skin effect; however, similar K_r estimates were obtained for wells where geotextile rings were installed to prevent short-circuiting suggesting that at least in this aquifer the role of the well skin was minimal. Xiang et al. (1997) investigated numerically the effect of K_s on the estimation of anisotropy ratios and found the estimated a ratio decreased when K_s/K_r increased. Peursem et al. (1999) used a mathematical analysis based on Stokes' stream functions to quantify the effect of a higher K_s zone near the well and observed that the presence of the higher K_s reduced the radial extent of the streamlines and that this effect was more pronounced for short distances between the chambers (i.e., low L).

Sutton et al. (2000) proposed an extension to the DFT by adding a conservative tracer; thus creating a dipole flow and tracer test (DFTT). The DFTT works in a similar fashion to the DFT except when a steady-state flow field has been established, a conservative tracer is released into the injection chamber and the tracer concentration is monitored in the extraction chamber. Recent efforts have built upon the flow system of the DFTT and suggested the use of reactive tracers to develop a new test for chemical and microbial aquifer parameters (Thomson et al., 2005; Reiha, 2006; Roos et al., 2008). The proposed test, termed the dipole flow and reactive tracer test (DFRTT), injects a suite of reactive tracers into the DFT flow field and uses a numerical model to interpret the breakthrough curves to estimate the desired aquifer parameters. The DFRTTs would be conducted in specific zones of K depending on the desired aquifer properties; DFRTTs could also be used to obtain a spatially averaged estimate of an aquifer parameter at a larger scale, consistent with objectives of bulk characterization. For example, if one was interested in the sorbing properties of an aquifer, a DFRTT could be completed with sorbing tracers across a lower K layer. The lower K layer would be identified with a series of DFTs, completed with the same dipole tool as the DFRTT, to estimate the vertical variation in K. The purpose of this paper is to demonstrate the use of a DFT as a site characterization tool to estimate small-scale variations in K.

2.2 Field site, materials and methods

2.2.1 Field site

The field site for the DFTs reported in this paper is located at Canadian Forces Base (CFB) Borden, ~80 km northwest of Toronto, Ontario, Canada. The aquifer at this location is unconfined and consists of glacio-lacustrine deposits of fine to medium sand with porosity 0.40 (Brewster et al., 1995; Sneddon et al., 2002). Mean K estimates for this aquifer range from 8.0 $x10^{-5}$ m/s (ln(K) variance 0.24 to 0.37) (Sudicky, 1986; Woodbury et al., 1991) for constant-head tests performed on homogenized core material to 2.6 $x10^{-5}$ m/s (ln(K) variance 1.1) for constant-head tests performed on intact soil cores (Tomlinson et al., 2003). Reported horizontal correlation lengths range from 1.8 m to 8.3 m and vertical correlation lengths range from 0.16 m to 0.26 m (Woodbury et al., 1991; Tomlinson et al., 2003). Tomlinson et al. (2003) completed slug tests whose K estimates ranged from 3.8 $x10^{-6}$ m/s to 6.1 $x10^{-5}$ m/s with a geometric mean of 2.5 $x10^{-5}$ m/s. Other slug test K estimates for the aquifer have ranged from 3.0 $x10^{-5}$ to 6.0 $x10^{-5}$ m/s (Nwankwor et al., 1984). Aquifer K estimates from a pumping test ranged from 1.4 $x10^{-4}$ m/s to 2.2 $x10^{-4}$ m/s (Nwankwor et al., 1984). Although the aquifer is relatively homogeneous, distinct horizontal bedding features at the cm scale have been observed (Mackay et al., 1986; Brewster et al., 1995). The sand unit is underlain by an aquitard comprised of silts and clays ~9 m below ground surface (bgs) (MacFarlane et al., 1983).

Six 5.1 cm diameter PVC monitoring wells (MW-3 to MW-8) were installed to a depth of 5.5 m bgs and completed with a 3 m screen (0.010" slot). The wells are evenly spaced over an area of ~1000 m^2. Four wells (MW-3, MW-5, MW-6 and MW-8) were installed using a jetting technique where a hollow steel casing (~7 cm ID) was hammered into the sandy aquifer material and the interior of the casing was flushed with water to remove the aquifer solids. The aquifer material was allowed to collapse around the inserted PVC monitoring well when the steel casing was removed (Kueper et al., 1993; Tomlinson et al., 2003) thereby creating a well with a no artificial filter pack. The remaining two wells (MW-4 and MW-7) were installed following a similar jetting technique with a larger steel casing (~13 cm ID) to allow the installation of a 5.1 cm radius artificial filter pack (d_{50} of 0.85 mm). The K of the filter pack material (K_s) was estimated using the Hazen equation (Hazen, 1911) to be ~3 $x10^{-3}$ m/s, 2 orders of magnitude

larger than the native aquifer material. Each monitoring well was developed by repeatedly surging and pumping until the extracted water was clear of sediment.

2.2.2 Dipole system

The prototype dipole probe consists of three rubber inflatable packers with brass end caps separated by two chambers (Figure 2.2). The packers are separated by adjustable spacer rods to create the injection and extraction chambers. The characteristic dimensions of the Waterloo prototype dipole probe are L = 0.22 m and Δ = 0.079 m. A 3.2 mm (1/8 in) HDPE inflation line connects the packers to a valve and pressure gage at ground surface. Two vented pressure transducers (Huba Control, Type 680 with range 0 – 2500 cm H_20) are mounted in the packers and connect to the chambers with 6.35 mm (¼ in) stainless steel tubing. The current measured by the transducers are recorded every second by a data logger (Onset Computer Corporation, H21-002) and used to determine the changes in chamber pressures. The peristaltic pump (Cole Parmer, K-07553-70) which controls the DFT is located at the surface. This dipole probe prototype was designed for use with DFRTTs where samples of the extracted solution will be collected aboveground; therefore, the pump is located at the surface instead of within the central packer as originally conceived by Kabala (1993).

The choice of packer length was dictated by the prevention of packer circumvention which occurs when water is drawn into the chambers from the well screen above or below the packers. Increased vertical flow due to packer circumvention will overestimate the K of the aquifer and underestimate the extent of the vertical variations in K (Butler et al., 1994). Following recommendations by Zlotnik et al. (2003) and Cole et al. (1994), a packer length to packer radius ratio >10 was selected for this dipole probe design.

2.2.3 Field methodology

Slug tests – Slug tests were completed in each of the six monitoring wells (MW-3 through MW-8). A minimum of six slug tests were completed at each well using two different slugs to ensure the K estimates were independent of the initial displacement (H_0) and to investigate changing well skin effects. Both falling head and rising head slug tests were completed to ensure the K estimate was not related to the direction of flow. The pressure changes in the monitoring well were measured with a pressure transducer (Onset Computer, U20-001-01) located below the

submerged slugs. The pressure transducer data was analyzed following the Bouwer and Rice method (Bouwer et al., 1976; Bouwer, 1989) to estimate a mean K (K_{SLUG}) along the monitoring well screen.

DFTs – DFTs were conducted at 0.10 m increments along the 3 m screen of each monitoring well. At each location tested in the naturally developed monitoring wells, DFTs were completed at three different flow rates. For the filter packed monitoring wells, DFTs were completed at a single flow rate due to limitations of the peristaltic pump. The flow rates for the DFTs ranged from 350 to 1460 mL/min. K_r^C (K_r estimated using pressure head change data from both dipole chambers) was estimated from Equation (1) developed by Zlotnik et al. (1998). Smaller scale estimates for K_r (K_r^I or K_r^E) were also estimated using only the injection (s_I) or extraction (s_E) pressure head changes (Zlotnik et al., 2001). Prior to conducting the DFTs, the monitoring wells were re-developed until the extracted groundwater was clear. To provide insight into the drawup and drawdown values obtained during the field DFTs, simulations were performed using the hydraulic head and flow component of the existing DFRTT interpretation model (Thomson et al., 2005; Thomson, 2009). The DFRTT interpretation model is a high-resolution two-dimensional radially symmetric model consisting of two major components: a steady-state groundwater flow component and a reactive transport component (Thomson et al., 2005; Reiha, 2006).

2.3 Results and discussion

2.3.1 Slug tests

The slug test estimates for K (K_{SLUG}) were not related to the size of the initial displacement (H_0), the order in which the tests were conducted, or the direction of water flow (i.e., rising head vs. falling head). The K_{SLUG} estimates for the non-filter packed wells ranged from 1.9 x10^{-5} (MW-8) to 4.1 x10^{-5} (MW-3) m/s with a geometric mean of 2.7 x10^{-5} m/s (Table 2.2). The mean coefficient of variation for the K_{SLUG} estimates was 0.05. The K_{SLUG} estimates are almost identical to the geometric mean slug test K estimate (2.5 x10^{-5} m/s) of Tomlinson et al. (2003) and similar to the K estimates of Sudicky (1986); differences between the K_{SLUG} estimates and

the previous K estimates may be attributed to different testing locations in the aquifer. Similar estimates for K_{SLUG} were obtained for the filter-packed wells (geometric mean 3.3 x10^{-5} m/s) indicating that the slug test was not sensitive to the presence of the filter pack presumably due to the horizontal flow field created during the test (Figure 2.3).

2.3.2 Dipole flow tests

The geometric mean K_r^C for the non-filter packed monitoring wells ranged from 1.5 x10^{-5} m/s (MW-8) to 5.8 x10^{-5} m/s (MW-3). The minimum and maximum K_r^C were 7.6 x10^{-6} m/s (4.3 m bgs MW-8) and 9.3 x10^{-5} m/s (4.2 m bgs MW-3), respectively. Previous work at CFB Borden has shown the stratigraphy consists of medium grained sand with some interbedding; therefore only a small range of K values was expected. For example, working with permeameters of undisturbed soil cores (5 cm), Tomlinson et al.'s (2003) K estimates ranged from 1.9 x10^{-7} m/s to 1.6 x10^{-3} m/s. The smaller K range estimated by the DFT is attributed to the averaging effect due to the DFT's larger scale of measurement (2.2 m (10aL) in the radial direction and 0.90 m (4L) in vertical direction) (Zlotnik et al., 1996). The DFT K_r^I and K_r^E estimates provide a smaller scale measurement of K_r than K_r^C. K_r^E ranged from 6.7 x10^{-6} m/s (4.3 m bgs MW-8) to 1.4 x10^{-4} m/s (3.9 m bgs MW-3) while the overall geometric mean for each monitoring well ranged from 1.5 x10^{-5} m/s (MW-8) to 6.7 x10^{-5} m/s (MW-3).

The slug test K estimates for a given monitoring well typically corresponded to the higher DFT K_r estimates (Table 2.2). For example, K_{SLUG} for MW-5 was estimated to be 4.5 x10^{-5} m/s while the DFT K_r^C estimate ranged from 1.3 x10^{-5} m/s to 4.4 x10^{-5} m/s (Figure 2.4). This is significant in that these results suggest the slug test is more influenced by higher K layers rather than lower K layers. This is supported by the results of previous numerical simulations which indicate the estimated K for a slug test will be a thickness-weighted arithmetic mean of the K_r of the individual layers (Butler et al., 1994).

As initially noted by Zlotnik et al. (2001), the drawup and drawdown of a given DFT can be used to find chamber specific estimates for K_r. Using the chamber specific interpretation of the pressure changes, two K_r profiles (K_r^I and K_r^E) can be obtained from the same series of DFTs

for a given monitoring well. In this manner, the DFTs can "self-verify" by comparing the two profiles ((Zlotnik et al., 2003). In general, good visual agreement was found between the K_r^I and K_r^E for the DFTs completed at in the non-filter packed wells (Figure 2.4(a-d)).

The DFTs completed in the filter packed monitoring wells MW-4 and MW-7 show a more uniform *K* profile (CV of 0.14) (Figure 2.4(e and f)) than the *K* profiles of the non-filter packed monitoring wells (Figure 2.4(a-d)). The geometric mean K_r^C estimated from the DFTs for wells MW-4 and MW-7 was 4.8 x10^{-4} m/s (standard deviation 7.4 x10^{-5} m/s), an order of magnitude greater than the geometric mean K_r^C of the non-filter packed wells (2.5 x10^{-5} m/s). There is also an order of magnitude difference between the MW-4 K_{SLUG} estimate (5.0 x10^{-5} m/s) and the mean MW-4 DFT K_r^C estimate (5.0 x10^{-4} m/s). The mean K for a well at CFB Borden is not known to vary by an order of magnitude over a short lateral distance so the difference in the *K* estimates is most likely due to the presence of the artificial filter pack. As the DFT induces a predominantly vertical flow field, short-circuiting through the disturbed zone (hydraulic conductivity K_s) may be more pronounced in the DFT than in other single-borehole tests (Kabala, 1993; Zlotnik et al., 1998). Therefore, a DFT completed with the current dimensions of the Waterloo dipole probe prototype (*L* 0.22 m and Δ 0.08 m) in a filter packed 5.1 cm diameter monitoring well will be measuring a combination of the *K* of the filter pack and the aquifer.

2.3.3 Pressure change analysis

Based on Equation (1) and the data shown in Figure 2.5(a), there exists a linear relationship between (s_I + s_E) (sum of the absolute drawup (s_I) and the absolute drawdown (s_E)) and flow rate. The linear relationship also extends to the drawup or drawdown in the individual chambers and flow rate (not shown). However, the difference between the drawup and drawdown (s_I - s_E) changes as a function of flow rate (Figure 2.5(b)) while the ratio (s_I / s_E) remains relatively constant (not shown). At some depths, the difference between the drawdown and drawup (s_I - s_E) increases with increasing *Q* while at others, the difference remains constant. The constant difference between drawdown and drawup seems to occur at higher conductivity layers (Figure 2.5(c)). Differences in the drawup and drawdown values during a DFT are therefore an indication of aquifer heterogeneity. For example, the presence of a higher

conductivity region in the vicinity of the extraction chamber results in less drawdown than the drawup measured in the injection chamber. Indelman et al. (1997) demonstrated numerically the pressure change in the dipole probe chamber is an amalgamation of the layers in the vicinity of the chamber and is therefore representative of the equivalent K of the formation at that location.

To provide insight into the drawup and drawdown values obtained during the field DFTs, simulations were performed using the hydraulic head and flow component of the existing DFRTT interpretation model (Thomson et al., 2005; Thomson, 2009). The flow component of the model can include a well skin and the effect of horizontal layers on the dipole flow field. Sudicky (1986) and Tomlinson et al. (2003) provide data that show that K at CFB Borden can vary by an order of magnitude over a vertical distance of 5 cm. To estimate the effect of horizontal layers or zones near a dipole tool on the K_r estimates from a DFT, K_r layers (hydraulic conductivity K_L) were simulated within an isotropic aquifer with a K_r of 7.0 x10^{-5} m/s. The thickness of the simulated layers was chosen to be equal to Δ (0.0785 m), half the chamber length of the prototype dipole probe. Simulations were performed with a high K_L (3.5 x10^{-4} m/s) layer and low K_L layer (1.4 x10^{-5} m/s) where the layers were simulated at half an order of magnitude higher or lower than the aquifer K_r. The DFRTT model simulated the chamber pressure changes (s_I and s_E) as would be captured by the pressure transducers as a DFT was completed at different distances above and below the high or low K layer. The simulated s_I and s_E values were then used to calculate a K_r^C profile (as well as K_r^E and K_r^I profiles) from Equation (1) (Figure 2.6).

Without the K_L layer present, the aquifer K_r calculated from the simulated s_I and s_E values was estimated to be 5.7 x10^{-5} m/s (slightly less than the simulated aquifer K_r 7.0 x10^{-5} m/s). Examining the K_r^E profile when there is a high K_r layer within the domain (Figure 2.6(a)), the K_r^E profile shows an increasing estimate of K_r as the dipole apparatus approaches the higher K_r layer. (Note that the K_r profiles in Figure 2.6 are plotted against depth where the K_L layer is centered at zero). The K_r^I and K_r^E profiles were similar for each set of simulations; therefore for clarity, only one profile is shown on Figure 2.6. The maximum K_r^E estimated was 1.2 x10^{-4} m/s for a K_L simulated at 3.5 x10^{-4} m/s (Figure 2.6(a)); the measured K_r^E is not expected to

estimate the simulated K_L as only half the chamber was covered by the K_L layer and therefore the s_I and s_E will be a function of both the aquifer K_r and the layer K_L. In addition to the K field directly adjacent to the chambers, the simulated s_I and s_E values sense the K field above and below the dipole chambers. For this series of simulations, if the dipole center is within 0.6 m of the K_L layer, s_I and s_E values are affected and the K_r estimate changes (Figure 2.6). For the simulations with the low K_L layer, similar results to the high K_L layer were obtained for the K_r^E profile (Figure 2.6(b)). The minimum K_r^E estimated was 3.7 x10^{-5} m/s when K_L was simulated at 1.4 x10^{-5} m/s. The K_r^C profile is a combination of both the s_I and s_E (drawup and drawdown) measurements and as such provides a less representative K_r profile than K_r^I and K_r^E. This can be observed directly from Figure 2.6(a-b)) where the K_r^C profile estimates two high (or low) K_r zones above and below the actual K_L layer. Similar K_r profiles were obtained when K_L was simulated at an order of magnitude different than the background aquifer K_r (data not shown). It is also interesting to note the chamber pressure changes are similar whether the top or bottom portion of the chamber lies across the K_L layer.

If the aquifer was completely homogenous, the chamber drawup and drawdown of a DFT would be identical and the difference between the drawdown and drawup (s_I - s_E) would plot against K_r as a vertical line. That the plot of (s_I - s_E) against K_r (Figure 2.5(c) does not show vertical lines is an indication of aquifer heterogeneity.

The hydraulic modeling confirms the K_r^I and K_r^E profiles provide more representative estimates of K_r than the K_r^C profile. The drawdown and drawup measurements are functions not only of the K field across the chamber but also of the K field in the vicinity of the chamber. Therefore, the K_r estimates should not be taken as point measurements (although they are often plotted as such) and care should be taken in the interpretation of the K_r^C profile in layered systems.

2.3.4 Spacing of *K* estimates

The DFTs were completed at 0.10 m intervals in the monitoring wells at CFB Borden in order to provide profiles of the vertical variation of K_r. Given that K is not known to vary widely at CFB Borden, the 0.10 m spacing of the K_r estimates may not have been required to sufficiently

characterize the vertical hydraulic profile. To demonstrate different measurement intervals, the summary statistics for K_r^E profiles of MW-6 at 0.20 m, 0.30 m, 0.40 m, and 0.50 m intervals are shown in Table 2.3 and the 0.20 m and 0.50 m intervals are shown on Figure 2.7(a) and (b). Collecting *K* estimates at 0.20 m intervals instead of 0.10 m shows similar variability in the data (0.10 m standard deviation 8.7 x10^{-6} m/s to 0.20 m standard deviation 8.3 x10^{-6} m/s). The two K_r^E profiles show the same general trends on Figure 2.7a. Further increasing the measurement interval to 0.30 m does not greatly alter the mean (2.1 x10^{-5} m/s) or standard deviation of the K_r^E estimates (8.4 x10^{-6} m/s). The K_r^E profile for the 0.30 m interval DFTs has the same general trend of the 0.10 m measurements; however, the small scale variations are not captured (data not shown). Further increasing the measurement interval (0.40 and 0.50m) and thereby decreasing the number of *K* estimates for the monitoring well, increased the CV of the data (Table 2.3). Again, the small scale variations of the K_r^E profile are not captured at the higher measurement intervals (Figure 2.7(b)). Based on the results of the DFT interval analysis, 0.20 m intervals appears to be the minimum interval for K_r profiles in the Borden aquifer for the current setup of the Waterloo dipole probe prototype. A different site with a more complex heterogeneous stratigraphy may require a more detailed K_r profile to fully characterize the *K* field around the monitoring well.

2.4 Conclusions

The spatial variations of *K* across a given site govern the advective transport of a contaminant. A series of DFTs, a single-well test which estimates the vertical distributions of the K_r, were completed to quantify small-scale variations in K_r in a relatively homogeneous aquifer. The DFTs conducted at 0.10 m increments along the length of the screen of non-filter packed monitoring wells provided similar estimates of *K* to slug tests and literature values. In general, good agreement was found between the injection K_r^I and extraction K_r^E profiles which provide a more representative estimate of *K* than the use of the K_r^C profile. This result was also supported by the dipole simulations which indicated the pressure drawdown and drawup measurements are functions not only of the *K* field across the chamber but also of the *K* field in the vicinity of the chamber. Therefore, the *K* estimates should not be taken as point measurements but rather as measurements at scale 2*L* (0.4 m).

The mean K_r^C estimated in the filter packed wells was approximately an order of magnitude greater than the mean K_r^C estimate for the non-filter packed wells. Higher variability in K_r estimates was also observed in the non-filter packed than the filter packed monitoring wells. As the DFT induces a predominantly vertical flow field, short-circuiting through the skin zone (hydraulic conductivity K_s) is more pronounced in the DFT performed in the filter packed wells. The slug test may be less sensitive to the skin effect than the DFT due to its primarily horizontal flow pattern.

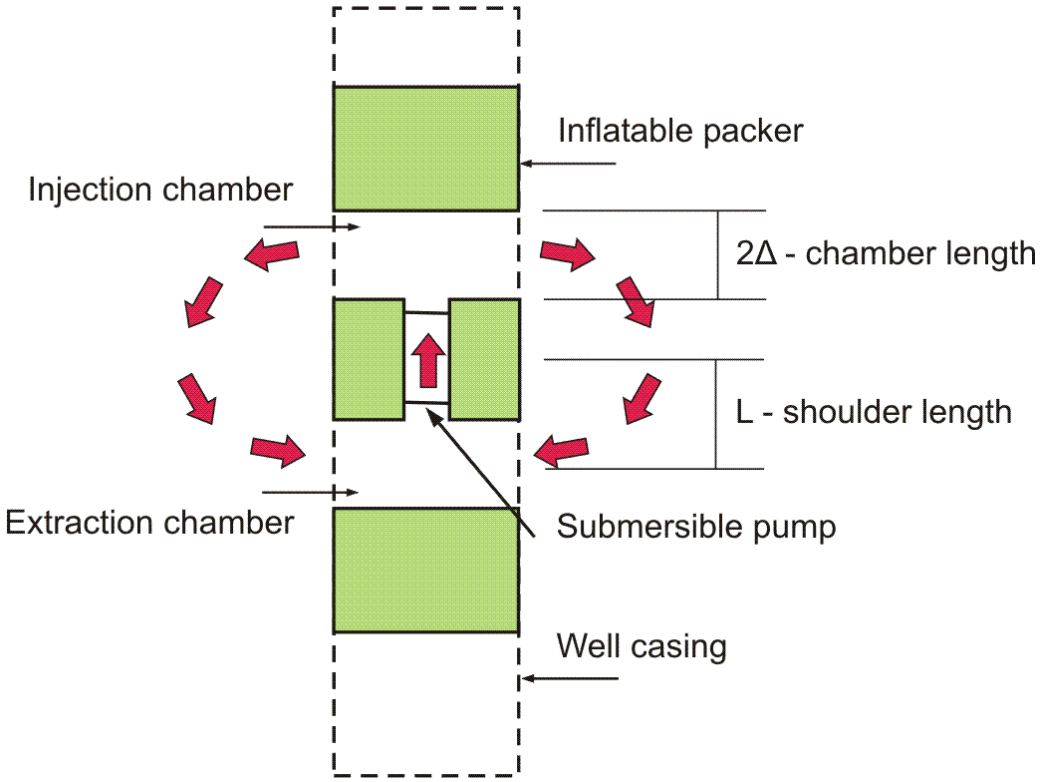

Figure 2.1. The dipole flow test (DFT) as proposed by Kabala (1993).

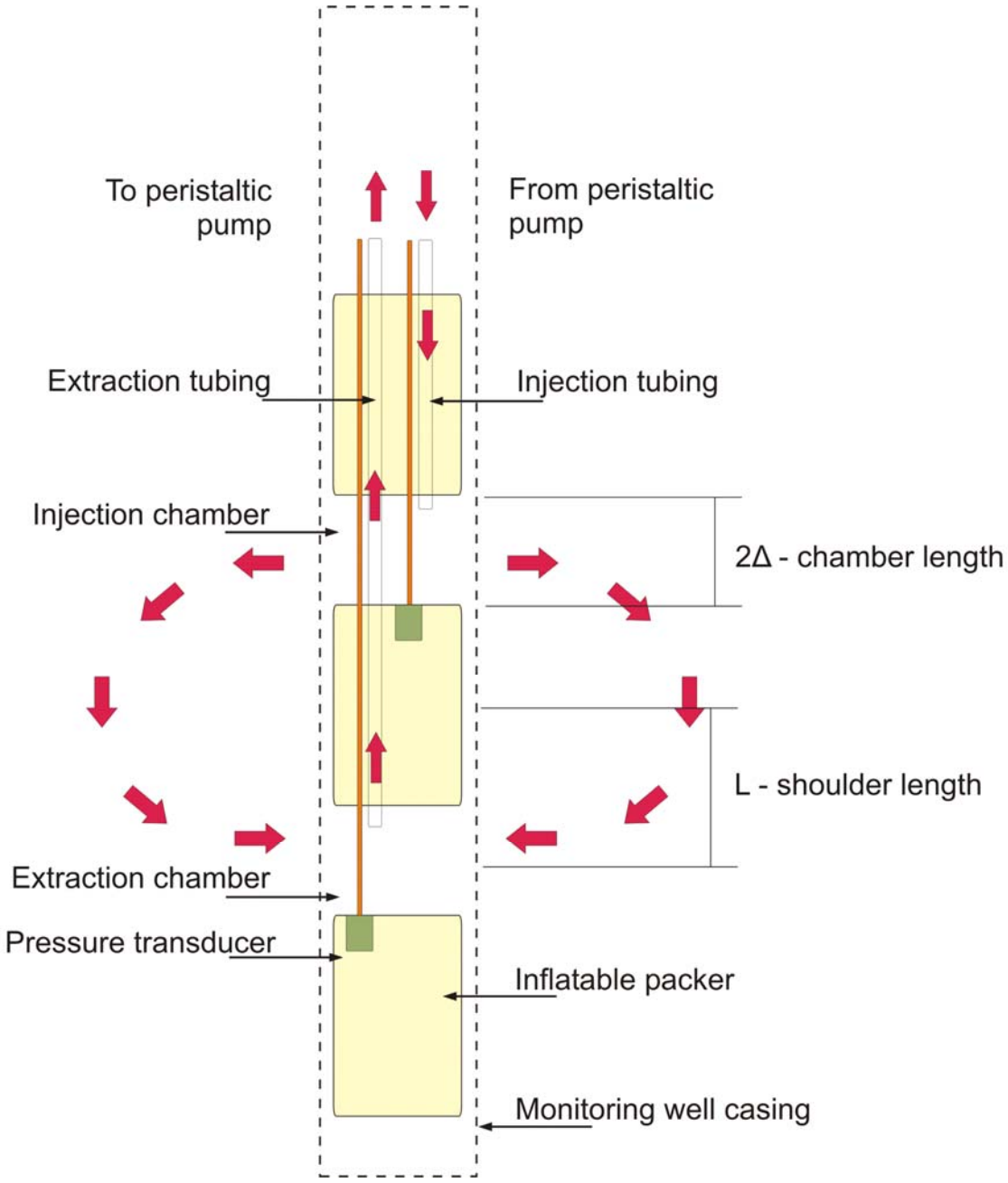

Figure 2.2. Schematic of the Waterloo prototype dipole probe and tracer test setup (arrows indicate tracer flow direction). Scale is exaggerated 3x in the horizontal direction.

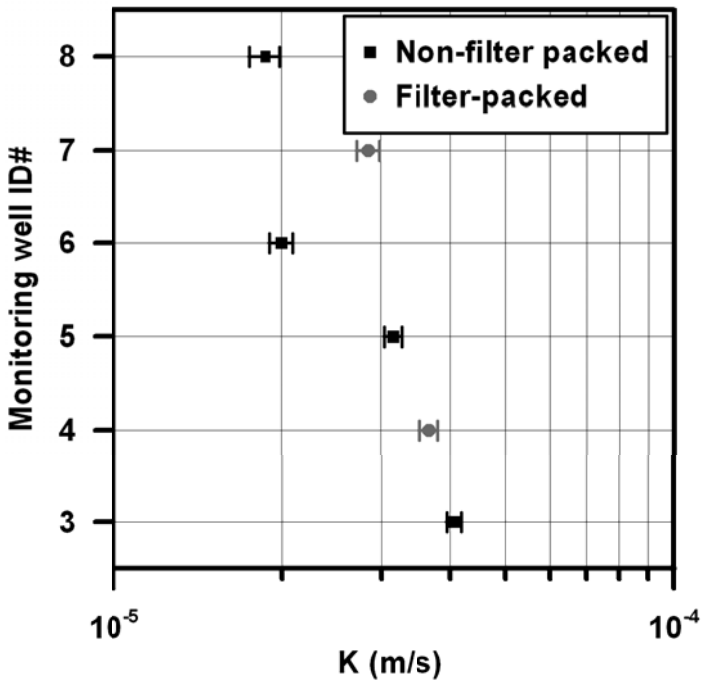

Figure 2.3. K_{SLUG} **estimates from the Bouwer and Rice analysis of the slug test data for the 6 CFB Borden monitoring wells (MW-3 to MW-8). The error bars show the standard deviations of the geometric mean** K_{SLUG} **estimates.**

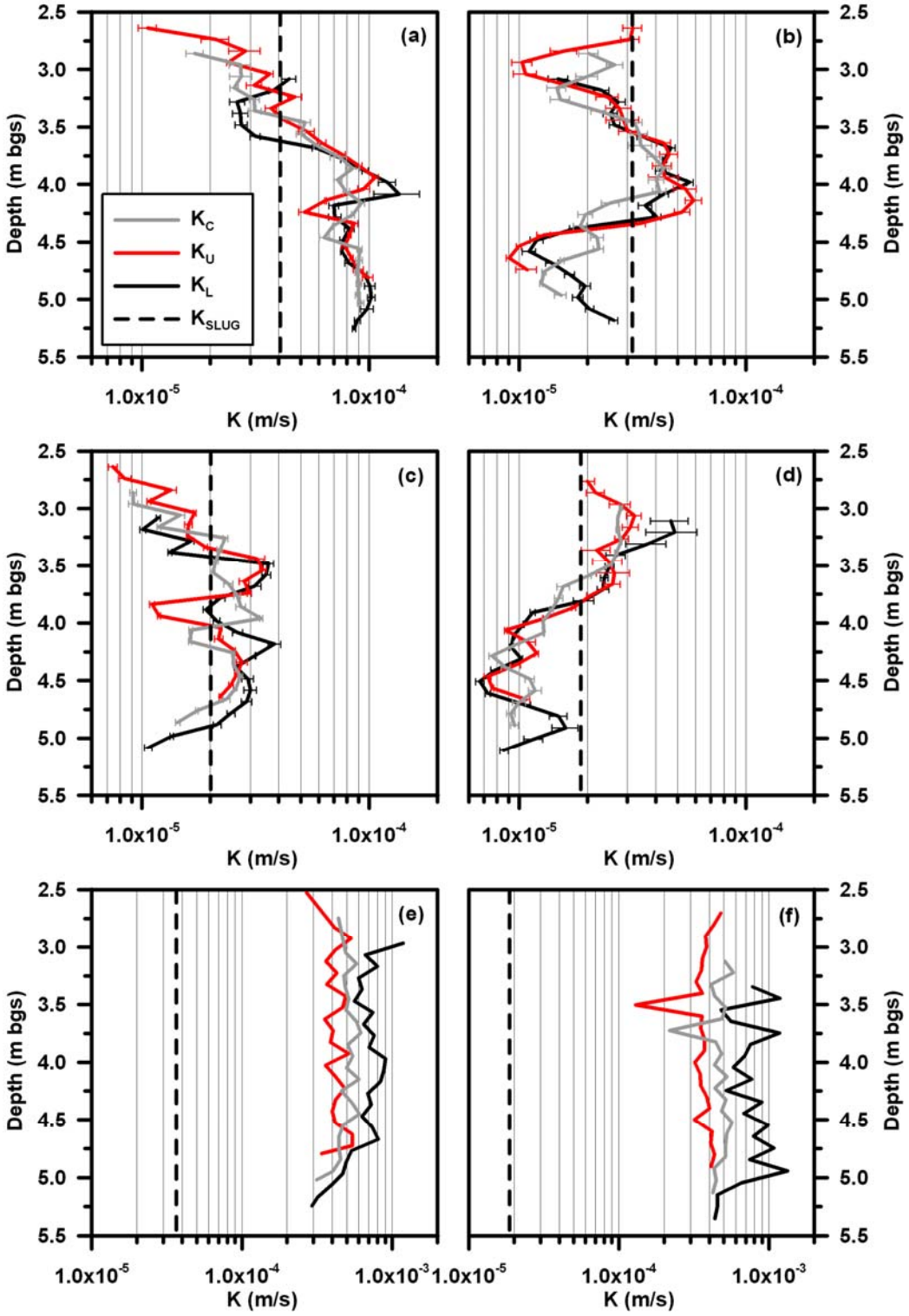

Figure 2.4. K_{BR} **estimates from slug tests and** K_r^C, K_r^I **and** K_r^E **estimates from DFTs completed at 0.10 m intervals in non-filter packed wells MW-3 (a), MW-5 (b), MW-6 (c), and MW-8 (d) and filter packed wells MW-4 (e) and MW-7 (f).**

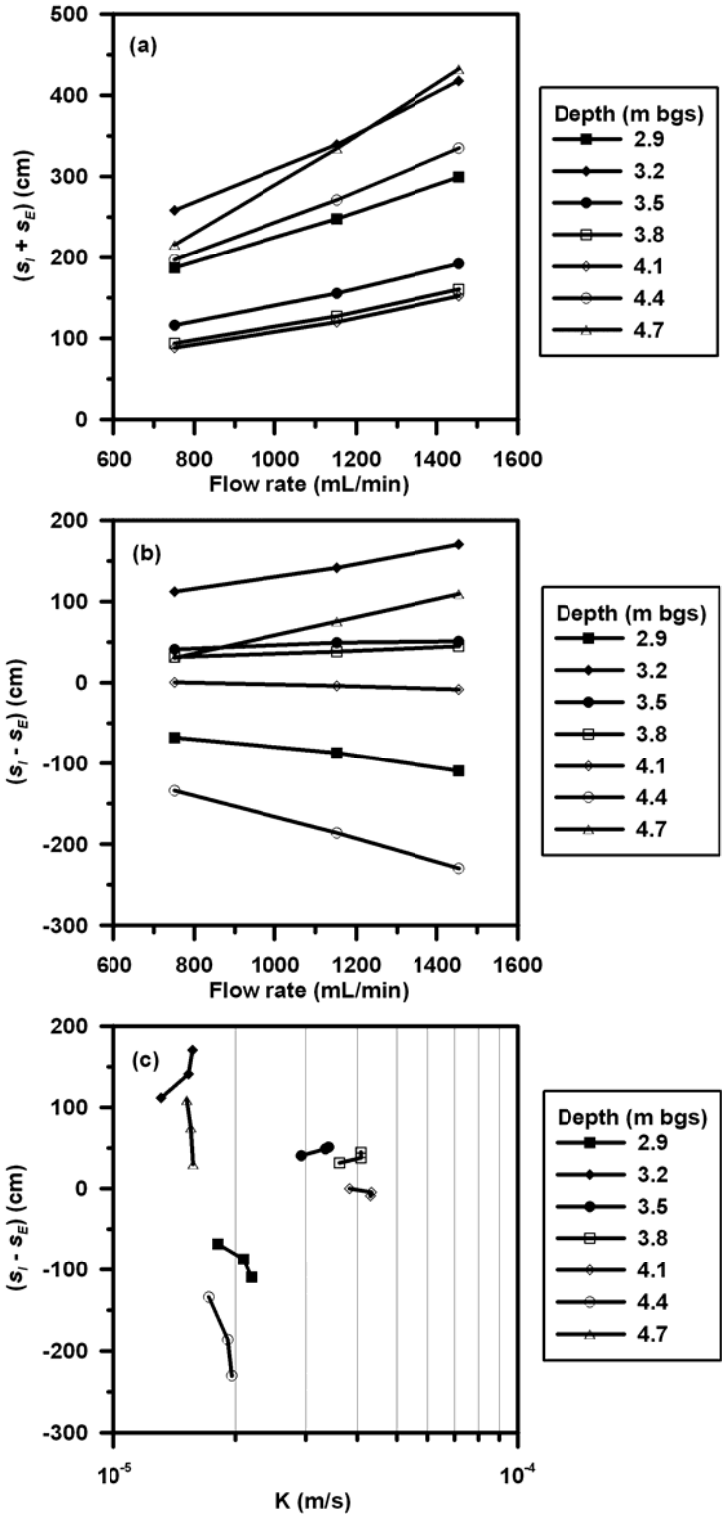

Figure 2.5. For DFTs in MW-5, (a) relationship between ($s_I + s_E$) (drawup + drawdown) and flow rate, (b) relationship between ($s_I - s_E$) (drawup - drawdown) and flow rate, and (c) relationship between the difference between ($s_I - s_E$) (drawup - drawdown) and K_r.

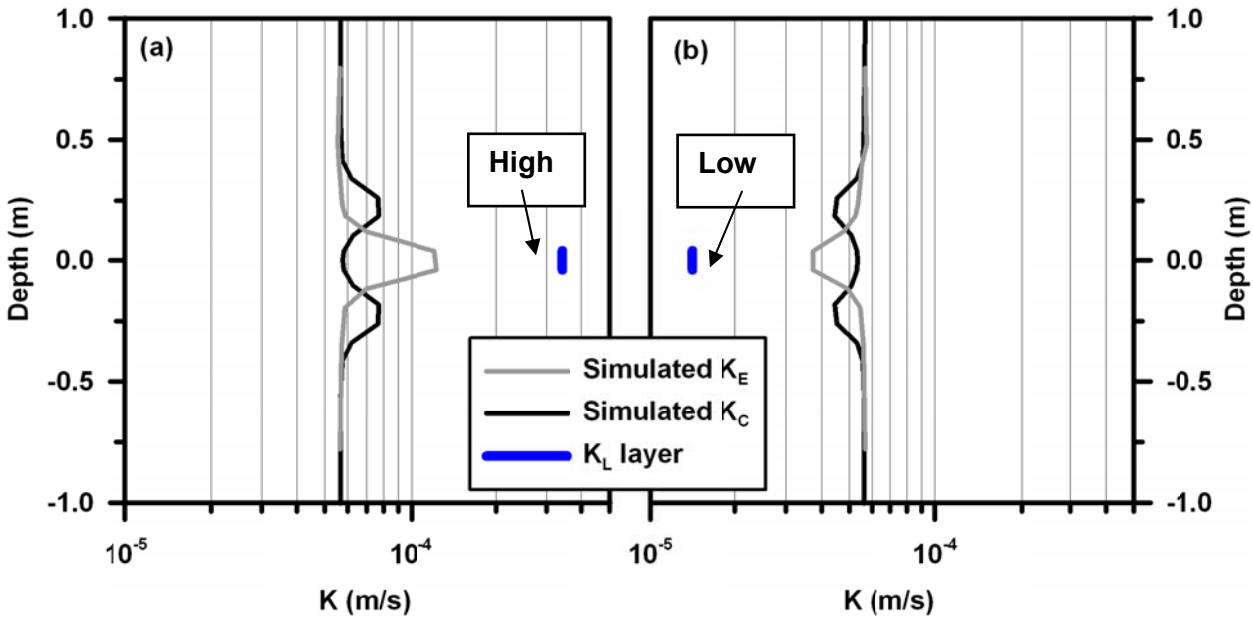

Figure 2.6. ***K_r*** **estimates calculated from drawup and drawdown values (** s_I **and** s_E**) from numerical model simulations of hydraulic head fields with a layer 0.0785 m (Δ) thick of different** ***K_r*** **than the aquifer** ***K_r*** **(7.0 x10^{-5} m/s). The** ***K_r*** **of the layers was simulated to be half an order of magnitude higher (3.5 x10^{-4} m/s (a)) or lower (1.4 x10^{-5} m/s (b)) than the aquifer** ***K_r*****.**

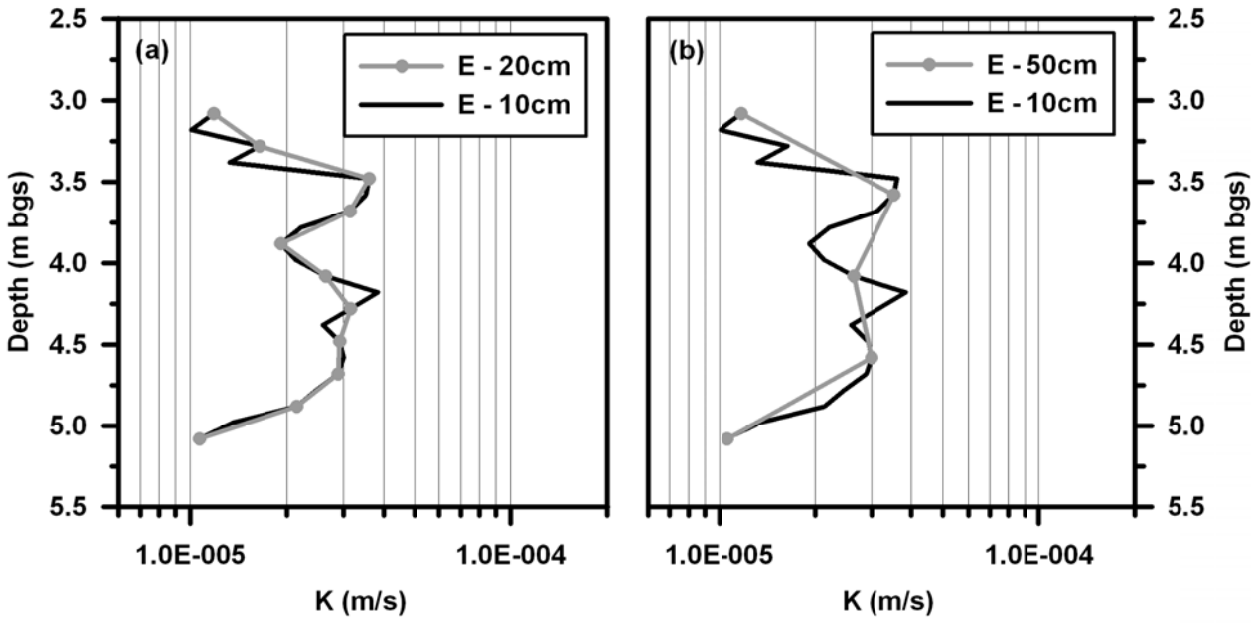

Figure 2.7. DFT ***K_L*** **estimates for monitoring well MW-6 from DFTs completed at 0.20 m (a) and 0.50 m (b) intervals. DFT** ***K_L*** **estimates at 0.10 m intervals shown as gray line.**

Table 2.1. Summary of setup parameters for published DFTs completed with symmetric dipole probes.

L (m)	Δ (m)	r_w (m)	Q (m^3/day)	s_I (m)	s_E (m)	$s_I + s_E$ (m)	Reference
0.27	0.25						
0.31	0.33	0.051	15 - 40	-	-	0.5 - 2.0	(Zlotnik et al., 1998)
0.40	0.34						
0.30	0.55	0.063	96	0.3 - 5.0	0.3 - 5.0	-	(Hvilshoj et al., 2000)
0.30	0.48						
0.84	0.43	0.057	26.6 - 28.2	1.46 – 1.49	1.52 – 1.83	2.98 – 3.29	(Sutton et al., 2000)
0.39	0.25	0.075	36.5 - 43.6	.003 - .37	.003 - .37	0.04 - 0.58	(Zlotnik et al., 2001)
0.53	0.25						
0.62	0.34	0.051	-	-	-	-	(Zlotnik et al., 2003)
0.53	0.25	0.051	13.7 – 28.6	-	-	0.35 – 1.30	(Zlotnik et al., 2007)
0.60	0.25						
0.22	0.08	0.025	0.43 - 1.01	0.07 – 3.93	0.03 – 2.95	0.04 – 6.47	This study

Table 2.2. *K* estimates from the slug tests (K_{SLUG}) and DFTs (K_r^C, K_r^I and K_r^E).

	MW-3	MW-5	MW-6	MW-8	MW-4	MW-7
K^C	5.8E-05	2.3E-05	1.9E-05	1.5E-05	4.9E-04	4.9E-04
CV	0.45	0.43	0.33	0.51	0.14	0.25
K^I	5.3E-05	2.5E-05	1.9E-05	1.7E-05	4.2E-04	3.6E-04
CV	0.53	0.65	0.43	0.50	0.18	0.18
K^E	6.7E-05	2.5E-05	2.2E-05	1.5E-05	6.4E-04	7.2E-04
CV	0.46	0.51	0.40	0.85	0.30	0.34
K_{SLUG}	4.1E-05	3.2E-05	2.0E-05	1.9E-05	3.7E-05	2.9E-05
CV	0.03	0.04	0.05	0.07	0.04	0.05

Table 2.3. K_r^E summary statistics for DFTs completed at 0.10 m, 0.20 m, 0.30 m, 0.40, and 0.50 m intervals in monitoring well MW-6 at CFB Borden.

DFT Interval	0.10 m	0.20 m	0.30 m	0.40 m	0.50 m
Geometric mean (m/s)	2.2E-05	2.2E-05	2.1E-05	2.1E-05	2.0E-05
Standard deviation (m/s)	8.7E-06	8.3E-06	8.0E-06	1.0E-05	1.0E-05
Coefficient of variation	0.40	0.37	0.37	0.49	0.50
Skew	-0.04	-0.26	-0.20	-0.04	-0.16

Chapter 3 Dipole Flow and Tracer Tests (DFTTs)

3.1 Introduction

The effective and efficient remediation of contaminated groundwater sites requires site specific information regarding the physical, chemical and biological properties of the aquifer (e.g., hydraulic conductivity, porosity, ion exchange capacity, redox capacity, and biodegradation potential). Hydraulic conductivity is known to vary both laterally and vertically (e.g., Molz et al., 1994; Butler, 2005; Zemansky et al., 2005; Dietrich et al., 2008), while biodegradation rates can vary due to differences in sediment texture, pH, temperature, microbial populations, carbon, oxygen and other nutrient availability (Schroth et al., 1998; Sandrin et al., 2004). To support the design of a remedial treatment system, aquifer parameter estimates specific to the site must be obtained. The use of literature values results in uncertain and potentially overly conservative predictions of remediation performance and may lead to unnecessarily cautious risk assessment and costly remediation strategies (Thomson et al., 2005).

Current aquifer parameter estimation methods are typically divided into *ex situ* and *in situ* techniques. *Ex situ* measurement techniques involve the removal of aquifer material from the impacted site for laboratory analysis. Although the materials can be tested to determine aquifer properties such as hydraulic conductivity, porosity, ion exchange capacity and biodegradation potential, *ex situ* techniques may provide parameter estimates not representative of the aquifer material due to the reduction of sample integrity during collection, transport, and laboratory setup and testing. Numerous *in situ* techniques are available for estimating aquifer physical and geologic characteristics (e.g., hydraulic conductivity, storativity, porosity, and fracture zones); however, few *in situ* methods are available to estimate biological or chemical properties. The main advantage to choosing an *in situ* technique over an *ex situ* technique is the opportunity to perform *in situ* techniques over multiple depths and locations across an impacted site while minimizing disturbance to the aquifer material sample. Recent work with partitioning inter-well tracer tests (PITTs) and push-pull tests indicate that *in situ* approaches present a potential opportunity to identify additional aquifer parameters.

A PITT consists of the simultaneous injection of several tracers with different partitioning coefficients at one or more injection wells and the subsequent measurement of tracer

concentrations at one or more monitoring wells to estimate the presence of non-aqueous phase liquids (NAPLs) (Jin et al., 1995). Typically, PITTs are conducted prior to and post source zone treatment to quantify the effectiveness of the remediation activities (e.g., Cain et al., 2000; Meinardus et al., 2002). The logistical and cost constraints tend to restrict the use of PITTs despite significant advances in their design and post-test analysis methods. Push-pull tests have been used to quantify microbial metabolic activities (Istok et al., 1997) and *in situ* reaction rate coefficients (Haggerty et al., 1998) in petroleum contaminated aquifers. Push-pull tests have also recently been used to estimate the natural oxidant demand of an aquifer (Mumford et al., 2004) and TCE degradation rates and permanganate consumption rates (Ko et al., 2007). One of the major disadvantages to using the push-pull test to estimate aquifer properties is the need to determine groundwater velocity direction and magnitude during the test as they are responsible for transporting the injected solution down-gradient of the monitoring well during the reaction phase.

The dipole flow test (DFT) is a single-well hydraulic test consisting of three inflatable packers isolating two chambers in a cased well and is used to estimate the vertical distribution of the radial (K_r) and vertical (K_z) hydraulic conductivity, and the specific storativity (S_s) in the vicinity of a test borehole. A submersible pump located in the central packer moves water at a constant flow rate from the aquifer into one chamber and transfers the water to the other chamber where it returns to the aquifer. Pressure transducers located in each chamber monitor pressure changes (drawup and drawdown). To estimate the hydraulic aquifer parameters (K_r, K_z and S_s) the transient chamber pressure changes are matched to type curves generated from an analytical solution (Kabala, 1993). Zlotnik et al. (1996) observed that the chamber pressures during a DFT reached steady-state quickly and suggested that the following could be used to estimate K_r

$$K_r = \frac{Q}{2\pi(s_I + s_E)\Delta} \ln\left(\frac{4a\Phi(\lambda)\Delta}{e r_w}\right), \tag{3}$$

$$\text{with } \Phi(\lambda) = \left(\frac{\lambda^2}{\lambda^2 - 1}\right)^{\lambda/2} \left(\frac{\lambda - 1}{\lambda + 1}\right)^{1/2}, \; a = \left(\frac{K_r}{K_z}\right)^{0.5} \text{ and } \lambda = \frac{L}{\Delta}, \tag{4}$$

where s_I and s_E are the steady-state absolute pressure head difference in the injection and extraction chamber respectively, r_w is the internal well radius, e = 2.718…, 2Δ is the chamber

length, $2L$ is the dipole shoulder defined as the distance between chamber centers ($L = D + \Delta$), and $2D$ is the dipole chamber separation. The function $\Phi(\lambda)$ increases from 0.5 to 1.0 as λ increases and the anisotropy ratio a must either be assumed or known prior to the test. Numerous DFTs have been conducted in various diameter wells with different dipole configurations and flow rates. Estimated K_r profiles generated from DFTs have shown similar trends and values to K estimates obtained through grain size analysis, permeameters, sieve analyses, flowmeters, and pump tests (Zlotnik et al., 1998; Zlotnik et al., 2001). Analysis of the individual chamber pressure changes (s_I or s_E) can provide estimates of K_r in the immediate vicinity of the chamber (K_r^I or K_r^E). One potential problem with the DFT is the short-circuiting of flow through the disturbed zone or well skin (hydraulic conductivity K_s). Since the DFT induces a predominantly vertical flow field, the well skin may be more pronounced in the DFT than in other single-borehole tests (Kabala, 1993; Zlotnik et al., 1998). In a series of DFTs performed in filter-packed wells in a heterogeneous highly permeable aquifer Zlotnik et al. (2001) observed a slight skin effect; however, similar K_r estimates were obtained for wells where geotextile rings were installed to prevent short-circuiting suggesting that at least in this aquifer the role of the well skin was minimal.

Sutton et al. (2000) proposed an extension to the DFT by adding a conservative tracer; thus creating a dipole flow and tracer test (DFTT). The DFTT works in a similar fashion to the DFT except when a steady-state flow field has been established, a conservative tracer is released into the injection chamber and the tracer concentration is monitored in the extraction chamber. The tracer is re-circulated since the extracted tracer solution is re-injected into injection chamber. Sutton et al. (2000) suggested that a combination of the chamber pressure changes and key properties of the tracer breakthrough curve (BTC) could be used to estimate the K_r and K_z, and the longitudinal dispersivity (α_L) along the DFT flowpaths. Using a combination of analytical flow and transport models, Sutton et al. (2000) showed that only 10% of the flow exiting from the injection chamber was responsible for the BTC peak concentration while the remaining 90% of the flow governed the shape of the BTC tail. As a consequence, the time to peak concentration and the peak concentration of the tracer were not affected by tracer recirculation. Field testing of the DFTT was performed in 12 cm diameter wells using a probe consisting of a 0.81 m central packer and two 0.61 m packers (L = 0.84 m and Δ = 0.43 m) with a fluorescent

tracer. The tracer BTCs exhibited numerous concentrations peaks which were attributed to some tracer movement through the well skin followed by the bulk of the tracer transport through the aquifer. In non-filter pack wells, the peak concentration arrival time was similar to the arrival time predicted by the numerical simulations (Sutton et al., 2000).

Recently, the dipole flow and reactive tracer test (DFRTT) has been proposed as *in situ* aquifer parameter estimation method (Thomson et al., 2005) and has a similar setup to the DFTT except that in addition to conservative tracer a suite of reactive tracers (i.e., sorbing, degrading, biodegrading, etc.) are injected either as a spike or for an extended period of time. The concentrations of the tracers and their breakdown products are monitored in the extraction chamber to produce a number of tracer BTCs. It is envisioned that these BTCs can then be analyzed with a suitable simulation model to estimate the required aquifer parameters (Thomson et al., 2005; Reiha, 2006). The difference between a conservative tracer BTC and a reactive tracer BTC will depend on the nature of the reactive tracer injected. For example a sorbing tracer such as trichlorofluoromethane will result in a retarded BTC relative to the conservative tracer, while a biodegrading tracer is expected to produce a BTC that shows signs of degradation relative to the conservative tracer BTC. These BTCs can be interpreted using simulation models in conjunction with optimization tools to estimate the value of controlling parameter(s) such as the distribution coefficient for the sorption process or the intrinsic degradation rate coefficient for the biodegradation process.

The purpose of the investigation described in this paper was to demonstrate the ability of a prototype dipole system to produce conservative tracer BTCs in conventional wells installed in a relatively homogeneous unconfined sandy aquifer. In particular, we were interested in the ability of our dipole system to produce repeatable BTCs at a given depth in a well, and the sensitivity of the DFTT BTCs to hydraulic conductivity variations along a single well and between wells, and to changes in operational parameters (flow rate, dipole dimensions, tracer injection duration, tracer recirculation, and natural or sand-packed wells). The results from this effort are now being used as the framework for our ongoing research effort exploring the utility of reactive tracers to characterize key aquifer properties *in situ*.

3.2 Field site, materials and methods

3.2.1 Field site

The field site for the testing reported in this paper is located at Canadian Forces Base (CFB) Borden, ~80 km northwest of Toronto, Ontario, Canada. The aquifer at this location is unconfined and consists of glacio-lacustrine deposits of fine to medium sand with porosity 0.40 (Brewster et al., 1995; Sneddon et al., 2002) and an organic carbon content of 0.2 mg/g (Mackay et al., 1986). Mean hydraulic conductivity estimates for this aquifer range from 8.0 $x10^{-5}$ m/s (Sudicky, 1986) for constant-head tests performed on homogenized core material to 2.6 $x10^{-5}$ m/s for constant-head tests performed on intact soil cores (Tomlinson et al., 2003). Although the aquifer is relatively homogeneous, distinct horizontal bedding features at the cm scale have been observed (Mackay et al., 1986; Brewster et al., 1995). The sand unit is underlain by an aquitard comprised of silts and clays ~9 m below ground surface (bgs) (MacFarlane et al., 1983).

Six 5.1 cm diameter PVC monitoring wells (MW-3 to MW-8) were installed to a depth of 5.5 m bgs and completed with a 3 m screen (0.010" slot). The wells are evenly spaced over an area of ~1000 m^2. Four wells (MW-3, MW-5, MW-6 and MW-8) were installed using a jetting technique where a hollow steel casing (~7 cm ID) was hammered into the sandy aquifer material and interior of the casing was flushed with water to remove the aquifer material. The aquifer material was allowed to collapse around the inserted PVC monitoring well when the steel casing was removed (Kueper et al., 1993; Tomlinson et al., 2003) thereby creating a well with a no artificial filter pack. The remaining two wells (MW-4 and MW-7) were installed following a similar jetting technique with a larger steel casing (~13 cm ID) to allow the installation of a 5.1 cm radius artificial filter pack (d_{50} of 0.85 mm). The hydraulic conductivity of the filter pack material (K_s) was estimated using the Hazen equation (Hazen, 1911) to be ~3 $x10^{-3}$ m/s. Each monitoring well was developed by repeatedly surging and pumping until the extracted water was clear of sediment.

3.2.2 Dipole system

Belowground dipole tool – The prototype dipole probe consists of three rubber inflatable packers with brass end caps separated by two chambers (Figure 3.1). The packers are separated by adjustable spacer rods to create the injection and extraction chambers. The characteristic

dimensions of the Waterloo prototype dipole probe are L = 0.22 m and Δ = 0.079 m. A 3.2 mm (1/8 in) HDPE inflation line connects the packers to a valve and pressure gage at ground surface. Two vented pressure transducers (Huba Control, Type 680 with range 0 – 2500 cm H_2O) are mounted in the packers and connect to the chambers with 6.35 mm (¼ in) stainless steel tubing. The current measured by the transducers was recorded every second by a data logger (Onset Computer Corporation, H21-002) and used to determine the changes in chamber pressures.

The choice of packer length was dictated by the prevention of packer circumvention which occurs when water is drawn into the chambers from the well screen above or below the packers. Increased vertical flow due to packer circumvention will overestimate the K of the aquifer and underestimate the extent of the vertical variations in K (Butler et al., 1994). Following recommendations by Zlotnik et al. (2003) and Cole et al. (1994), a packer length to packer radius ratio >10 was selected for this dipole probe design.

Aboveground DFTT control and monitoring equipment – The surface equipment controls and monitors the injection and extraction streams (Figure 3.2). The peristaltic pump (Cole Parmer, K-07553-70) draws water from the extraction chamber through the 6.35 mm (1/4 in) ID HDPE extraction line and passes it through the fluorometer (Turner Designs, 10-AU-005-CE). If a fluorescent tracer is used the fluorometer can provide almost continuous measurements. Downstream of the fluorometer a sampling port is available to manually sample the extracted groundwater, and an acrylic flow-through cell (constructed by the University of Waterloo), with ports for four probes, provides in-line monitoring. For the tests performed in this investigation, in-line probes were selected to monitor dissolved oxygen (DO), pH, electrical conductivity (EC), and oxidation reduction potential (ORP) (Thermo Orion, 083005MD, 9106BNWP, 013010MD, and 9678BNWP, respectively). Each probe is connected to a meter (Themo Orion, 1219000 or 1215000) which transmits data to a field notebook computer every 15 seconds. A syringe pump (Cole-Parmer, K-75900-00) is used to inject the tracer solutions into the injected groundwater through a three-way valve at a prescribed flow rate for a given duration. To ensure complete mixing of the injected tracer solution a static inline mixer (Cole-Parmer, K-04668-04) was placed downstream of the syringe pump. Finally, prior to being injected into the dipole probe injection chamber, a sampling port is available to manually sample the injected solution.

3.2.3 Field methodology

To investigate the properties of the conservative tracer BTCs, DFTTs were completed to assess the repeatability of the BTCs as well as the sensitivity of the BTCs to hydraulic conductivity variations along a single well and between wells, and to changes in operational parameters (flow rate, dipole dimensions, tracer injection duration, tracer recirculation, and natural or filter-packed wells).

DFTs were conducted at 10 cm increments to establish the vertical distribution of K_r along the 3 m screen of the monitoring wells. At each location tested in the non-filter packed monitoring wells, DFTs were completed at three different flow rates. For the filter packed monitoring wells, DFTs were completed at a single flow rate due to limitations of the peristaltic pump. The flow rates for the DFTs ranged from 347 to 1455 mL/min and K_r was estimated from Equation (1) developed by Zlotnik et al. (1998). Smaller scale estimates for K_r (K_r^I or K_r^E) were also calculated using only the injection (s_I) or extraction (s_E) pressure head changes (Zlotnik et al., 2001).

Before conducting a DFTT at a specific depth in a monitoring well, the well was re-developed by pumping until the water was clear and the fluorometer readings had stabilized. The packers of the dipole probe were inflated to ~200 kPa (30 psi) at the desired test depth in the monitoring well and then the peristaltic pump was powered on at the specified flow rate. After the dipole flow field reached steady-state conditions (constant pressure transducer readings for ~5 min), the injection valve was turned and the syringe pump injected the tracer into the injection line (Figure 3.2) for a specified period of time. Samples of the injected solution at the downstream monitoring port were collected during the tracer injection phase (10 mL samples collected every 2 – 10 min depending on the fluorometer readings). In addition to the online monitoring of the extracted solution with the fluorometer and probes, periodic samples of the extracted solution were collected throughout the DFTT to complement the BTC produced by the fluorometer.

Flow rates selected for the DFTTs ranged from 320 to 1860 mL/min. For DFTTs completed without tracer recirculation, the extracted solution was collected in a holding tank and a second pump, operating at the extraction flow rate, pumped clean water from a holding tank into the injection line. The effect of the dipole probe dimensions was investigated by modifying the

prototype by reducing L from 0.22 to 0.18 m, and Δ from 0.079 to 0.05 m. DFTTs were completed in both the non-filter pack and artificial filter pack wells.

The conservative tracer injection solutions were prepared using NaBr (Fisher Scientific) at concentrations ranging from 6,500 to 20,000 mg/L as Br^-, and either rhodamine WT (Cole-Parmer) or sulforhodamine B (Sigma-Aldrich) at concentrations from 50 to 75 mg/L. Bromide was selected as a conservative tracer due to its low sorption and low concentrations in natural ground waters (Davis et al., 1980; Mackay et al., 1986; LeBlanc et al., 1991). The fluorescent dyes were chosen due to the low detection limits and ease of detection in the field with a fluorometer (Davis et al., 1980; Smart et al., 1998). Rhodamine WT (RWT) is one of the most commonly used fluorescent dyes in groundwater tracer studies and has been used as both a conservative (Pang et al., 1998) and sorbing tracer (Sabatini et al., 1991). Rhodamine WT consists of two isomers with different sorption characteristics (Shiau et al., 1993; Sutton et al., 2001) which may make tracer BTC interpretation more difficult. Sulforhodamine B (SRB) (also known as acid rhodamine B) sorbs less than rhodamine WT (Kasnavia et al., 1999).

Fluorescent dye concentrations of the extracted solution were measured directly in the field with the fluorometer set up for continuous flow monitoring. Fluorescent dye concentrations of the collected samples were measured in the laboratory with the fluorometer in discrete sample mode. The fluorometer was calibrated with a 25 ppb solution (MDL 0.1 ppb). Bromide concentrations were determined by ion chromatography (IC) (Dionex AS18 4 x 250 mm column; 29 mM potassium hydroxide eluent; 1.0 mL/min flow rate) with a MDL of 1.0 mg/L. Bromide standards were prepared with a 7 point calibration curve (1 – 100 mg/L). Repeat measurements of the 10 mg/L calibration standard were used throughout all IC runs to ensure accurate bromide measurements.

3.3 Expected breakthrough curve (BTC) behaviour

Given the hydraulic conductivity and porosity of the CFB Borden aquifer are well established and the dipole probe configuration and operating parameters can be controlled, it was of interest to investigate the expected behaviour of conservative tracer BTCs using an existing DFRTT simulation model. The DFRTT model was developed as a high-resolution two-dimensional radially symmetric finite volume model consisting of two major components: a steady-state

groundwater flow component and a reactive transport component (Thomson et al., 2005). The model was designed so that it could provide an accurate representation of key first-order processes (e.g., biodegradation rate), have the ability to conform to a variety of field configurations and site conditions, and be able to handle a range of input parameters. The major assumptions used to develop this model are: (1) homogeneous aquifer parameters in the vicinity of the test well, and (2) the ambient groundwater flow field does not affect the dipole flow field. For more details regarding the DFRTT model, the interested reader is referred to Thomson (2009).

The hydrogeological and dipole system parameters used as the base case simulation are listed in Table 3.1. The base case BTC (Figure 3.3(a)) shows a time to peak of 51 min and a peak concentration of 0.0063. Figure 3.3(a) also shows how the base case BTC is affected by an increase or decrease in flow rate, the higher flow rate shifted the BTC to the left and increasing the peak concentration to 0.0088, and the lower flow rate shifting the curve to the right and reducing the peak concentration to 0.0038. The impact of tracer recirculation (Figure 3.3(b)) has minimal impact on the peak concentration but affects the shape of the BTC tail. Figure 3.3(c) demonstrates that increasing the tracer injection duration by a factor of 5 (from 2 min to 10 min) has a pronounced effect on the time to peak and peak concentration of the tracer BTC. The streamfunctions for the base case dimensions of the dipole probe and a smaller dipole probe (L = 0.18 m and Δ = 0.05 m) are shown on Figure 3.3(f). The shorter distance between the chambers of the smaller dipole probe pulls the streamlines closer to the well casing and produces a BTC with a shorter time to peak Figure 3.3(e).

Preliminary simulations were also performed to investigate the effect of the well skin on the shape of the BTC. Numerous concentrations peaks have been observed on field-measured tracer BTCs which have been attributed to some tracer movement through the well skin followed by the bulk of the tracer transport through the aquifer (Sutton et al., 2000). Holding the radius of the well skin constant (r_s 6.4 mm) and increasing the K_s/K_r ratio produces BTCs with progressively more skin effect (Figure 3.3(d)).

3.4 Dipole flow and tracer test (DFTT) results

A total of 46 DFTTs were completed in the monitoring wells at CFB Borden to investigate the properties of the BTCs. Test setup parameters for the DFTTs discussed in this paper are presented in Table 3.2. Definite tracer breakthrough in the extraction chamber was observed during all DFTTs, indicating that a dipole flow field was created between the two chambers of the dipole apparatus. Of the 46 DFTTs, 6 DFTTs were completed without tracer recirculation to investigate the role tracer recirculation plays on the shape of the BTC. BTCs were completed with a variety of tracer injection periods (13 DFTTs with 10 min injection, 7 DFTTs with 5 min injection, 22 DFTTs with 2 min injection and 3 DFTTs with 1 min injection). To compare the effect of the dipole tool dimensions, 14 DFTTs were completed with the smaller version of the dipole tool. Five tests were conducted in a filter packed monitoring well and the remainder in the non-filter packed wells.

To distinguish the DFTTs, each test was labelled with the monitoring well number, the depth of the dipole center bgs at which the DFTT was completed and the test number at that aquifer location. As an example, DFTT 6-4.3-C was completed in well MW-6 at 4.3 m bgs and was the third DFTT completed at that location. The BTCs are plotted as C/C_0 where C_0 is the concentration of the mixed injected tracer as estimated from samples collected from the port after the in-line mixer (Figure 3.2). In order to compare BTCs of various DFTTs conducted at different flow rates, we scaled the tracer concentration by M_0/Qt_c and non-dimensionalize the time (t_D) by dividing by the characteristic time t_c, defined as

$$t_c = \frac{l_c}{v_c} = \frac{2(L-\Delta)}{Q//4\pi\theta r_w\Delta} = \frac{8\pi\theta r_w\Delta(L-\Delta)}{Q}, \tag{5}$$

where l_c is the distance between the edges of the extraction and injection chambers ($2L$ - 2Δ), v_c is the characteristic pore-scale velocity along the chamber face, and M_0 is the injected tracer mass (Sutton et al., 2000). Theoretically, scaled BTCs should have a similar time to peak concentration, magnitude of the peak concentration and shape of the falling limb. In addition to the BTCs, the cumulative mass curves (CMCs) are also used to provide a measure of the amount of injected tracer recovered in the extraction chamber.

The fluorometer was an important monitoring tool for the breakthrough of the conservative fluorescing tracers since data could be obtained every second and used to produce detailed BTCs. In the absence of a fluorometer, the EC probe provided a good indication of relative bromide concentrations at the beginning of the DFTT; however, the calibration drifted and the conductivity readings increased during the constant or diminishing tail of the BTCs. The effluent pH remained constant during each DFTT. Due to pressure pulses from the peristaltic pump, the DO probe was removed from the flow-through cell and dissolved oxygen concentrations were measured by collecting a discrete sample from the sampling valve and measuring the DO concentration in a small flow cell at a lower flow rate. The DO concentration in the groundwater were low (typically 0.5 – 2 mg/L) and highly variable. The E_H measurements from the ORP probe typically started high and decreased during a conservative DFTT which indicates the length of time required for the ORP probe to equilibrate. The E_H measurements may also have been affected by the streaming effect of the flowing water in the flow-through cell (Nordstrom et al., 2005).

3.4.1 Hydraulic profiles

DFTs were performed at 0.10 m intervals and K_r was estimated using Equation (1) and the steady state pressure head changes. The estimated DFT K_r^C (combined chamber K_r estimates) profiles are shown on Figure 3.4. Despite the small area over which the wells are located, different K_r profiles are observed. For example, a lower K_r zone is observed in the upper portion of the screened interval of MW-3 and MW-6, but not in MW-8 despite this wells being separated ~50 m. The overall geometric mean K_r^E for each monitoring well varied from 1.5 x10^{-5} m/s (MW-8) to 2.2 x10^{-5} m/s (MW-6) and 6.7 x10^{-5} m/s (MW-3). The minimum and maximum K_r^E encountered were 6.7 x10^{-6} m/s (dipole center at 4.29 m bgs MW-8) and 1.4 x10^{-4} m/s (3.86 m bgs MW-3), respectively. The range of K_r^E values (max K_r^E – min K_r^E) encountered in each monitoring well varied from 2.8 x10^{-5} m/s (MW-6) to 1.1 x10^{-4} m/s (MW-3).

3.4.2 "Type" or response curves

The observed DFTT BTCs can be categorized into four "type curves" based on the shape of the conservative tracer BTC which is affected by flow rate, tracer injection duration, the presence of an artificial or naturally developed filter pack and aquifer properties including hydraulic

conductivity and porosity. BTC tailing is often observed during tracer tests (including tests other than DFTTs) due to aquifer heterogeneities (Luo et al., 2007; Riva et al., 2008). Key properties that define the shape of a BTC are the time to the maximum or peak concentration as well as the magnitude of the peak concentration (as C/C_0). An additional parameter is the time to tracer front as defined as the time to 10% of the peak concentration and is a measure of dispersivity. The time to the well skin peak concentration and the magnitude of the skin peak are also important for characterizing the well skin in the vicinity of a DFTT.

Type 1 BTC - The Type 1 BTC is characterized by a small initial peak followed by a higher peak (Figure 3.5(a)). The initial small peak results from tracer transport through a small disturbed zone around the monitoring well casing, while the second higher peak captures the bulk of the tracer movement through the aquifer. The results of dipole simulations indicate Type 1 BTCs are produced when there is only a small difference in K between the skin zone and the aquifer (K_s/K_r only slightly greater than one) (Figure 3.3(d)). Alternatively, the radius of the developed zone around the monitoring well casing is small and therefore the majority of the injected tracer travels through the aquifer.

Type 2 BTC - The Type 2 BTC is characterized by a rapid concentration peak which decreases quickly and the tail of the BTC flattens out to a fairly constant value (Figure 3.5(b)). Due to the rapid arrival time in the extraction chamber ($t_D < 5$), the Type 2 BTC response is dominated by tracer transport through the well skin. The arrival of tracer transported through the undisturbed aquifer may be masked by the dominant skin effect.

Type 3 BTC - Type 3 BTCs are characterized by at least two high concentration peaks (Figure 3.5(c)). A typical Type 3 curve has a rapid skin peak followed by an aquifer peak of similar magnitude. The Type 3 BTC is similar to the Type 1 curve; however, the peak magnitudes are different. The greater mass tracer transport through the skin zone of the Type 3 BTC results from a more permeable skin zone than the Type 1 BTC (Figure 3.3(d)). As initially noted by Roos et al. (2008), the DFTT BTCs are sensitive to variations in the ratio K_s/K_r. Some of the BTCs classed as Type 3 exhibit more than two concentration peaks. As the DFTTs are operated in recirculation mode, the additional peaks may be caused by recirculation of the injected tracers.

Type 4 BTC - The Type 4 BTC is characterized by a rapid concentration peak followed by a rapid drop off to a constant concentration (Figure 3.5(d)). Type 4 BTCs appear similar to Type 2 BTCs; however, the Type 4 response does not follow the exponential decay to the constant concentration. The constant concentration of the tail is supported by tracer recirculation through the aquifer and the skin zone of the monitoring well.

Of the 36 BTCs observed from the DFTTs completed in the non-filter packed monitoring wells, 14 BTCs were classified as Type 1 BTCs, 10 as Type 2 BTCs, 9 as Type 3 BTCs and 3 as Type 4 BTCs. To aid in classifying the type curves, the BTC dimensionless times to peak tracer concentration, skin peak and tracer front are shown on Figure 3.6(a-c). The skin peaks typically arrive at the extraction chamber less than $5t_D$ while the times to peak vary from $6.8t_D$ to $22.9t_D$ (preceded by the times to tracer front). The Type 1 and Type 3 BTCs can be easily differentiated from the Type 2 BTCs by the length of time between the skin peak and the aquifer peak. For example, the Type 1 DFTTs completed at 4.3 m bgs in MW-6 show a skin peak at ~$2.8t_D$, a tracer front at $6.2t_D$ and a tracer peak at ~$12t_D$ while the Type 2 BTCs of the DFTTs completed at 3.3 m bgs are characterized by a time to tracer peak at $2.1t_D$.

3.4.3 Relation of tracer breakthrough curves (BTCs) to hydraulic conductivity (*K*) field

The shape of the dipole flow field for a given dipole apparatus is governed by the hydraulic conductivity field surrounding the monitoring well (Zlotnik et al., 1994; Zlotnik et al., 1996; Xiang et al., 1997; Reiha, 2006) and will therefore affect tracer transport during a DFTT. For example, the presence of a lower hydraulic conductivity layer near one of the chambers will 'shift' the flow field away from the lower hydraulic conductivity layer. A lower hydraulic conductivity layer between the dipole chambers will cause the flow path to extend further into the aquifer delaying the peak of the BTC. If a more permeable layer falls across the injection chamber, the time to peak could be shortened (less travel time) or the peak concentration less (tracer injected further into aquifer).

As noted in section 3.4.1, the geometric mean K_r differs slightly between the three non-filter packed wells with the mean K_r estimate at MW-3 higher than at MW-6 or MW-8. The majority of the DFTTs completed in monitoring well MW-3 followed an ideal Type 1 BTC with a small skin peak followed by a higher aquifer peak. Since the shape of the BTC is sensitive to the ratio

of K_s/K_r, if the aquifer is more permeable at the location of MW-3, there may be less inducement for skin zone creation either during monitoring well installation or development. Therefore, the majority of the injected tracer migrates through the undisturbed aquifer and only a small percentage of the injected tracer short circuits through the skin zone. Based on the K_r profiles obtained through the DFTs (Figure 3.4), MW-8 is located in a less permeable area than MW-3 and MW-6. None of the BTCs obtained from the DFTTs completed in MW-8 followed the ideal Type 1 BTC. While the entire screen length was not tested, the results of the 8 DFTTs in MW-8 suggest the well is more heavily influenced by the well skin than either MW-3 or MW-6. The dominance of the skin zone may be due to the increased resistance to flow in a low *K* zone or may be a result of the development of a more prominent natural filter pack around the well casing as the small grain size materials are removed from the skin zone during well development.

As expected from the results of supporting numerical simulations, the presence of lower *K* zones within the dipole flow field affects the shape of the BTC. DFTT 3-4.3-A does not follow a Type 1 BTC response despite the fact that DFTTs 3-4.0-A, B, and C (completed above) and DFTT 3-5.0-A (completed below) follow a Type 1 BTC response. The hydraulic profile of MW-3 (Figure 3.4 (a)) indicates a low *K* layer present across the center of the dipole tool for DFTT 3-4.3-A. This low *K* layer would have affected the shape of the dipole flow field and thus affected the shape of the DFTT BTC. The series of DFTTs completed at 3.3 m bgs in MW-6 (6-3.3-A through H) produced Type 2 BTCs heavily dominated by the skin effect. This may be due to the MW-6 K_r profile (Figure 3.4(b)) which indicates a lower *K* zone present across the upper injection chamber of the dipole tool during these DFTTs. Since the flow field was deflected away from this low *K* zone, a short circuit near the well casing is produced that yields a Type 2 BTC.

3.4.4 Repeatability of dipole flow and tracer test (DFTT) breakthrough curves (BTCs)

To assess the ability of the DFTT to generate repeatable BTCs at the same depth within a given monitoring well, two series of DFTTs were performed. The first series (DFTTs 3-3.8-A, 3-3.8-B, and 3-3.8-C), which has a Type 1 BTC response, was completed at a depth of 3.8 m bgs in monitoring well MW-3 using a flow rate of ~540 mL/min. The BTCs from this series are shown in Figure 3.7(a) and indicate that portions of the tracer BTCs are repeatable. Some of the variability between the MW-3 DFTT BTCs is due to the use of discrete samples to build the

BTC and hence the resolution of the BTC is not as high as the BTCs represented by data from the fluorometer. Nevertheless, a comparison of the BTCs shows similar times to peak concentration ($7.6t_D$) and similar magnitudes of peak concentration (~0.13) (Figure 3.7(a)). The rising limb of the aquifer peak of the BTC shows a similar shape for each DFTT however there is some difference in the falling limbs. The tail of the BTCs for tests 3-3.8-A and 3-3.8-C follow a straight line (slope -1.86×10^{-4}) while the tail of BTC 3-4-3.0-B initially follows the same sloped line but then deviates to follow a plateau (slope -1.04×10^{-4}). While the sample resolution at early time in the DFTT is low (samples collected every 5 min), the three MW-3 BTCs seem to show early skin peaks (3-3.8-A is a possible exception). As noted in section 3.4.2, the skin peak is a function of tracer transport along the flow paths closest to the well casing in the skin zone. The hydraulic properties of the skin zone (e.g., K_s) may change depending on activities in the monitoring well (e.g., further well development, pumping, and other DFTTs). The differences in the BTCs may be caused by changes in the well skin as the well becomes more developed. If more tracer is transported through the well skin than less tracer will be available for aquifer characterization. Note however that, despite the differences in the BTCs, the CMCs are very similar between the DFTTs (Figure 3.7(b)).

The second series to examine the repeatability of DFTT BTCs was conducted in MW-6 (DFTTs 6-3.3-D, 6-3.3-E, and 6-3.3-F) at a flow rate of ~590 mL/min and produced a Type 2 BTC (Figure 3.7(c)). The MW-6 DFTT BTCs show similar times to peak concentration (~6 min) and varying magnitudes of peak concentration (0.03 – 0.065). The early BTC peak is created by tracer movement through the skin zone around the well casing. Therefore the varying magnitudes of peak concentration are a reflection of the variable nature of the skin zone. Since only 10 to 13% of the flow is involved in the peak concentration (Sutton et al., 2000; Reiha, 2006), small-scale heterogeneities present in the injection chamber can create large differences in the peak concentration. This is supported by the differences in CMCs for the MW-6 DFTTs (Figure 3.7(d)) which show similar shapes in the early mass arrival; however, the magnitude of the early mass arrival increases with the order in which the DFTTs were completed (i.e., 6-3.3-F was the last DFTT of the series to be performed and has the highest peak and most tracer mass transport of the three DFTTs). This increase in tracer transport in the skin zone seems to suggest

the skin zone around the well casing is becoming more prominent with increased activity in the monitoring well.

The two series of DFTTs completed to assess the repeatability of the BTCs demonstrate that portions of the DFTT BTCs are repeatable. The Type 1 and Type 2 BTCs showed similar times to peak concentration between DFTTs. The Type 1 BTCs showed similar magnitudes of peak concentration; however the early skin concentration peaks were not as repeatable between the DFTTs. This is similar to the differing magnitudes of the peak concentration for Type 2 DFTs which emphasizes the influence of the skin zone on the BTC shape, especially for the Type 2 BTC.

3.4.5 Influence of flow rate

Given that the dipole flow field is defined by the aquifer properties and the dimensions of the dipole apparatus, changing the flow rate of a DFTT does not affect the spatial distribution of the flow field but will affect tracer transport velocity and the shape of the BTC. In order to be able to compare BTCs of DFTTs completed at different flow rates, we use Equation (5) to define a dimensionless time scale and scale the tracer concentration.

The effect of flow rate (360, 550 and 710 mL/min) on the shape of a Type 1 BTC was investigated at a depth of 4.9 m bgs in MW-3 (DFTTs 3-4.9-C, 3-4.9-D, and 3-4.9-B, respectively). As expected from numerical simulations (Figure 3.3(a)), the BTCs of the DFTTs completed at higher flow rates show earlier times to peak concentration and greater magnitudes of peak concentration. The time to the skin peak also decreases as the flow rate increases however the magnitude of the peak skin concentration is more related to the heterogeneity of the skin zone than the flow rate. When the BTCs are scaled, the times to peak concentration ($\sim 12.4 t_D$) and times to skin peak ($\sim 3.4 t_D$) are similar between DFTTs (Figure 3.8(c)). The scaled magnitude of the peak concentration (0.027) is similar for the DFTTs completed at 550 and 710 mL/min (DFTTs 3-4.9-D and 3-4.9-B) however the 360 mL/min DFTT has a scaled peak concentration of 0.033. One possible reason for the discrepancy between the tests is increased dispersion at lower flow rates. The magnitudes of the skin peak concentration also vary between DFTTs. The most pronounced skin peak was observed on the 500 mL/min BTC (DFTT 3-4.9-D). DFTT 3-4.9-D was the most recent DFTT to be completed at this aquifer location. As the

skin peak captures the movement of the tracer through a developed zone around the monitoring well casing, a more prominent developed zone may have been created around the casing of MW-3 during well development activities. Examining the CMCs (Figure 3.8(b)), more tracer mass was observed in the extraction chamber during the duration of the tests for DFTTs completed at higher flow rates as expected; however, the scaled CMCs are similar in shape indicating the tracer is following the same flow paths for each DFTT at that location despite the different flow rates (Figure 3.8(d)).

The effect of flow rate on the shape of a Type 2 BTC is less dramatic than the effect on a Type 1 BTC. Three DFTTs were completed at flow rates 420, 600, and 800 mL/min at a depth of 3.3 m bgs in MW-6 (DFTTs 6-3.3-G, 6-3.3-D, and 6-3.3-H, respectively). Slight differences between the times to peak concentration can be observed on the BTCs (Figure 3.9(a)) as the time to peak decreased from 11.0 min for the 420 mL/min DFTT to 5.0 min for the 800 mL/min DFTT. Similar to the Type 1 BTCs discussed above, scaling the BTCs shows similar times to peak concentration (~$1.8t_D$) (Figure 3.9(c)); however some differences are apparent between the DFTT BTCs. A second peak (15.4 min or $3.8t_D$) is visible on the BTC of DFTT 6-3.3-D, which is likely due to tracer recirculation through the skin zone as the time to the second peak is approximately double that of the initial peak. As the bulk of the Type 2 BTC is defined by tracer travel through the skin zone, the CMCs for these DFTTs (Figure 3.9(b) and (d)) are less similar to each other than for the Type 1 BTCs (Figure 3.8(d)) due to the varying nature of the skin zone.

DFTTs can be completed at higher flow rates than the 500 mL/min typically chosen for the tests reported in this paper. Conducting a DFTT at a higher flow rate would allow more tests to be completed in the same amount of time. Although Sutton et al. (2000) employed a 19,000 mL/min flow rate with a larger dipole (L = 0.84 m and Δ = 0.43 m), at high flow rates there may be concerns about mobilizing the fine grained fraction of the aquifer (Zlotnik et al., 2001). An additional concern for tests completed with reactive tracers at high flow rates may be the contact required for tracer sorption to aquifer materials or for tracer degradation. Therefore there is an upper limit to the flow rate for a given DFTT or DFRTT. To examine the influence of a higher flow rate for our dipole prototype system, DFTT 6-4.3-C was completed at 1350 mL/min, the maximum flow rate of the peristaltic pump at that aquifer location. The BTC follows a typical Type 1 curve (Figure 3.10(a)) with a rapid low concentration skin peak followed by the main

aquifer peak. As expected, the BTC peak arrives more quickly than the peak of DFTT 6-4.3-A (750 mL/min) and more mass is returned to the chamber in the same amount of time (Figure 3.10b). The scaled BTCs (Figure 3.10c) show similar dimensionless times to peak ($12.5t_D$). Slight differences in the falling limb of the BTCs are observed. These differences between the BTCs are possibly due to the effect of the flow rate. The scaling CMCs indicates that a similar mass of recirculated tracer (60% of the injected tracer mass) arrived at the extraction chamber within the same dimensionless time period ($90t_D$) for the two DFTTs. This indicates that repeatable DFTTs can be completed with the Waterloo dipole probe at CFB Borden to a flow rate of at least 1350 mL/min. The maximum flow rate at which representative conservative BTCs could be obtained under similar conditions (apparatus dimensions, aquifer parameters) was not determined.

Field testing at CFB Borden has found that BTCs of DFTTs completed at the same aquifer locations but at different flow rates can be scaled to produce similar BTCs. Both Type 1 and Type 2 BTCs can be scaled; however, more variability was found for the Type 2 BTC than the Type 1 BTCs. Repeatable DFTT BTCs were obtained with the Waterloo dipole probe at CFB Borden at flow rates up to 1350 mL/min, indicating that conservative DFTTs can be completed in less time in the Borden aquifer; however the maximum flow rate was not determined.

3.4.6 Tracer recirculation

The results from dipole simulation efforts have shown the magnitude of the peak concentration of the BTC is not affected by the recirculation of the injected tracer for DFTTs in non-filter pack wells (Figure 3.3(b)). It is simplest from a practical point of view in the field to conduct the DFTT with tracer recirculation where the extracted solution is subsequently re-injected into the dipole flow field. However, at times it may be simpler to interpret the shape of the BTCs from DFTTs completed without tracer recirculation as the tails are a reflection of only a single tracer injection.

To assess the effect of tracer recirculation on the observed BTCs collected as part of this investigation, a series of recirculation and non-recirculation DFTTs were completed at the same aquifer locations. DFTT 3-4.9-E, completed without tracer recirculation, serves as a comparison to DFTTs 3-4.9-B, 3-4.9-C, and 3-4.9-D completed with tracer recirculation. The general shape

of the tracer BTC at this aquifer location (4.9 m bgs in monitoring well MW-3) is a Type 1 curve characterized by a small early skin peak followed by a greater aquifer peak (Figure 3.11(a)). The BTC of DFTT 3-4.9-E follows those of the recirculating DFTTs until ~25t_D (105 min) when it diverges (Figure 3.11(a)). This is consistent with simulation efforts (Figure 3.3(b)). The CMC for the non-recirculating DFTT also diverges at 25t_D (105 min) (Figure 3.11(b)) indicating that the peak of the observed BTC was largely defined by the aquifer properties and not affected by tracer recirculation. Furthermore, the recirculation of the tracer which created the early skin peak on the BTC did not affect the overall shape of the aquifer peak of the BTC. The small amount of tracer that did travel through the well skin would have been re-injected and only a small fraction of that re-injected tracer would have followed the short circuit flow path.

Similar to the Type 1 BTC discussed above, non-reciculatory DFTTs 8-4.9-B and 8-4.9-C were completed to compare the effects of recirculation against a Type 2 DFTT with tracer recirculation (8-4.9-D). The BTCs for all three DFTTs show early skin peaks (2t_D); however the magnitude of the skin peak concentrations differs between the tests in a manner similar to that observed during the repeatability tests in MW-6. As expected, more tracer mass is observed in the extraction chamber for recirculatory DFTT 8-4.9-D (60%) than for non-recirculatory DFTTs 8-4.9-B and 8-4.9-C (45%) at 53t_D (Figure 3.11(d)). The CMCs diverge in shape at ~20t_D indicating the lengthy tail of the recirculatory BTCs is supported by tracer recirculation.

For Type 1 BTCs, the peak is largely defined by the aquifer properties and not affected by tracer recirculation. Although some of the early skin peak tracer mass will re-circulate due to its short travel distance, this small amount of tracer is not enough to affect the shape of the BTC. The peak of Type 2 BTCs are more affected by the well skin properties and is therefore vulnerable to changes in the skin zone. Nevertheless, the CMCs of the recirculatory and non-recirculatory DFTTs do diverge in shape indicating the lengthy tail of the recirculatory BTCs is supported by tracer recirculation. If a long test is desired (e.g., for a biodegrading tracer), a recirculatory DFTT may be preferred over a DFTT without tracer recirculation.

3.4.7 Duration of tracer injection

To initiate a DFTT the selected tracer(s) may be added as a spike or as a continuous injection. The results of numerical simulations have shown a longer tracer injection period produces a BTC

with a higher and later concentration peak (Figure 3.3(c)). To investigate the effect of the duration of the tracer injection, DFTTs 6-3.3-D and 6-3.3-E were completed with a 2 min ($0.5t_D$) tracer injection while DFTT 6-3.3-C was completed with a 10 min ($1.8t_D$) tracer injection period. The same mass of tracer was injected for each test; however the rate at which the tracer was injected was varied. The scaled BTCs have similar Type 2 curve shapes in that the BTCs are dominated by a skin peak (Figure 3.12(a)). However, the time to peak of DFTT 6-3.3-C ($0.5t_D$) is greater than the time to peak of DFTTs 6-3.3-D and 6-3.3-E ($0.25t_D$). As expected, the longer tracer injection duration spreads out the tracer mass resulting in a delayed and lower peak concentration. It is not expected that the difference in tracer injection rates (25 mL/min vs 5 mL/min) affect the shape of the BTCs. Note that the scaling method developed by Sutton et al. (2000) does not account for the effect of the injection duration. The CMCs for the DFTTs indicate the longer tracer injection period (DFTT 6-3.3-C) has mass arriving more quickly than the shorter injection period (Figure 3.12(b)). This result may not be a function of the tracer injection duration but rather the variability of the developed zone around the well casing at this location observed during the repeatability tests described in section 3.4.4 (Figure 3.7(d)).

The effect of longer tracer injection on a Type 1 curve was investigated with DFTTs 3-4.9-D (2 min ($0.5t_D$) tracer injection) and 3-4.9-F (10 min ($2.3t_D$) tracer injection) completed at 4.9 m bgs in monitoring well MW-3. Both BTCs follow a Type 1 curve however the time to peak concentration of DFTT 3-4.9-F ($14t_D$) lags that of DFTT 3-4.9-D ($12.5t_D$) (Figure 3.12(c)). It is also interesting to note similar lag times between the respective skin peaks of the BTCs. Similar to the BTCs, the CMCs are comparable in shape (Figure 3.12(d)) however the CMC of the longer injection DFTT (3-4.9-F) lags that of the shorter injection DFTT (3-4.9-D). Slightly less tracer mass returned to the extraction chamber for the longer tracer injection (3-4.9-F) than the shorter injection.

As expected, the longer duration of tracer injection delays the peak concentration of the BTC for both the Type 1 and Type 2 curves. The early skin peak of the longer injection period Type 1 BTC was also delayed relative to the shorter injection period BTC. While the CMCs for the Type 2 curves are difficult to interpret due to the variability of the developed zone, the CMC for the Type 1 curves show delayed tracer mass arrival for longer injection periods.

3.4.8 Dipole probe dimensions

The dimensions of the dipole apparatus (and the aquifer anisotropy) determine the dipole flow field and therefore the portion of the aquifer characterized by the DFTT BTC. The results of numerical simulations show that increasing L, half the distance between chamber centers, increases the time to peak concentration and decreases the magnitude of the peak concentration (Figure 3.3(e)). The shape of the BTC is also more sensitive to the L dimension of the dipole probe than Δ, the half chamber length (Reiha, 2006). To compare the effect of the dipole probe dimensions, DFTTs were completed with two configurations of the dipole probe prototype. The base case dipole probe had slightly longer chambers ($\Delta = 0.08$ m) and chamber spacing ($L = 0.22$ m) than the modified dipole probe ($L = 0.18$ m and $\Delta = 0.05$ m).

The BTCs for DFTTs 3-3.8-A and 3-3.8-B, completed with the smaller modified probe, show earlier times to peak ($8t_D$) than the BTC for DFTT 3-3.8-D ($15t_D$) completed with the larger base case probe (Figure 3.13(a)). All three DFTTs were completed at similar flow rates (~540 mL/min) with the dipole probe center located at 3.8 m bgs in monitoring well MW-3. The magnitude of the peak concentration is greater for the smaller probe DFTTs (0.07) than the larger base case probe (0.04). The differences in the CMCs between the DFTTs (Figure 3.13(b)) also indicate the injected tracer is following different flow paths through the aquifer. Due to the difference in the L dimension of the probes, the tracer injected in the smaller probe DFTTs appears more quickly in the extraction chamber and more mass is recovered during the DFTT (Figure 3.13(b)). This is supported by Figure 3.3(f) which shows the simulated flow lines of the smaller probe drawn closer to the well than the flow lines for the larger dipole probe. Although Sutton et al. (2000) scaling method is supposed to account for differences in L, Figure 3.13(a) and Figure 3.13(b) indicate slightly different portions of the aquifer are sampled during these DFTTs with different probe dimensions.

3.4.9 Filter packed wells

Until now, the analysis has been limited to non-filter pack monitoring wells and has not included a discussion of the monitoring wells installed with artificial filter packs. Figure 3.14(a) shows a comparison between the BTCs for DFTTs completed in an artificial filter packed well (DFTT 4-3.4-A) and a non-filter pack monitoring well (DFTT 3-4.9-A). The two DFTTs were conducted at similar flow rates (~560 mL/min). Although the BTCs are not directly comparable as the

DFTTs were completed in different monitoring wells, the differences in the time to peak concentration as well as the magnitude of the peak concentration emphasize the difference in tracer flow between the two types of monitoring wells. Similar to the BTCs presented by Sutton et al. (2000), the BTC for the DFTT conducted in the filter packed well had a much faster peak concentration arrival time than the BTCs in the non-filter packed wells. Monitoring wells installed with artificial filter packs are designed so the K_s is greater than the K_r of the aquifer to increase water flow to the monitoring well (Driscoll, 1986). The radius of the skin zone (r_s) will also be much greater (at a minimum the borehole diameter) for an artificially filter packed well than for a non-filter pack monitoring well. Due to the increase in the skin zone parameters (K_s and r_s) between the two monitoring well types, rapid and high concentration peaks were expected in the filter packed wells.

The CMCs also illustrated the differences between the two DFTTs (data not shown). During the first 15 min of DFTT 4-3.2-A completed at 3.2 m bgs in filter packed monitoring well MW-4, 50% of the injected tracer mass had already travelled from the injection chamber to the extraction chamber. In comparison, no tracer was visible in the extraction chamber of the non-filter pack well at 15 min. At the end of the DFTT, 211% and 0.2% of the injected tracer mass had been observed in the extraction chamber for the filter packed and non-filter pack wells, respectively. The high percentage of tracer return during the DFTT in the filter packed well is due to cumulative tracer recirculation. The difference in the cumulative mass is due to the difference in flow paths between the two different types of monitoring wells. Although obvious recycled tracer peaks are not visible on the BTC, that 211% of the injected tracer mass was observed in the extraction chamber confirms the tracer was recirculating within the dipole flow system established in the filter packed well.

To investigate the portion of the BTC that is recirculation in filter packed wells, DFTTs were completed with and without recirculation at 4.9 m bgs in monitoring well MW-4 (Figure 3.14(b)). The recirculation DFTT 4-4.9-A is characterized by an early time to peak ($1.5t_D$) followed by a three successively lower tracer peaks. The non-recirculation DFTT BTC 4-4.9-B is characterized by the same early time to peak ($1.5t_D$) but does not show the three successive peaks of the recirculation DFTT (Figure 3.14(b)). The two BTCs diverge before the second concentration peak ($2t_D$). The differences between these two BTCs confirms Sutton et al.'s

(2000) hypothesis that the multiple peaks observed on BTCs in filter packed wells are due to tracer recirculation. As expected, the CMC of the recirculation DFTT continues to rise after diverging from the non-recirculation CMC (data not shown). It is interesting to note that although recirculation was not present during DFTT 4-5.1-B, the CMC still reached ~100% of the injected tracer mass. This indicates the bulk of the tracer mass flows through the filter pack and little tracer mass flows through the aquifer as longer arrival times are expected for tracer travel through the aquifer.

The differences between the BTCs of DFTTs completed in filter packed wells and non-filter pack wells emphasize the importance of well construction on the interpretation of DFTT BTCs. The differences in the BTCs completed at the same location demonstrate the importance of tracer recirculation in the DFTTs completed in filter packed wells. Successive peaks are not a signal of tracer movement through the aquifer, rather they are the initial concentration peak recirculated through the filter pack. In order to separate the two aquifer signal from the recirculation signal, DFTTs can be completed with and without tracer recirculation (as was done in this case). The DFTTs completed in the filter packed wells may or may not include tracer movement through the aquifer in addition to tracer movement through the filter pack. However, as initially noted by Sutton et al. (2000), DFTTs in filter packed wells can yield estimates of K_s and r_s which will allow other aquifer characterization methods to provide more accurate estimates of aquifer formation parameters.

3.5 Conclusions

The dipole flow and reactive tracer test (DFRTT) has been proposed as *in situ* aquifer parameter estimation method. The DFRTT involves the injection of a suite of reactive and conservative tracers into one chamber of the dipole apparatus and the subsequent monitoring of the tracer concentrations in the other chamber to produce the BTCs. To estimate the aquifer parameters, the BTCs are analyzed with the DFRTT model. The aquifer parameters estimated will depend on the nature of the reactive tracers injected. For example, the use of biodegrading tracers will yield biodegradation information that will aid in assessing the feasibility of selecting monitored natural attenuation as a remedial strategy rather than other more costly techniques.

The dipole apparatus was constructed at the University of Waterloo and field tested to estimate hydraulic profiles and complete 46 DFTTs at CFB Borden. The shape of the BTC for a conservative tracer is affected by test set up parameters, well construction and aquifer formation properties. The BTCs from the DFTTs completed in the non-filter pack monitoring wells can be categorized into four "type curves" based on the curve properties (time to peak, peak concentration, etc.). The differences between the type curves are largely defined by the ratio of K between the skin zone and the aquifer (K_s/K_r).

In order for aquifer parameters to be estimated from the BTC of a DFTT, one must have confidence the BTC is representative of the aquifer conditions. One measure of confidence is the repeatability of the BTC: for a given DFTT setup at a specific location, will the shape of the BTC be consistent between tests? The series of DFTTs completed to assess the repeatability of the BTCs demonstrate portions of the DFTT BTCs are repeatable and the Type 1 and Type 2 BTCs showed similar times to peak concentration between DFTTs. Field testing at CFB Borden found that BTCs of DFTTs completed at the same locations but at different flow rates can be scaled by the method suggested by Sutton et al. (2000) to produce similar BTCs. Investigating the effect of tracer recirculation, it was found the peak of the field BTCs was largely defined by the aquifer properties and not affected by tracer recirculation; however tracer recirculation was important for controlling the shape of the tail of the BTC. Longer durations of tracer injection were found to delay the peak concentration of the BTC.

The differences between the BTCs of DFTTs completed in filter packed wells and non-filter pack wells emphasize the importance of well construction on the interpretation of DFTT BTCs. The differences in the BTCs completed at the same location demonstrate the importance of tracer recirculation in the DFTTs completed in filter packed wells. Successive peaks on the recirculatory BTC were not visible on the non-recirculation BTC indicating the initial concentration peak was recirculated through the filter pack. The DFTTs completed in the filter packed wells may or may not include tracer movement through the aquifer in addition to tracer movement through the filter pack. However, as initially noted by Sutton et al. (2000), DFTTs in filter packed wells can yield estimates of K_s and r_s which will allow other aquifer characterization methods to provide more accurate estimates of aquifer formation parameters.

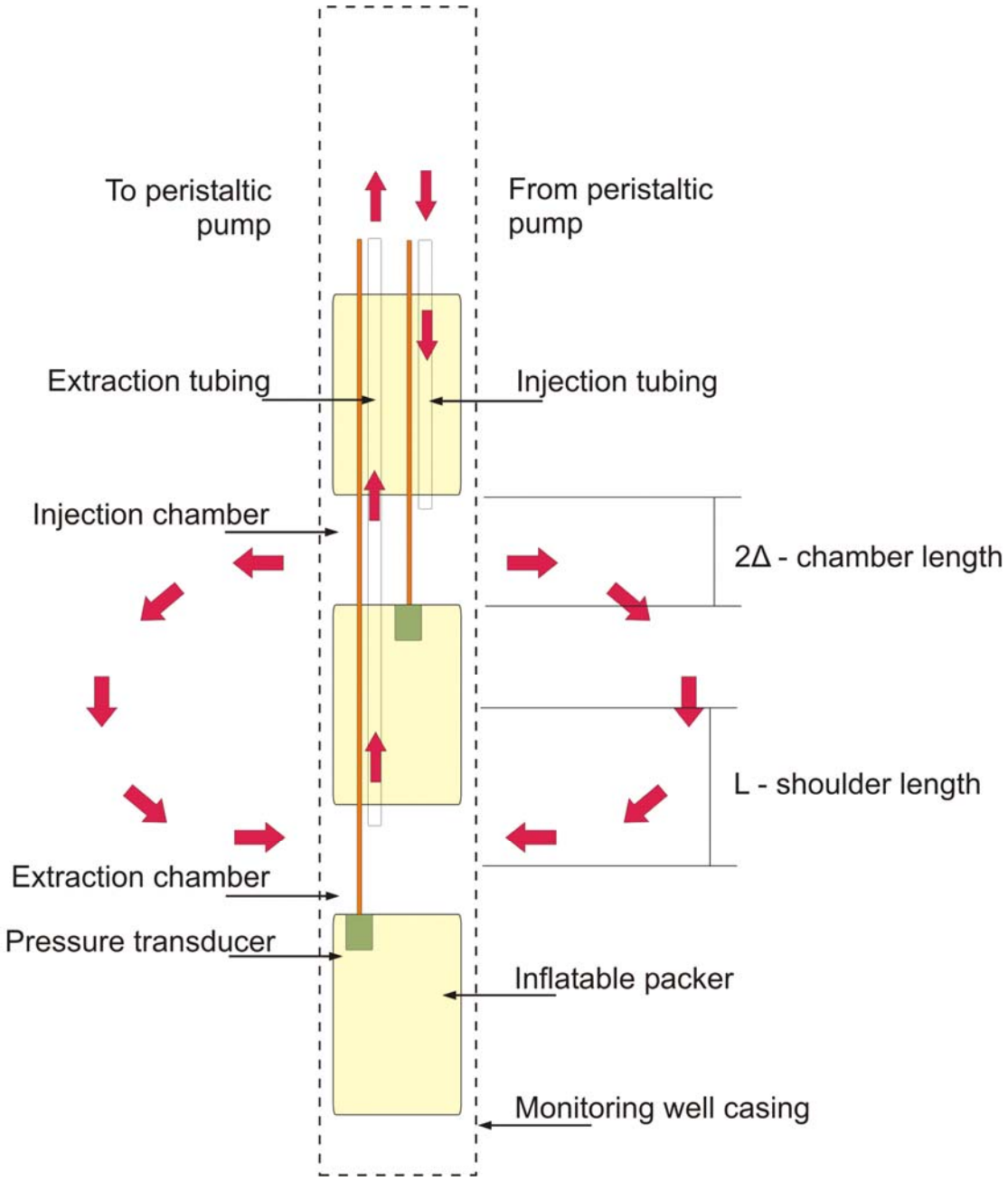

Figure 3.1. Schematic of the Waterloo prototype dipole probe (arrows indicate tracer flow direction). Scale is exaggerated 3x in the horizontal direction.

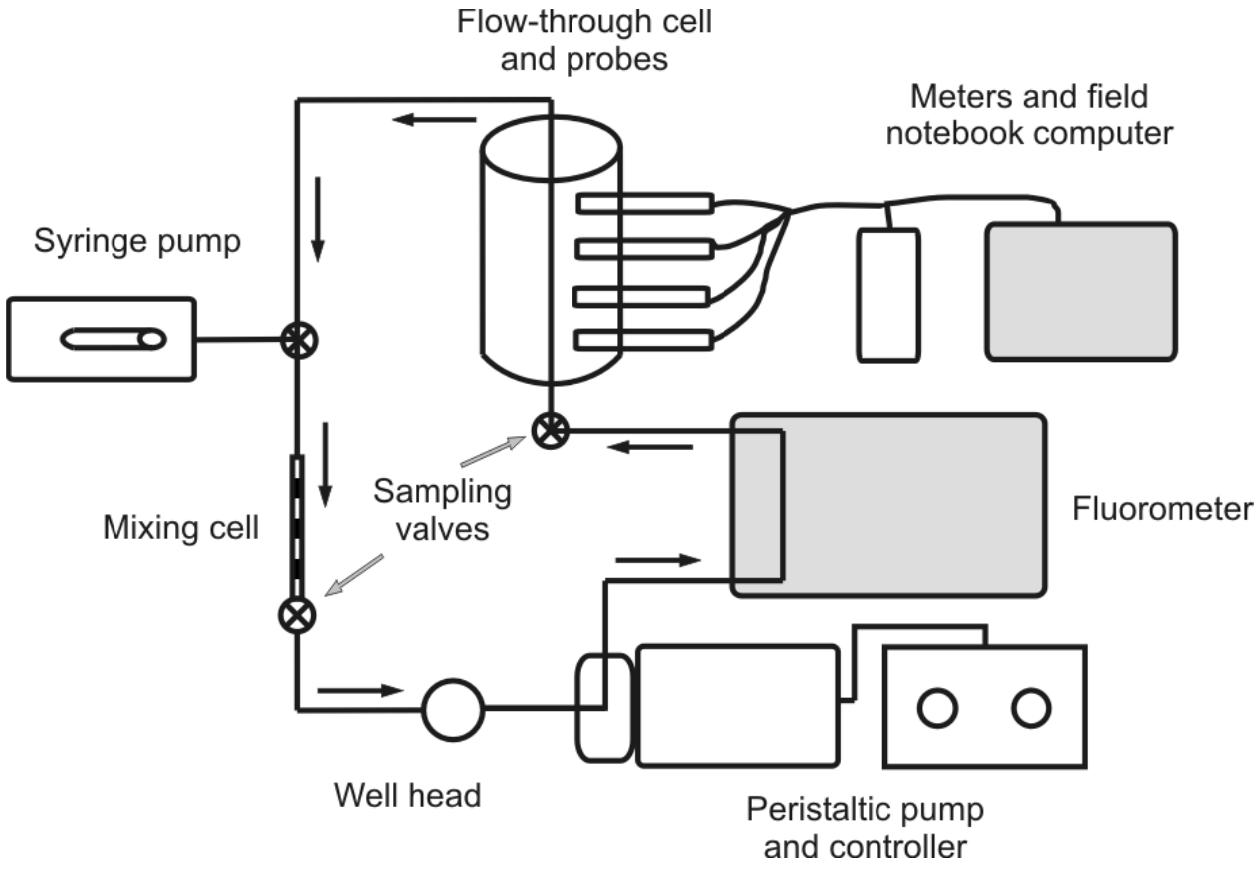

Figure 3.2. Schematic of aboveground equipment for controlling and monitoring DFTTs.

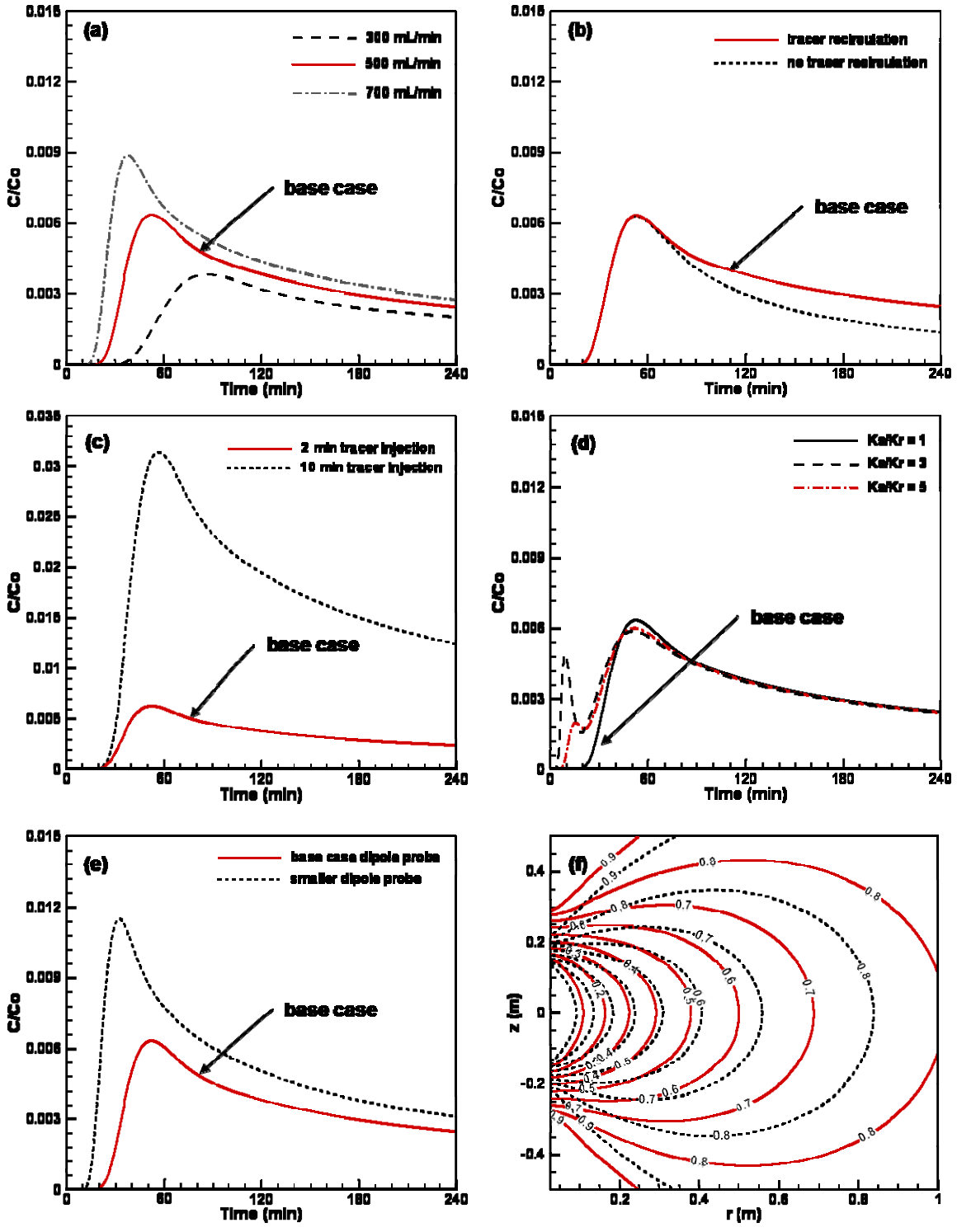

Figure 3.3. Comparison of simulated tracer BTCs for DFTTs completed with the base case parameters outline in Table 3.1 and : (a) flow rates 300, 500, and 700 mL/min, (b) with and without tracer recirculation, (c) 2 and 10 min tracer injection periods, (d) varying K_s/K_r ratio from 1 to 5, and (e) dipole probe of base case dimensions and a smaller dipole probe. The simulated streamfunctions for the base case dipole probe and smaller dipole probe are shown on (e).

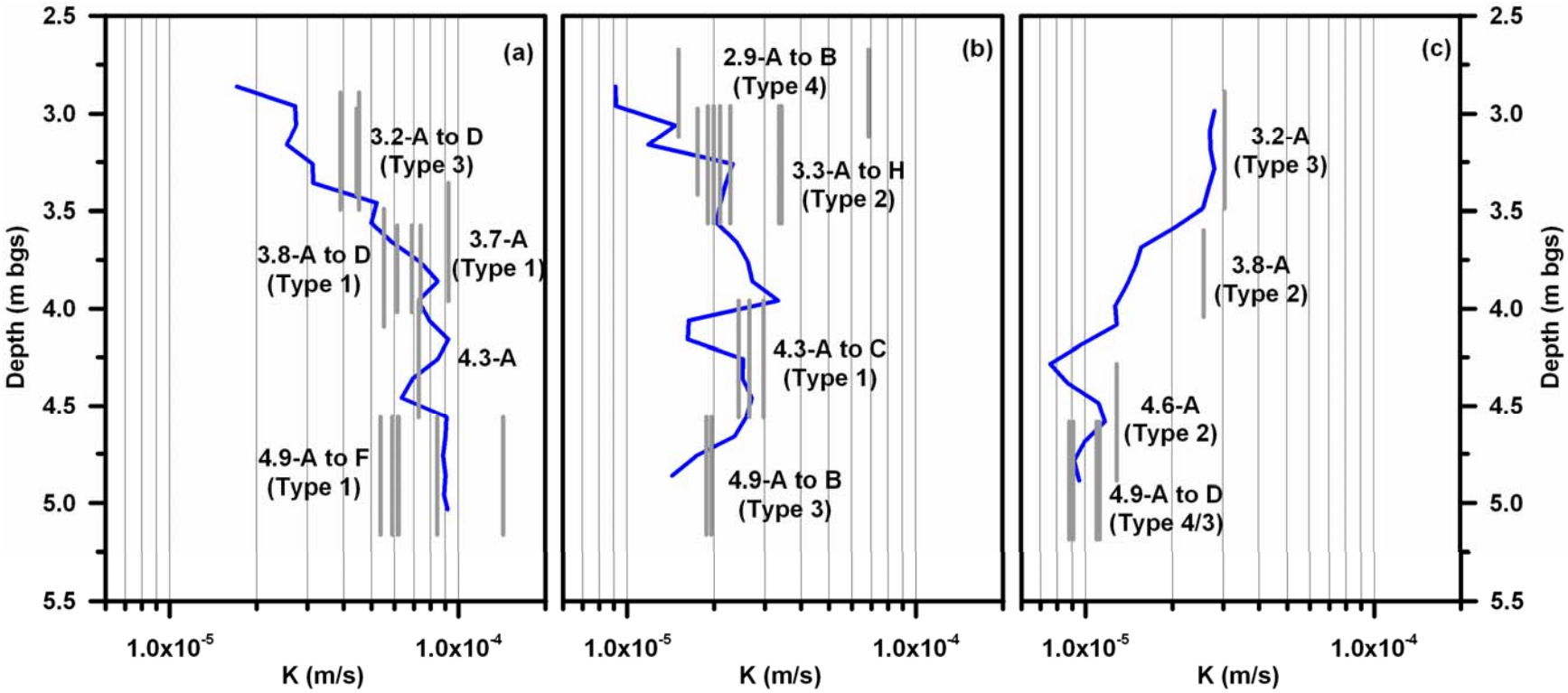

Figure 3.4. K_r^C **profiles for MW-3 (a), MW-6 (b), and MW-8 (c) showing the showing the location of the DFTTs.**

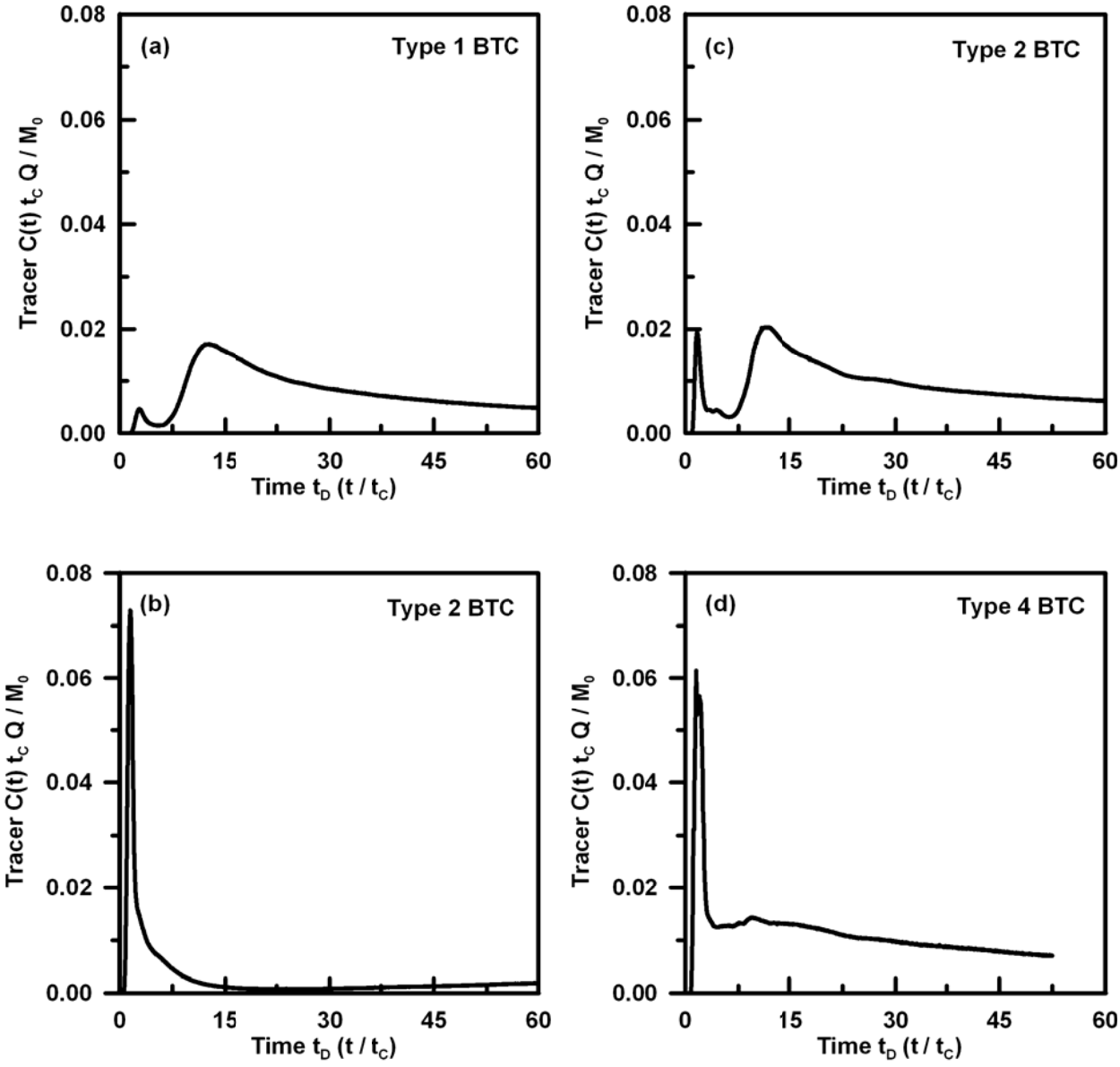

Figure 3.5. Four type or response BTCs observed in field tests of the DFTT (a) Type 1 BTC; (b) Type 2 BTC; (c) Type 3 BTC; and (d) Type 4 BTC.

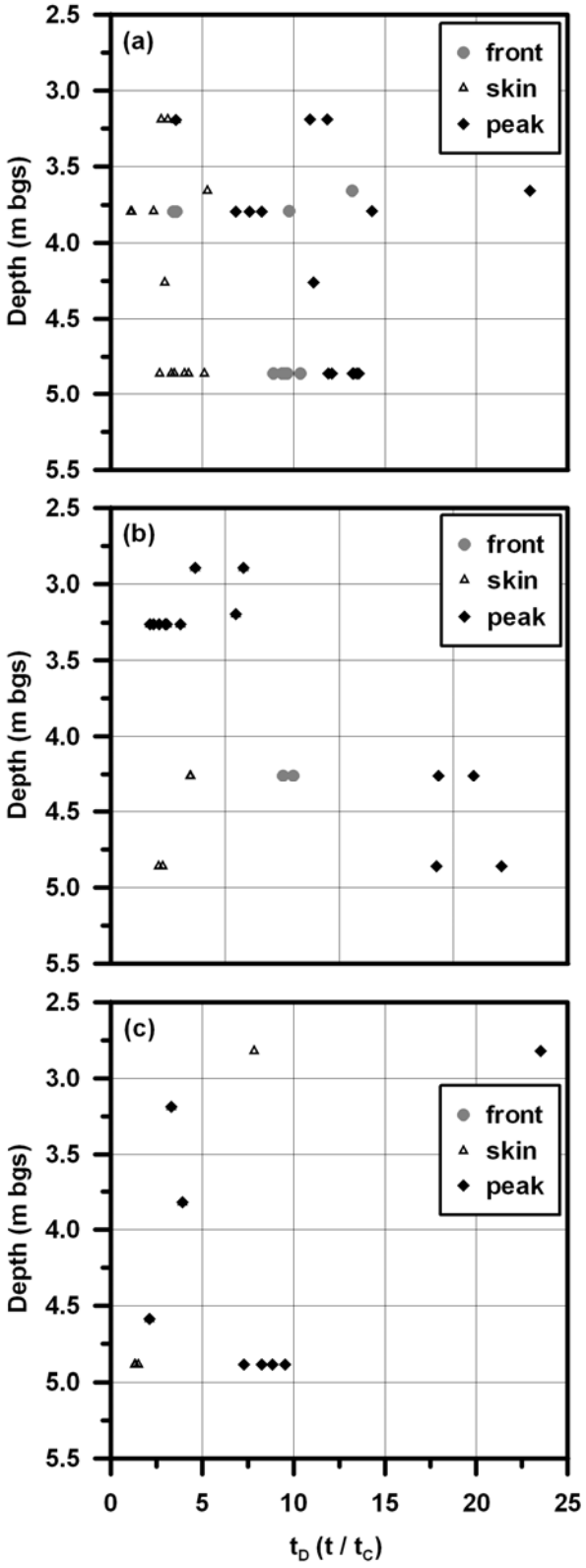

Figure 3.6. Dimensionless times (t_D) to tracer skin, front and peak plotted against depth for monitoring wells MW-3 (a), MW-6 (b), and MW-8 (c).

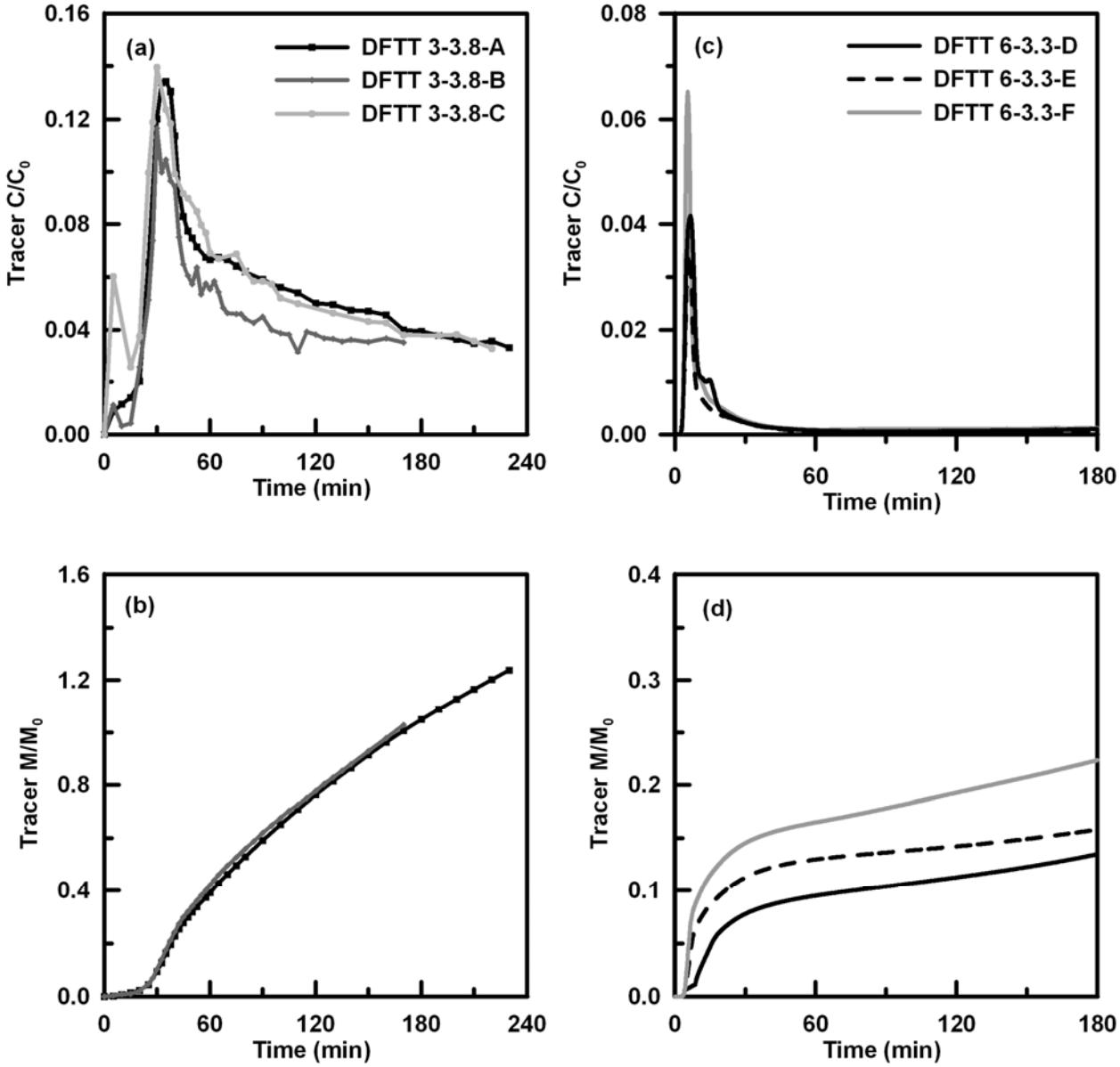

Figure 3.7. BTCs (a) and CMCs (b) for DFTTs completed at similar flow rates (~540 mL/min) at a depth of 3.8 m bgs in MW-3 (DFTTs 3-3.8-A, 3-3.8-B, and 3-3.8-C). BTCs (c) and CMCs (d) for DFTTs completed at similar flow rates (~590 mL/min) at a depth of 3.3 m bgs in MW-6 (DFTTs 6-3.3-D, 6-3.3-E and 6-3.3-F).

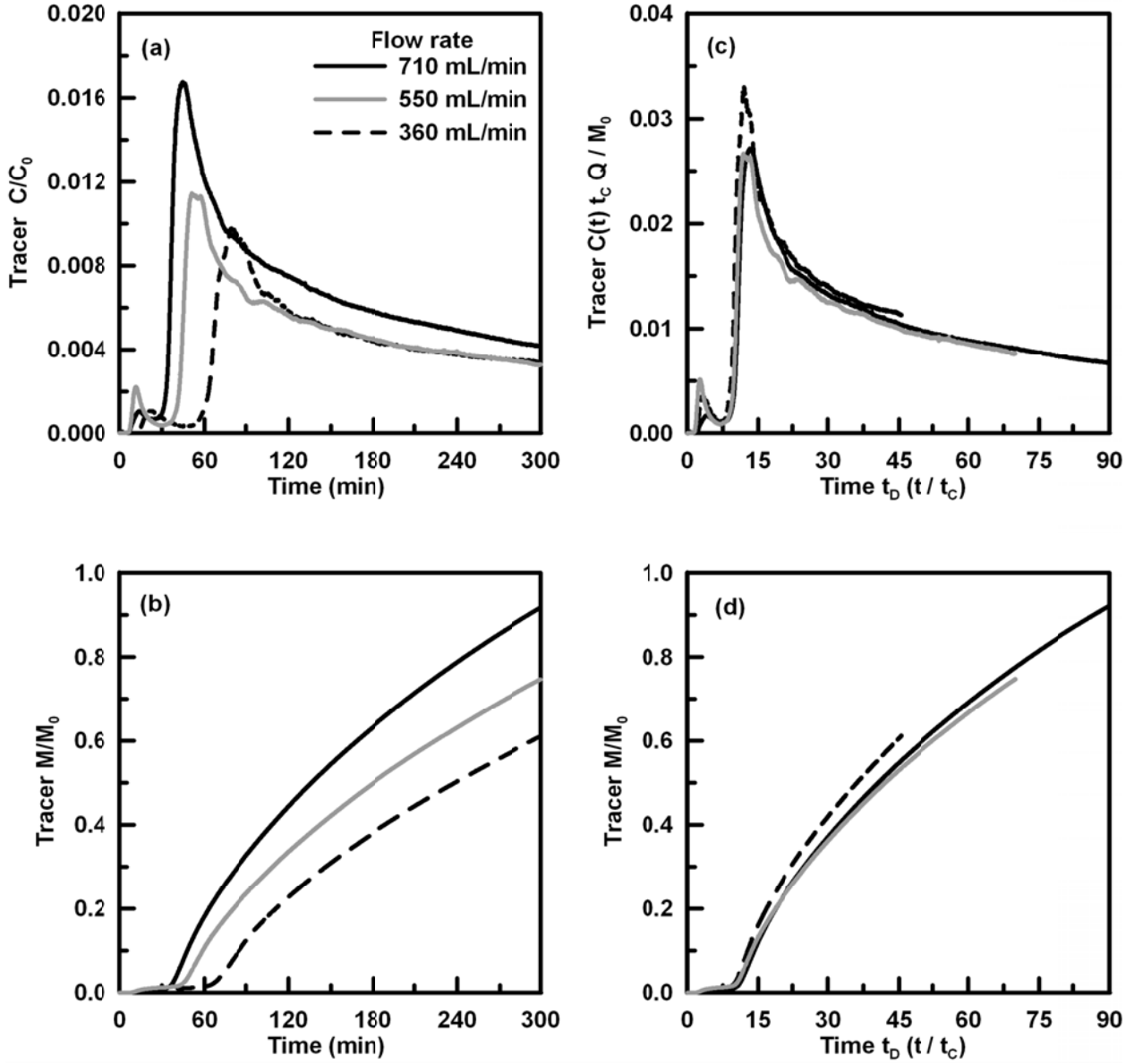

Figure 3.8. BTCs (a) and CMCs (b) for DFTTs completed at flow rates 710, 550, and 360 mL/min (DFTTs 3-4.9-B, 3-4.9-D, and 3-4.9-C, respectively). Scaled BTCs (c) and CMCs (d) for DFTTs 3-4.9-B, 3-4.9-D, and 3-4.9-C.

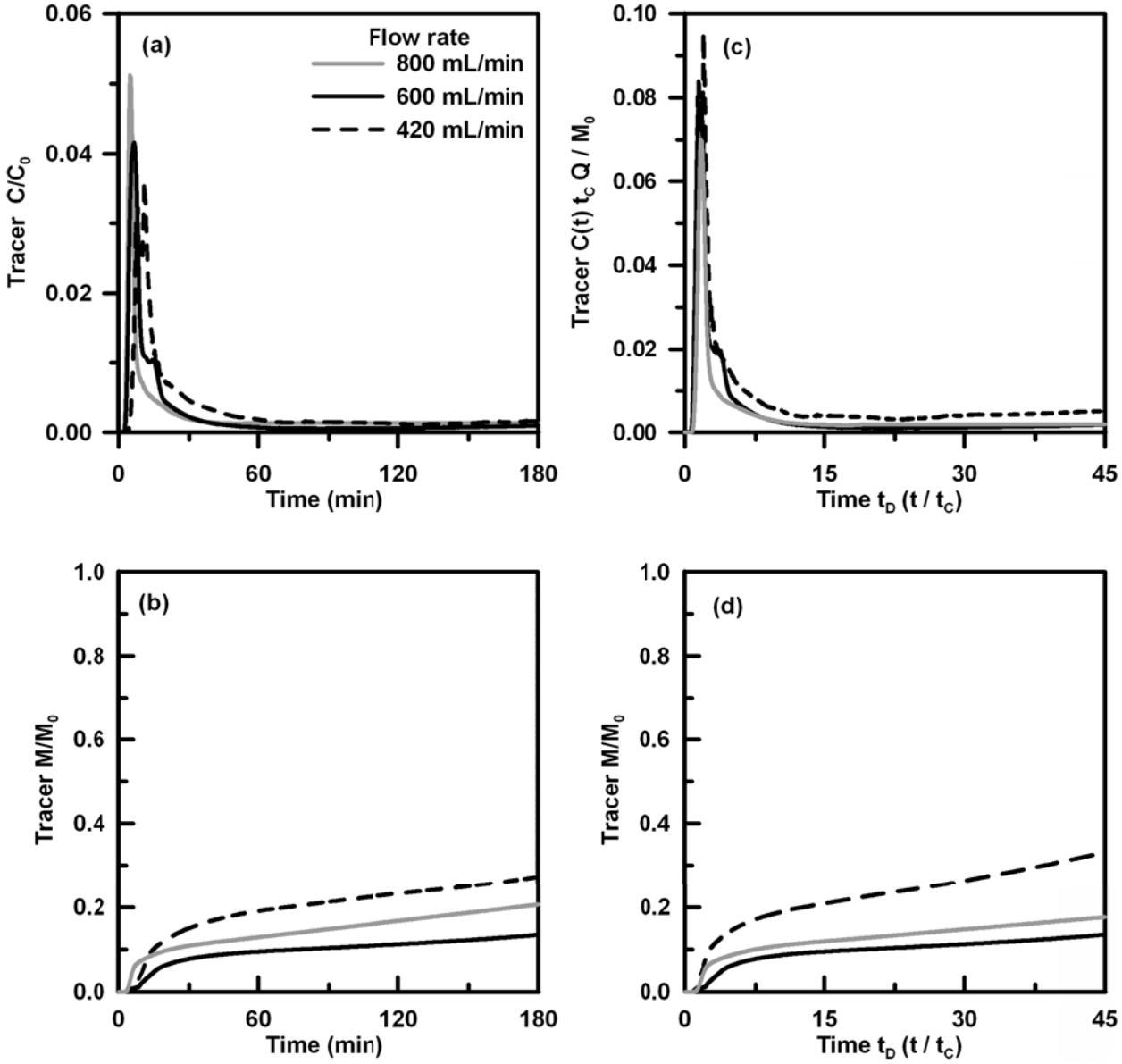

Figure 3.9. BTCs (a) and CMCs (b) for DFTTs completed at flow rates 800, 600, and 420 mL/min (DFTTs 6-3.3-H, 6-3.3-D, and 6-3.3-G, respectively). Scaled BTCs (c) and CMCs (d) for DFTTs 6-3.3-H, 6-3.3-D, and 6-3.3-G.

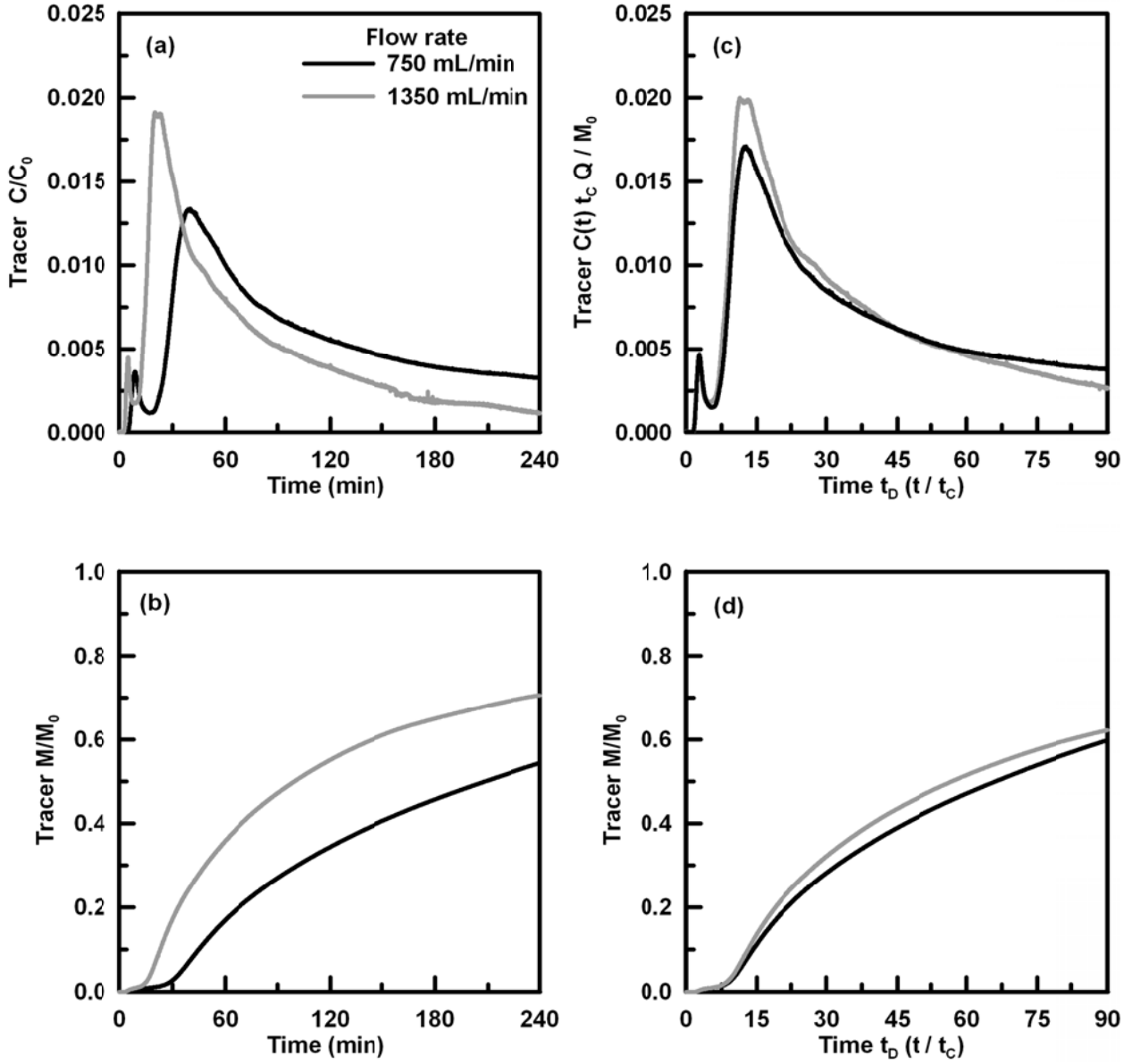

Figure 3.10. BTCs (a) and CMCs (b) for DFTTs completed at flow rates 1350 and 750 mL/min (DFTTs 6-4.3-C and 6-4.3-A, respectively). Scaled BTCs (c) and CMCs (d) for DFTTs 6-4.3-C and 6-4.3-A.

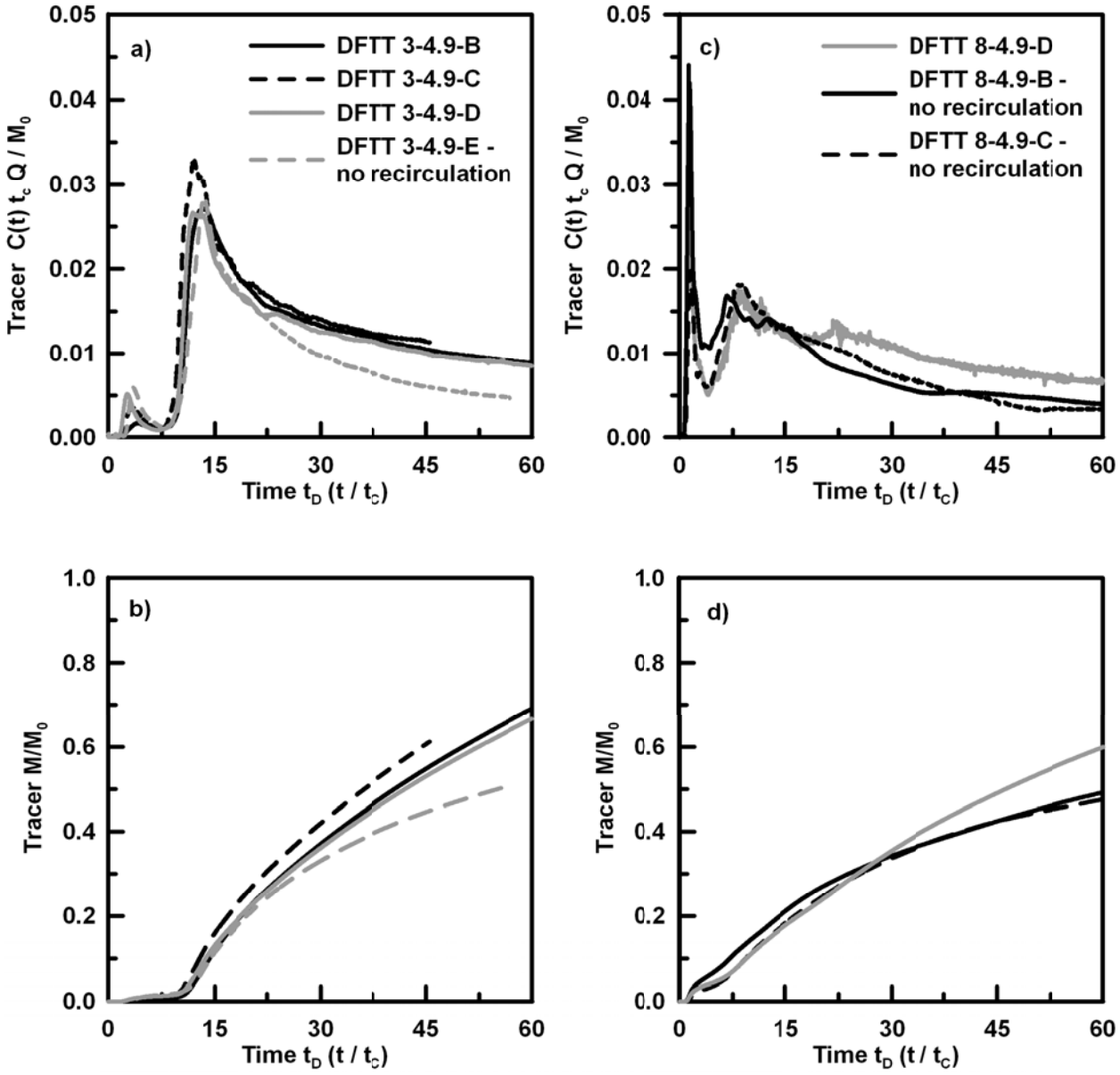

Figure 3.11. BTCs (a) and CMCs (b) for DFTTs completed with (DFTTs 3-4.9-B, 3-4.9-C, and 3-4.9-D) and without (DFTT 3-4.9-E) tracer recirculation at 4.9 m bgs in MW-3. BTCs (c) and CMCs (d) for DFTTs completed with (DFTT 8-4.9-D) and without (DFTTs 8-4.9-B and 8-4.9-C) tracer recirculation at 4.9 m bgs in MW-8.

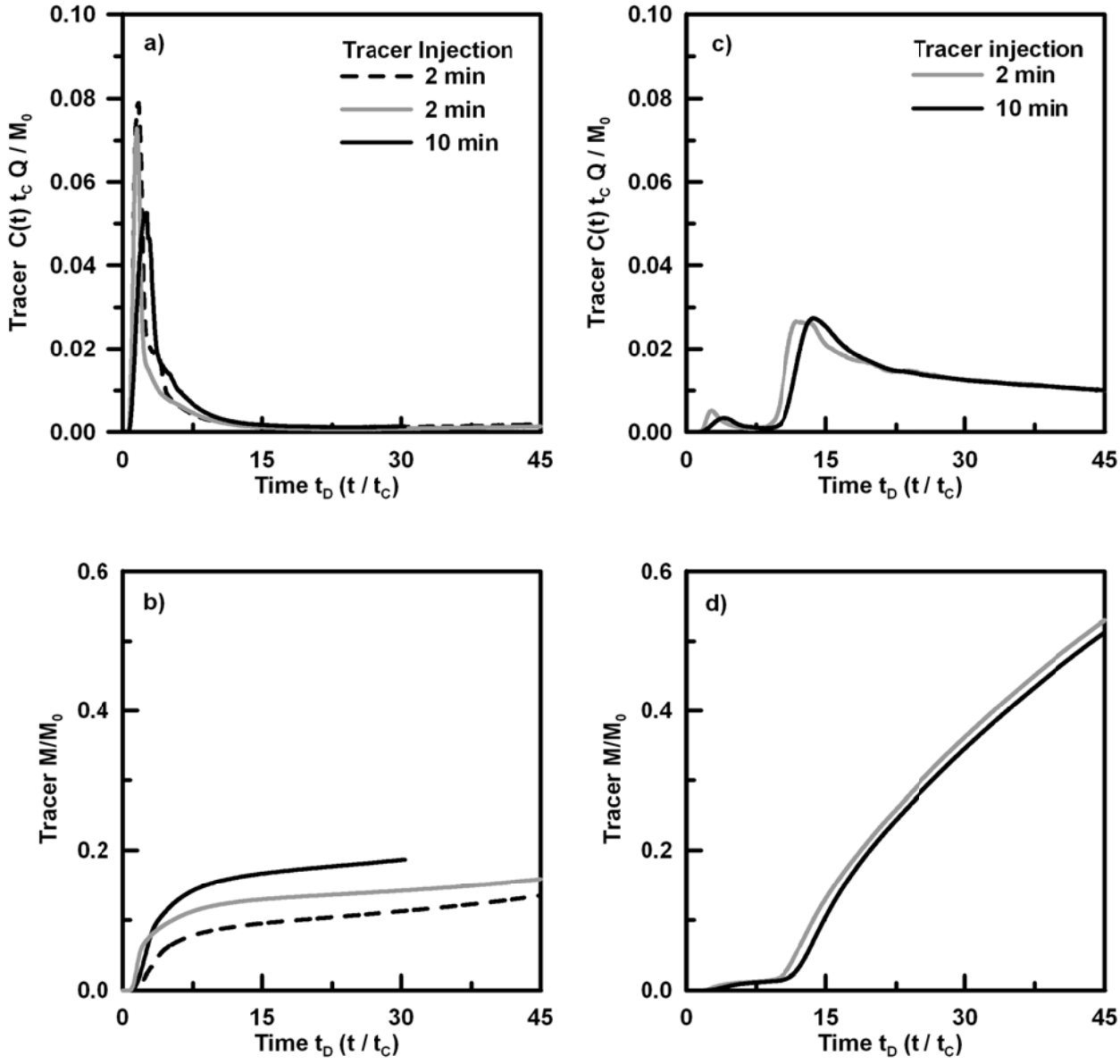

Figure 3.12. Scaled tracer BTCs (a) and CMCs (b) for DFTTs completed with a 2 min ($0.5t_D$) tracer injection (DFTTs 6-3.3-D and 6-3.3-E) and completed with a 10 min ($1.8t_D$) tracer injection (DFTT 6-3.3-C) at 3.3 m bgs in MW-6.

Scaled tracer BTCs (c) and CMCs (d) for DFTTs completed with a 2 min ($0.5t_D$) tracer injection (DFTT 3-4.9-D) and completed with a 10 min ($2.3t_D$) tracer injection period (DFTT 3-4.9-F) at 4.9 m bgs in MW-3.

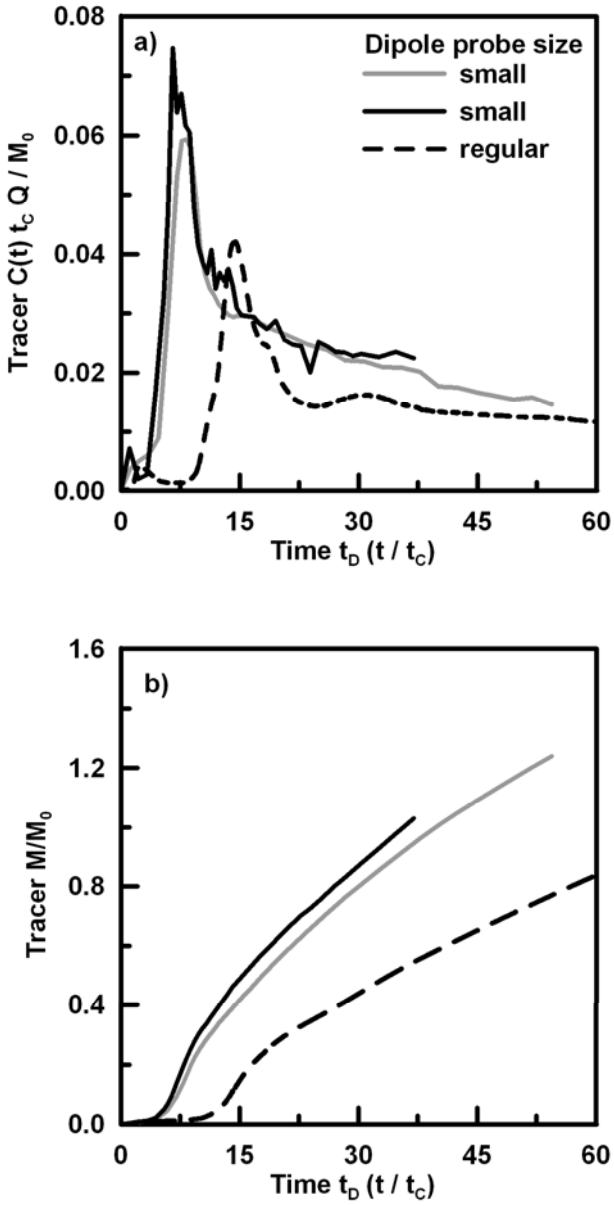

Figure 3.13. Scaled tracer BTCs (a) and CMCs (b) for DFTTs completed with the smaller dipole probe (solid lines DFTT 3-3.8-A and 3-3.8-B) and larger dipole probe (dashed line DFTT 3-3.8-D). DFTTs were completed at similar flow rates (~540 mL/min) with the probe centers located at 3.8 m bgs in MW-3.

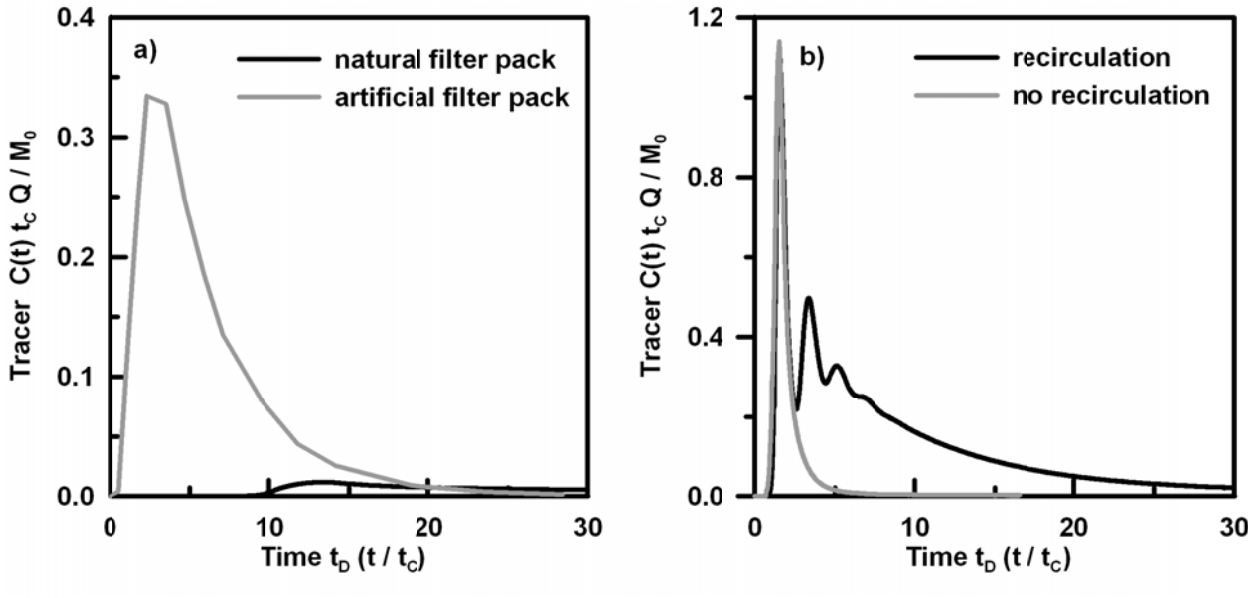

Figure 3.14. (a) Comparison of BTCs for DFTTs completed in filter packed MW-4 (DFTT 4-3.2-A) and non-filter packed MW-3 (DFTT 3-4.9-A) flow rate 560 mL/min. (b) Comparison of BTCs for DFTTs completed with (DFTT 4-4.9-A) and without (4-4.9-B) tracer recirculation in filter packed MW-4.

Table 3.1 Base case values for parameters for numerical simulations of DFTTs.

Parameter	Description	Value	Unit	Reference
L	dipole shoulder	0.222	m	Waterloo dipole probe prototype
Δ	half dipole chamber	0.0785	m	Waterloo dipole probe prototype
r_w	well radius	0.0254	m	-
Q	flow rate	500	mL/min	-
t_{inj}	tracer injection time	2	min	-
K_r	radial hydraulic conductivity	2.5×10^{-5}	m/s	Geometric mean estimated by CFB Borden DFTs
K_z	vertical hydraulic conductivity	2.5×10^{-5}	m/s	Assuming aquifer is isotropic
θ	porosity	0.40	-	(Brewster et al., 1995; Sneddon et al., 2002)
αL	longitudinal dispersivity	0.01	m	(Sudicky et al., 1983)

Table 3.2 DFTT setup and selected results for the DFTTs discussed in this paper.

Test ID	L/Δ[1]	Q (mL/min)	R[2]	s_E (cm)	s_I (cm)	K_C (m/s)	Q_{inj} (mL/min)	RWT (mg/L)	SRB (mg/L)	Br^- (mg/L)	V_{inj} (mL)	t_{inj} (min)	BTC Type
3-3.8-A	S	560	Y	26.7	10.3	7.4E-05	27	50	-	6,500	250	9.3	1
3-3.8-B	S	515	Y	29.7	14.9	6.1E-05	27	-	-	10,000	250	9.3	1
3-3.8-C	S	540	Y	19.1	20.5	6.9E-05	30	50	-	-	300	10.0	1
3-3.8-D	W	543	Y	16.1	28.2	5.5E-05	25	-	50	15,000	50	2.0	1
3-4.9-B	W	706	Y	22.6	31.4	5.9E-05	25	50	-	10,000	50	2.0	1
3-4.9-C	W	359	Y	10.2	16.1	6.2E-05	25	-	50	20,000	50	2.0	1
3-4.9-D	W	553	Y	20.2	20.0	6.2E-05	25	-	50	15,000	50	2.0	1
3-4.9-E	W	551	N	22.4	23.8	5.4E-05	25	-	50	15,000	50	2.0	1
3-4.9-F	W	553	Y	7.8	9.7	1.4E-04	5	-	50	15,000	50	10.0	1
4-3.2-A	S	560	Y	1.8	2.2	6.9E-04	27	50	-	6,500	250	9.3	2
4-4.9-A	W	650	Y	4.4	6.2	2.8E-04	10	-	50	15,000	10	1.0	2
4-4.9-B	W	650	N	8.9	0.9	3.0E-04	10	-	50	15,000	10	1.0	2
6-3.3-C	W	398	Y	32.6	52.6	2.1E-05	5	-	50	20,000	50	10.0	2
6-3.3-D	W	591	Y	51.4	81.6	2.0E-05	25	-	50	20,000	50	2.0	2
6-3.3-E	W	589	Y	48.4	91.1	1.9E-05	25	-	50	15,000	50	2.0	2
6-3.3-F	W	592	Y	26.6	51.1	3.4E-05	25	-	50	15,000	50	2.0	2
6-3.3-G	W	422	Y	40.8	49.6	2.1E-05	25	-	50	15,000	50	2.0	2
6-3.3-H	W	800	Y	22.4	84.8	3.4E-05	25	-	50	15,000	50	2.0	2
6-4.3-A	W	754	Y	42.0	85.9	2.7E-05	25	75	-	20,000	50	2.0	1
6-4.3-C	W	1354	Y	106.3	99.2	3.0E-05	25	-	50	15,000	50	2.0	1
8-4.9-B	W	589	N	166.7	133.4	8.8E-06	25	-	50	15,000	50	2.0	3
8-4.9-C	W	590	N	155.1	136.7	9.1E-06	25	-	50	15,000	50	2.0	3
8-4.9-D	W	592	Y	117.9	119.4	1.1E-05	25	-	50	15,000	50	2.0	3

[1] S – smaller modified dipole probe; W – Waterloo dipole probe prototype

[2] Y – tracer recirculation; N – no tracer recirculation

Chapter 4 Conclusions and Recommendations

4.1 Dipole flow test (DFT) conclusions

A series of DFTs, a single-well test which estimates the vertical distributions of the K_r, were completed to quantify small-scale variations in K_r in a relatively homogeneous aquifer. The DFTs conducted at 0.10 m increments along the length of the screen of non-filter packed monitoring wells provided similar estimates of K to slug tests and literature values. In general, good agreement was found between the injection K_r^I and extraction K_r^E profiles which provide a more representative estimate of K than the use of the K_r^C profile. This result was also supported by the dipole simulations which indicated the pressure drawdown and drawup measurements are functions not only of the K field across the chamber but also of the K field in the vicinity of the chamber. Therefore, the K estimates should not be taken as point measurements but rather as measurements at scale $2L$ (0.4 m).

The mean K_r^C estimated in the filter packed wells was approximately an order of magnitude less than the mean K_r^C estimate for the non-filter packed wells. Higher variability in K_r estimates was also observed in the non-filter packed than the filter packed monitoring wells. As the DFT induces a predominantly vertical flow field, short-circuiting through the skin zone (hydraulic conductivity K_s) is more pronounced in the DFT performed in the filter packed wells. The slug test may be less sensitive to the skin effect than the DFT due to its primarily horizontal flow pattern. These results indicate short-circuiting through the skin zone (hydraulic conductivity K_s) is more pronounced in the DFTs completed with the prototype dipole probe in the filter packed monitoring wells than the non-filter packed wells.

The K_r profiles were measured in order to determine intervals for completing the DFRTTs, small-scale tracer tests completed within the same flow field as the DFT estimates. Due to the small scale of the DFRTTs, the BTCs are sensitive to variations in the K field. Based on the results of the DFT interval analysis, 0.20 m intervals appears to be the minimum interval for K_r profiles at CFB Borden for the DFRTT at the scale of the Waterloo dipole probe prototype. For DFRTTs completed at a different site with a more heterogeneous stratigraphy, a more detailed K_r profile may be required to fully characterize the K field around the monitoring well. Note that

changing the scale of the dipole probe (L or Δ) may change the measurement interval required in the K_r profile.

4.2 Dipole flow and tracer test (DFTT) conclusions

The dipole flow and reactive tracer test (DFRTT) has been proposed as *in situ* aquifer parameter estimation method. The DFRTT involves the injection of a suite of reactive and conservative tracers into one chamber of the dipole apparatus and the subsequent monitoring of the tracer concentrations in the other chamber to produce the BTCs. To estimate the aquifer parameters, the BTCs are analyzed with the DFRTT model. The aquifer parameters estimated will depend on the nature of the reactive tracers injected. .

The dipole apparatus was constructed at the University of Waterloo and field tested to estimate hydraulic profiles and complete 46 DFTTs at CFB Borden. The shape of the BTC for a conservative tracer is affected by test set up parameters, well construction and aquifer formation properties. The BTCs from the DFTTs completed in the non-filter pack monitoring wells can be categorized into four "type curves" based on the curve properties (time to peak, peak concentration, etc.). The differences between the type curves are largely defined by the ratio of K between the skin zone and the aquifer (K_s/K_r).

In order for aquifer parameters to be estimated from the BTC of a DFTT, one must have confidence the BTC is representative of the aquifer conditions. One measure of confidence is the repeatability of the BTC: for a given DFTT setup at a specific location, will the shape of the BTC be consistent between tests? The series of DFTTs completed to assess the repeatability of the BTCs demonstrate portions of the DFTT BTCs are repeatable and the Type 1 and Type 2 BTCs showed similar times to peak concentration between DFTTs. BTCs from DFTTs completed at the same locations but at different flow rates can be scaled (by the method suggested by Sutton et al. (2000)) to produce similar BTCs. Investigating the effect of tracer recirculation, it was found the peak of the field BTCs was largely defined by the aquifer properties and not affected by tracer recirculation; however tracer recirculation was important for controlling the shape of the tail of the BTC. Longer durations of tracer injection were found to increase and delay the peak concentration of the BTC, as expected from numerical simulations.

The differences between the BTCs of DFTTs completed in filter packed wells and non-filter pack wells emphasize the importance of well construction on the interpretation of DFTT BTCs. The differences in the BTCs completed at the same location demonstrate the importance of tracer recirculation in the DFTTs completed in filter packed wells. Successive peaks on the recirculatory BTC were not visible on the non-recirculation BTC indicating the initial concentration peak was recirculated through the filter pack. The DFTTs completed in the filter packed wells may or may not include tracer movement through the aquifer in addition to tracer movement through the filter pack. However, as initially noted by Sutton et al. (2000), DFTTs in filter packed wells can yield estimates of K_s and r_s which will allow other aquifer characterization methods to provide more accurate estimates of aquifer formation parameters.

The dipole flow and reactive tracer test (DFRTT) has been proposed as a method to obtain site specific *in situ* estimates of aquifer parameters to aid in the design of a remedial system for a contaminated site. The BTCs generated during this study were found to be repeatable and behaved as expected from numerical simulations. The DFRTT model will subsequently be used to provide estimates of aquifer parameters based on the field BTCs.

4.3 Recommendations

This research focused on the field implementation of the DFT and DFTT. The following recommendations are made for extending the results of this study:

- Increase the L dimension of the dipole probe prototype when completing DFTs, DFTTs, or DFRTTs in filter packed wells to decrease the effect of the skin zone on the BTC;

- Complete a parameter estimation and sensitivity analysis for the generated BTCs to confirm if the DFTT BTCs are sufficiently repeatable to provide accurate parameter estimates;

- Acquire a sorbing tracer that would meet with regulatory approval for the DFRTTs. For the biodegradation DFRTTs, complete tests of longer duration with two tracer injections to provide an acclimation period for the microbial community in the aquifer. Once DFRTTs can be reproduced at CFB Borden, complete DFRTTs at well-documented contaminated sites; and

- Investigate the effect of much longer tracer injection periods (at least one hour) on tracer movement through the dipole flow field. This would be in support of using the dipole probe to deliver chemical oxidants at a contaminated site.

References

Anderson, R.T., Vrionis, H.A., Ortiz-Bernad, I., Resch, C.T., Long, P.E., Dayvault, R., Karp, K., Marutzky, S., Metzler, D.R., and Peacock, A. 2003. Stimulating the in situ activity of Geobacter species to remove uranium from the groundwater of a uranium-contaminated aquifer. Applied and Environmental Microbiology, 69(10): 5884-5891.

ATSDR 2000. Toxicological profile for toluene, U.S. Department of Health and Human Services, Public Health Service, Agency for Toxic Substances and Disease Registry.

Boman, G.K., Molz, F.J., and Boonec, K.D. 1997. Borehole flowmeter application in fluvial sediments: Methodology, results, and assessment. Ground Water, 35(3): 443-450.

Bouwer, H. 1989. Bouwer and Rice slug test - An update. Ground Water, 27(3).

Bouwer, H., and Rice, R.C. 1976. A slug test for determining hydraulic conductivity of unconfined aquifers with completely or partially penetrating wells. Water Resources Research, 12(3): 423-428.

Brewster, M.L., Annan, A.P., Greenhouse, J.P., Kueper, B.H., Olhoeft, G.R., Redman, J.D., and Sander, K.A. 1995. Observed migration of a controlled DNAPL release by geophysical methods. Ground Water, 33(6): 977-987.

Butler, J.J., Jr. 2005. Hydrogeological methods for estimation of spatial variations in hydraulic conductivity. *In* Hydrogeophysics. Springer, Dordrecht, The Netherlands. p. 23–58.

Butler, J.J., Jr., McElwee, C.D., and Liu, W. 1996. Improving the quality of parameter estimates obtained from slug tests. Ground Water, 34(3): 480-490.

Butler, J.J., Jr., Bohling, G.C., Hyder, Z., and McElwee, C.D. 1994. The use of slug tests to describe vertical variations in hydraulic conductivity. Journal of Hydrology, 156(1-4): 137-162.

Butler, J.J., Jr., Dietrich, P., Wittig, V., and Christy, T. 2007. Characterizing hydraulic conductivity with the direct-push permeameter. Ground Water, 45(4): 409-419.

Cain, R.B., Johnson, G.R., McCray, J.E., Blanford, W.J., and Brusseau, M.L. 2000. Partitioning tracer tests for evaluating remediation performance. Ground Water, 38(5): 752-761.

Cole, K., and Zlotnik, V.A. 1994. Modification of Dagan's numerical method for slug and packer test interpretation. *In* Computational Methods in Water Resources X. *Edited by* A. Peters et al. Kluwer Academic, pp. 719-726.

Cooper, H.H., Jr., Bredehoeft, J.D., and Papadopulos, I.S. 1967. Response of a finite-diameter well to an instantaneous charge of water. Water Resources Research, 3(1): 263-269.

Davis, S.N., Thompson, G.M., Bentley, H.W., and Stiles, G. 1980. Ground-water tracers: A short review. Ground Water, 18(1): 14-23.

Dietrich, P., Butler, J.J., and Faiss, K. 2008. A rapid method for hydraulic profiling in unconsolidated formations. Ground Water, 46(2): 323-328.

Driscoll, F.G. 1986. Groundwater and wells. Johnson Filtration Systems Inc., St. Paul, Minnesota.

Haggerty, R., Schroth, M.H., and Istok, J.D. 1998. Simplified method of "push-pull" test data analysis for determining in situ reaction rate coefficients. Ground Water, 36(2): 314-324.

Hazen, A. 1911. Discussion of 'Dams on sand foundations' by A.C. Koenig. Transactions, American Society of Civil Engineers, 73: 199-203.

Hvilshoj, S., Jensen, K.H., and Madsen, B. 2000. Single-well dipole flow tests: Parameter estimation and field testing. Ground Water, 38(1): 53-62.

Hvorslev, M.J. 1951. Time lag and soil permeability in groundwater observations, Waterways Experiment Station, Corps of Engineers, U.S. Army, Vicksburg, Mississippi.

Hyder, Z., Butler, J.J., Jr., McElwee, C.D., and Liu, W. 1994. Slug tests in partially penetrating wells. Water Resources Research, 30(11): 2945–2958.

Indelman, P., and Zlotnik, V.A. 1997. Average steady nonuniform flow in stratified formations. Water Resources Research, 33(5): 927-934.

Istok, J.D., Humphrey, M.D., Schroth, M.H., Hyman, M.R., and O'Reilly, K.T. 1997. Single-well, "push-pull" test for in situ determination of microbial activities. Ground Water, 35(4): 619-631.

Jin, M., Delshad, M., Dwarakanath, V., McKinney, D.C., Pope, G.A., Sepehrnoori, K., Tilburg, C.E., and Jackson, R.E. 1995. Partitioning tracer test for detection, estimation, and remediation performance assessment of subsurface nonaqueous phase liquids. Water Resources Research, 31(5): 1201-1211.

Kabala, Z.J. 1993. The dipole flow test: a new single-borehole test for aquifer characterization. Water Resources Research, 29(1): 99-107.

Kasnavia, T., Vu, D., and Sabatini, D.A. 1999. Fluorescent dye and media properties affecting sorption and tracer selection. Ground Water, 37(3): 376-381.

Kleikemper, J., Schroth, M.H., Sigler, W.V., Schmucki, M., Bernasconi, S.M., and Zeyer, J. 2002. Activity and diversity of sulfate-reducing bacteria in a petroleum hydrocarbon-contaminated aquifer. Applied and Environmental Microbiology, 68(4): 1516.

Ko, S.-O., and Ji, S.-H. 2007. In situ push-pull tests for the determination of TCE degradation and permanganate consumption rates. Environmental Geology, 53(2): 359.

Kueper, B.H., Redman, D., Starr, R.C., Reitsma, S., and Mah, M. 1993. A field experiment to study the behavior of tetrachloroethylene below the water table: Spatial distribution of residual and pooled DNAPL. Ground Water, 31(5): 756-766.

LeBlanc, D.R., Garabedian, S.P., Hess, K.M., Gelhar, L.W., and Quadri, R.D. 1991. Large-scale natural gradient tracer test in sand and gravel, Cape Cod, Massachusetts 1. Experimental design and observed tracer movement. Water Resources Research, 27(5): 895-910.

Luo, J., Dentz, M., Cirpka, O.A., and Kitanidis, P.K. 2007. Breakthrough curve tailing in a dipole flow field. Water Resources Research, 43: W09403.

MacFarlane, D.S., Cherry, J.A., Gillham, R.W., and Sudicky, E.A. 1983. Migration of contaminants in groundwater at a landfill: A case study: 1. Groundwater flow and plume delineation. Journal of Hydrology, 63(1-2): 1-29.

Mackay, D.M., Freyburg, D.L., Roberts, P.V., and Cherry, J.A. 1986. Natural gradient experiment on solute transport in a sand aquifer: 1. Approach and overview of plume movement. Water Resources Research, 22(13): 2017-2029.

Mackay, D.M., deSieyes, N.R., Einarson, M.D., Feris, K.P., Pappas, A.A., Wood, I.A., Jacobson, L., Justice, L.G., Noske, M.N., Scow, K.M., and Wilson, J.T. 2006. Impact of ethanol on the natural attenuation of benzene, toluene, and o-xylene in a normally sulfate-reducing aquifer. Environmental Science and Technology, 40(19): 6123-6130.

MacQuarrie, K.T.B., Sudicky, E.A., and Frind, E.O. 1990. Simulation of biodegradable organic Contaminants in groundwater 1. Numerical formulation in principal directions. Water Resources Research, 26(2): 207-222.

Meinardus, H.W., Dwarakanath, V., Ewing, J., Hirasaki, G.J., Jackson, R.E., Jin, M., Ginn, J.S., Londergan, J.T., Miller, C.A., and Pope, G.A. 2002. Performance assessment of NAPL remediation in heterogeneous alluvium. Journal of Contaminant Hydrology, 54(3-4): 173-193.

Molz, F.J., Boman, G.K., Young, S.C., and Waldrop, W.R. 1994. Borehole flowmeters: field application and data analysis. Journal of Hydrology, 163(3-4): 347.

Mumford, K.G., Lamarche, C.S., and Thomson, N.R. 2004. Natural oxidant demand of aquifer materials using the push-pull technique. Journal of Environmental Engineering, 130(10): 1139–1146.

Nordstrom, D.K., and Wilde, F.D. 2005. Reduction-oxidation potential (electrode method) (version 1.2): U.S. Geological Survey Techniques of Water-Resources Investigations, book 9, chap. A6., section 6.5.

Nwankwor, G.I., Cherry, J.A., and Gillham, R.W. 1984. A comparative study of specific yield determinations for a shallow sand aquifer. Ground Water, 22(6): 764-772.

Pang, L., Close, M., and Noonan, M. 1998. Rhodamine WT and Bacillus subtilis transport through an alluvial gravel aquifer. Ground Water, 36(1): 112-122.

Peursem, D.V., Zlotnik, V., and Ledder, G. 1999. Groundwater flow near vertical recirculatory wells: effect of skin on flow geometry and travel times with implications for aquifer remediation. Journal of Hydrology, 222(1-4): 109.

Pombo, S.A., Pelz, O., Schroth, M.H., and Zeyer, J. 2002. Field-scale 13C-labeling of phospholipid fatty acids (PLFA) and dissolved inorganic carbon: tracing acetate assimilation and mineralization in a petroleum hydrocarbon-contaminated aquifer. FEMS Microbiology Ecology, 41(3): 259-267.

Reiha, B. 2006. A numerical interpretation model for the dipole flow and reactive tracer test, M.A.Sc. Thesis, Department of Civil and Environmental Engineering, University of Waterloo, Waterloo, Ontario.

Riva, M., Guadagnini, A., Fernandez-Garcia, D., Sanchez-Vila, X., and Ptak, T. 2008. Relative importance of geostatistical and transport models in describing heavily tailed breakthrough curves at the Lauswiesen site. Journal of Contaminant Hydrology, 101(1-4): 1.

Roos, G., Thomson, N.R., Wilson, R.D., and Thornton, S.F. 2008. The dipole flow and reactive tracer test for aquifer parameter estimation. *In* GeoEdmonton'08 - 61st Canadian Geotechnical Conference and the 9th Joint CGS/IAH-CNC Groundwater Conference. Edmonton, AB. September 21-24, 2008, pp. 1500-1506.

Ross, H.C., and McElwee, C.D. 2007. Multi-level slug tests to measure 3-D hydraulic conductivity distributions. Natural Resources Research, 16(1): 67-79.

Sabatini, D.A., and Austin, T.A. 1991. Characteristics of rhodamine WT and fluorescein as adsorbing ground-water tracers. Ground Water, 29(3): 341-349.

Sandrin, S.K., Brusseau, M.L., Piatt, J.J., Bodour, A.A., Blanford, W.J., and Nelson, N.T. 2004. Spatial variability of in situ microbial activity: Biotracer tests. Ground Water, 42(3): 374-383.

Schroth, M.H., Istok, J.D., Conner, G.T., Hyman, M.R., Haggerty, R., and O'Reilly, K.T. 1998. Spatial variability in in situ aerobic respiration and denitrification rates in a petroleum-contaminated aquifer. Ground Water, 36(6): 924-937.

Shiau, B.-J., Sabatini, D.A., and Harwell, J.H. 1993. Influence of rhodamine WT properties on sorption and transport in subsurface media. Ground Water, 31(6): 913-920.

Smart, C.C., Zabo, L., Alexander, E.C., and Worthington, S.R.H. 1998. Some advances in fluorometric techniques for water tracing. Environmental Monitoring and Assessment, 53(2): 305-320.

Sneddon, K.W., Powers, M.H., Johnson, R.H., and Poeter, E.P. 2002. Modeling GPR data to interpret porosity and DNAPL saturations for calibration of a 3-D multiphase simulation, US Geological Survey Open File Report 02-451.

Sudicky, E.A. 1986. A natural gradient experiment on solute transport in a sand aquifer: spatial variability of hydraulic conductivity and its role in the dispersion process. Water Resources Research, 22(13): 2069-2082.

Sudicky, E.A., Cherry, J.A., and Frind, E.O. 1983. Migration of contaminants in groundwater at a landfill: A case study; 4. A natural-gradient dispersion test. Journal of Hydrology, 63(1-2): 81-108.

Sutton, D.J., Kabala, Z.J., Schaad, D.E., and Ruud, N.C. 2000. The dipole-flow test with a tracer: a new single-borehole tracer test for aquifer characterization. Journal of Contaminant Hydrology, 44: 71-101.

Sutton, D.J., Kabala, Z.J., Francisco, A., and Vasudevan, D. 2001. Limitations and potential of commercially available rhodamine WT as a groundwater tracer. Water Resources Research, 37(6): 1641-1656.

Taylor, K., Wheatcraft, S., Hess, J., Hayworth, J., and Molz, F. 1990. Evaluation of methods for determining the vertical distribution of hydraulic conductivity. Ground Water, 28(1): 88-98.

Thomson, N.R. 2009. The dipole flow and reactive tracer test interpretation model. In preparation.

Thomson, N.R., Reiha, B., McKnight, D., Smalley, A.L., and Banwart, S.A. 2005. An overview of the dipole flow in situ reactor. *In* Proceedings, 33rd Annual Conference of the Canadian Society for Civil Engineering. Toronto, Ontario. June 2-4, 2005.

Tomlinson, D.W., Thomson, N.R., Johnson, R.L., and Redman, J.D. 2003. Air distribution in the Borden aquifer during in situ air sparging. Journal of Contaminant Hydrology, 67(1-4): 113-132.

Weigand, H., and Totsche, K.U. 1998. Flow and reactivity effects on dissolved organic matter transport in soil columns. Soil Science Society of America Journal, 62(5): 1268-1274.

Woodbury, A.D., and Sudicky, E.A. 1991. The geostatistical characteristics of the Borden aquifer. Water Resources Research, 27(4): 533-546.

Xiang, J., and Kabala, Z.J. 1997. Performance of the steady-state dipole flow test in layered aquifers. Hydrological Processes, 11: 1595-1605.

Zemansky, G.M., and McElwee, C.D. 2005. High-resolution slug testing. Ground Water, 43(2): 222-230.

Zlotnik, V., and Ledder, G. 1994. Effect of boundary conditions on dipole flow. *In* Computational methods in Water Resources X. Kluwer Academic Publishers, Netherlands. pp. 907-914.

Zlotnik, V., and Ledder, G. 1996. Theory of dipole flow in uniform anisotropic aquifers. Water Resources Research, 32(4): 1119-1128.

Zlotnik, V.A., and Zurbuchen, B.R. 1998. Dipole probe: Design and field applications of a single-borehole device for measurements of vertical variations of hydraulic conductivity. Ground Water, 36(6): 884-893.

Zlotnik, V.A., and Zurbuchen, B.R. 2003. Field study of hydraulic conductivity in a heterogeneous aquifer: Comparison of single-borehole measurements using different instruments. Water Resources Research, 39(4): 1101.

Zlotnik, V.A., Zurbuchen, B.R., and Ptak, T. 2001. The steady-state dipole-flow test for characterization of hydraulic conductivity statistics in a highly permeable aquifer: Horkheimer Insel site, Germany. Ground Water, 39(4): 504-516.

Zlotnik, V.A., Eisenhauer, D.E., Schlautman, D.J., Zurbuchen, B.R., and Van Peursem, D. 2007. Entrapped air effects on dipole flow test in sand tank experiments: Hydraulic conductivity and head distribution. Journal of Hydrology, 339(3-4): 193.

Appendix A – Dipole Flow Test (DFT) Data

Table A.1. K_r^E summary statistics for DFTs completed at 0.10 m, 0.20 m, 0.30 m, 0.40, and 0.50 m intervals in MW-3 at CFB Borden.

DFT Interval	0.10 m	0.20 m	0.30 m	0.40 m	0.50 m
Geometric mean (m/s)	6.7E-05	6.8E-05	6.7E-05	6.4E-05	6.8E-05
Standard deviation (m/s)	3.1E-05	3.3E-05	2.9E-05	2.7E-05	4.1E-05
Coefficient of variation	0.46	0.48	0.44	0.43	0.61
Skew	0.14	0.39	0.09	-0.47	0.77
Kurtosis	0.25	0.91	-0.64	-1.26	0.31

Table A.2. K_r^E summary statistics for DFTs completed at 0.10 m, 0.20 m, 0.30 m, 0.40, and 0.50 m intervals in MW-5 at CFB Borden.

DFT Interval	0.10 m	0.20 m	0.30 m	0.40 m	0.50 m
Geometric mean (m/s)	2.5E-05	2.5E-05	2.6E-05	2.4E-05	2.2E-05
Standard deviation (m/s)	1.3E-05	1.3E-05	1.6E-05	1.2E-05	1.3E-05
Coefficient of variation	0.51	0.51	0.59	0.49	0.58
Skew	0.56	0.27	0.49	0.40	0.43
Kurtosis	-0.76	-1.53	-1.09	-1.57	-1.51

Table A.3. K_r^E summary statistics for DFTs completed at 0.10 m, 0.20 m, 0.30 m, 0.40, and 0.50 m intervals in MW-6 at CFB Borden.

DFT Interval	0.10 m	0.20 m	0.30 m	0.40 m	0.50 m
Geometric mean (m/s)	2.20E-05	2.23E-05	2.15E-05	2.07E-05	2.04E-05
Standard deviation (m/s)	8.67E-06	8.33E-06	8.00E-06	1.01E-05	1.03E-05
Coefficient of variation	0.40	0.37	0.37	0.49	0.50
Skew	-0.036	-0.258	-0.198	-0.039	-0.156
Kurtosis	-1.071	-1.187	-1.536	-1.712	-1.829

Table A.4. K_r^E summary statistics for DFTs completed at 0.10 m, 0.20 m, 0.30 m, 0.40, and 0.50 m intervals in MW-8 at CFB Borden.

DFT Interval	0.10 m	0.20 m	0.30 m	0.40 m	0.50 m
Geometric mean (m/s)	1.5E-05	1.5E-05	1.7E-05	1.5E-05	1.5E-05
Standard deviation (m/s)	1.3E-05	1.3E-05	1.4E-05	1.5E-05	1.6E-05
Coefficient of variation	0.85	0.86	0.81	0.96	1.10
Skew	1.61	1.38	1.35	1.61	1.34
Kurtosis	2.34	1.20	1.50	1.72	0.78

Table A.5. K_r^E summary statistics for DFTs completed at 0.10 m, 0.20 m, 0.30 m, 0.40, and 0.50 m intervals in MW-4 at CFB Borden.

DFT Interval	0.10 m	0.20 m	0.30 m	0.40 m	0.50 m
Geometric mean (m/s)	6.4E-04	6.9E-04	6.7E-04	7.4E-04	7.1E-04
Standard deviation (m/s)	2.0E-04	2.2E-04	2.4E-04	2.4E-04	2.9E-04
Coefficient of variation	0.31	0.32	0.35	0.32	0.41
Skew	0.24	0.20	1.10	0.91	0.93
Kurtosis	1.01	1.20	2.12	1.86	-0.40

Table A.6. K_r^E summary statistics for DFTs completed at 0.10 m, 0.20 m, 0.30 m, 0.40, and 0.50 m intervals in MW-7 at CFB Borden.

DFT Interval	0.10 m	0.20 m	0.30 m	0.40 m	0.50 m
Geometric mean (m/s)	7.2E-04	6.6E-04	6.5E-04	8.6E-04	7.0E-04
Standard deviation (m/s)	2.6E-04	2.0E-04	1.8E-04	3.2E-04	1.7E-04
Coefficient of variation	0.36	0.30	0.28	0.37	0.24
Skew	0.70	1.41	0.58	-0.21	-1.47
Kurtosis	-0.37	3.11	-0.06	-0.48	3.10

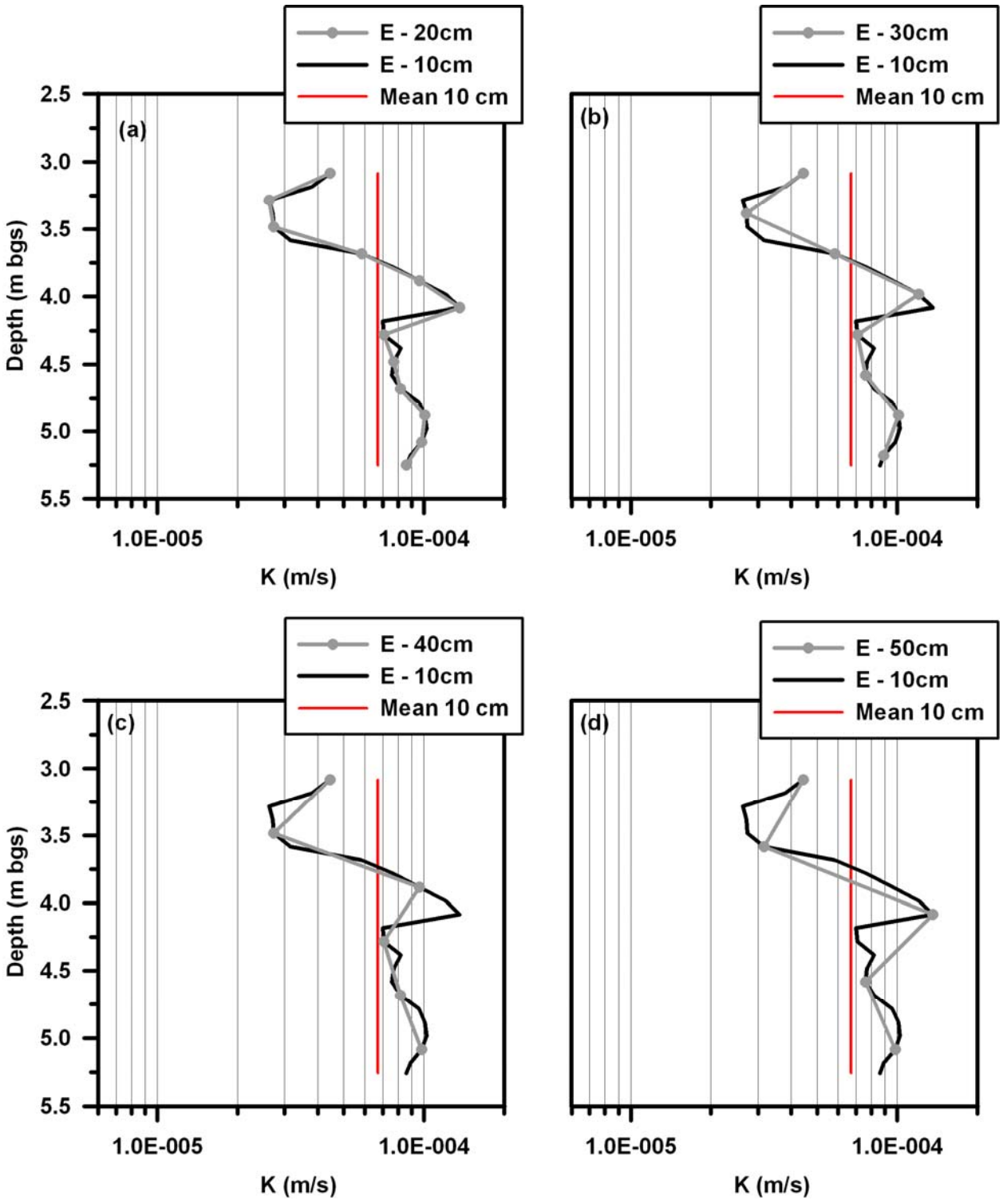

Figure A.1. DFT K_r^E estimates for monitoring well MW-3 from DFTs completed at 0.20 m (a), 0.30 m (b), 0.40 m (c), and 0.50 m (d) intervals. DFT K_r^E estimates at 0.10 m intervals shown as gray line and mean K_r^E for well shown in red.

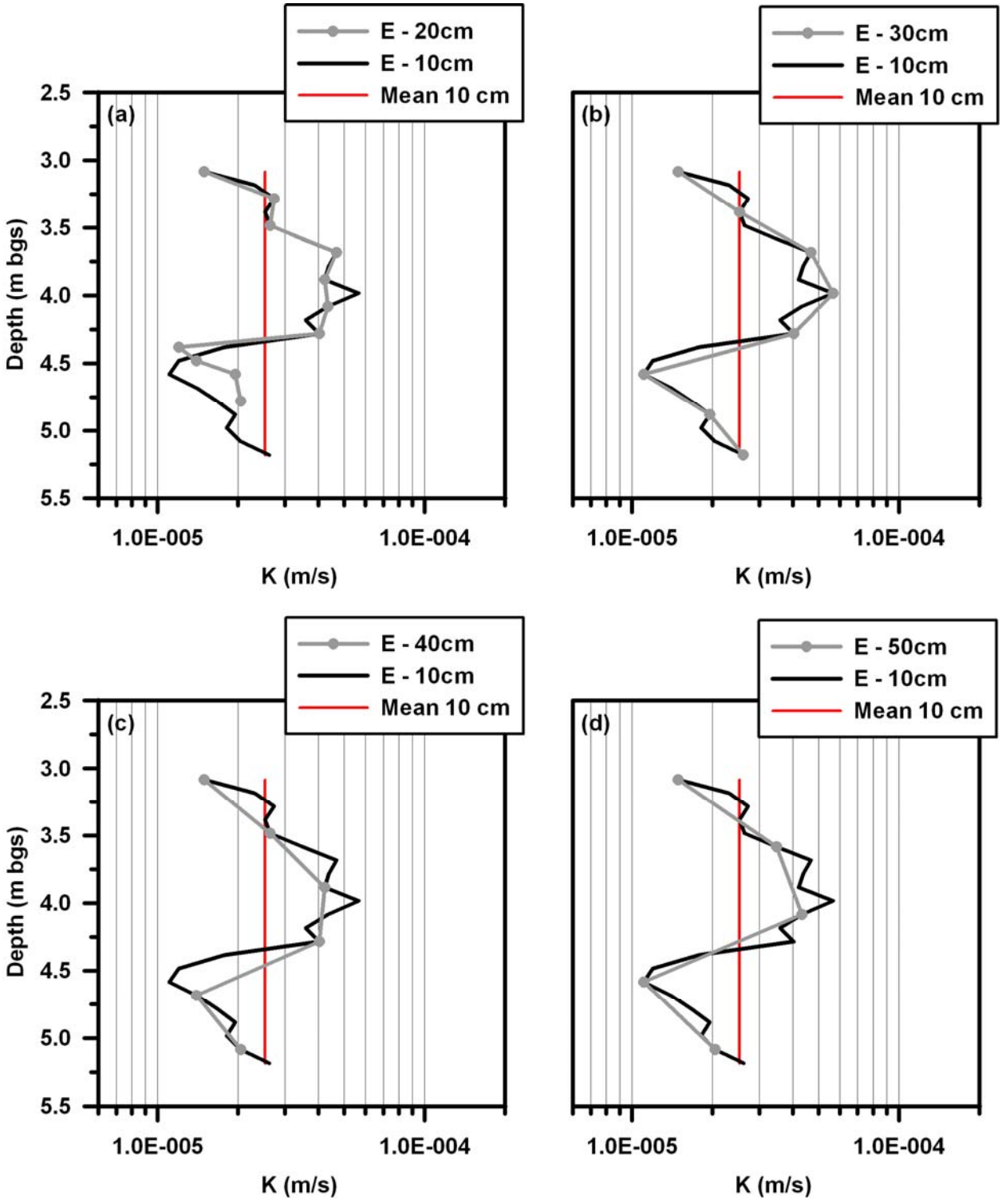

Figure A.2. DFT K_r^E estimates for monitoring well MW-5 from DFTs completed at 0.20 m (a), 0.30 m (b), 0.40 m (c), and 0.50 m (d) intervals. DFT K_r^E estimates at 0.10 m intervals shown as gray line and mean K_r^E for well shown in red.

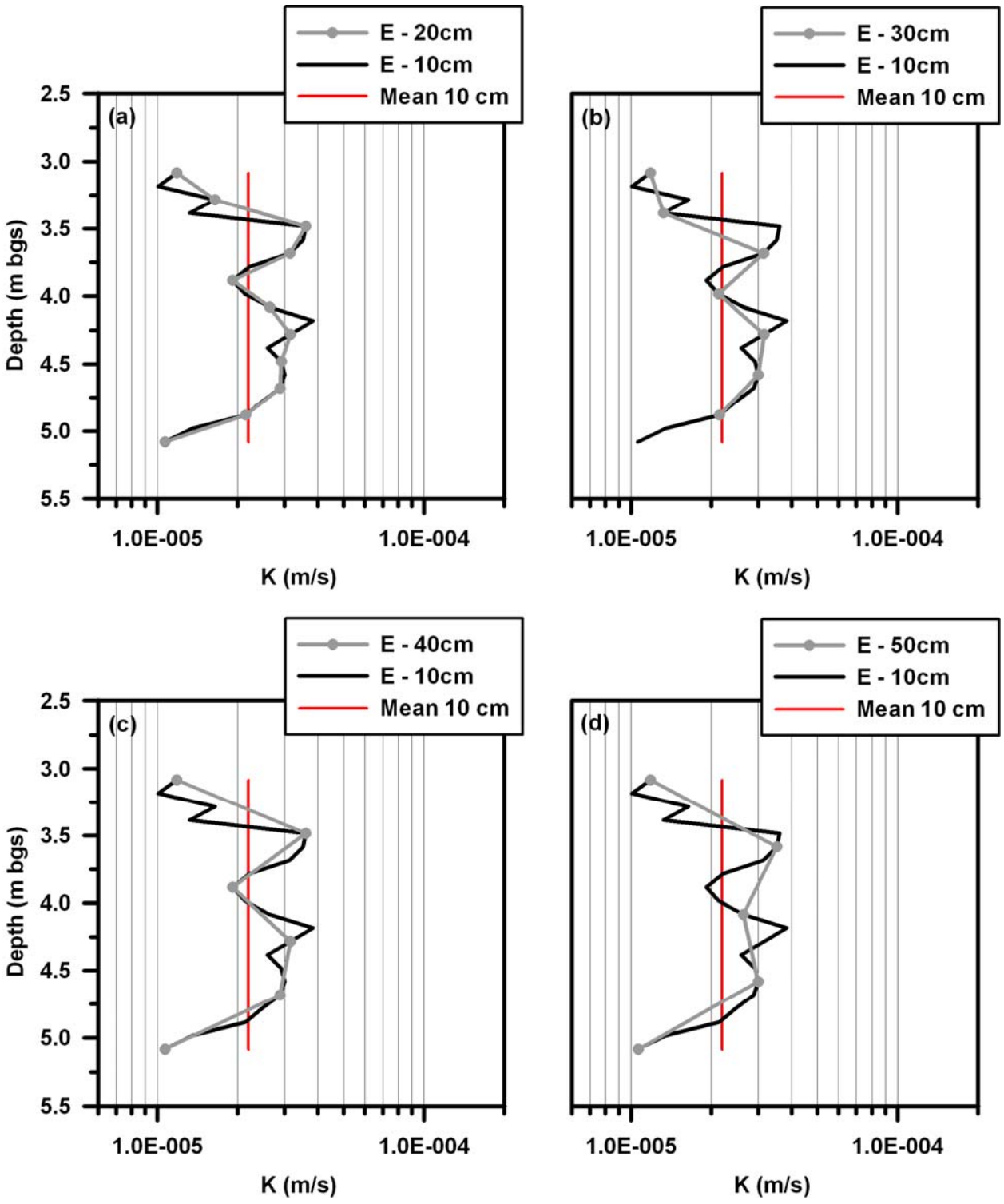

Figure A.3. DFT K_r^E estimates for monitoring well MW-6 from DFTs completed at 0.20 m (a), 0.30 m (b), 0.40 m (c), and 0.50 m (d) intervals. DFT K_r^E estimates at 0.10 m intervals shown as gray line and mean K_r^E for well shown in red.

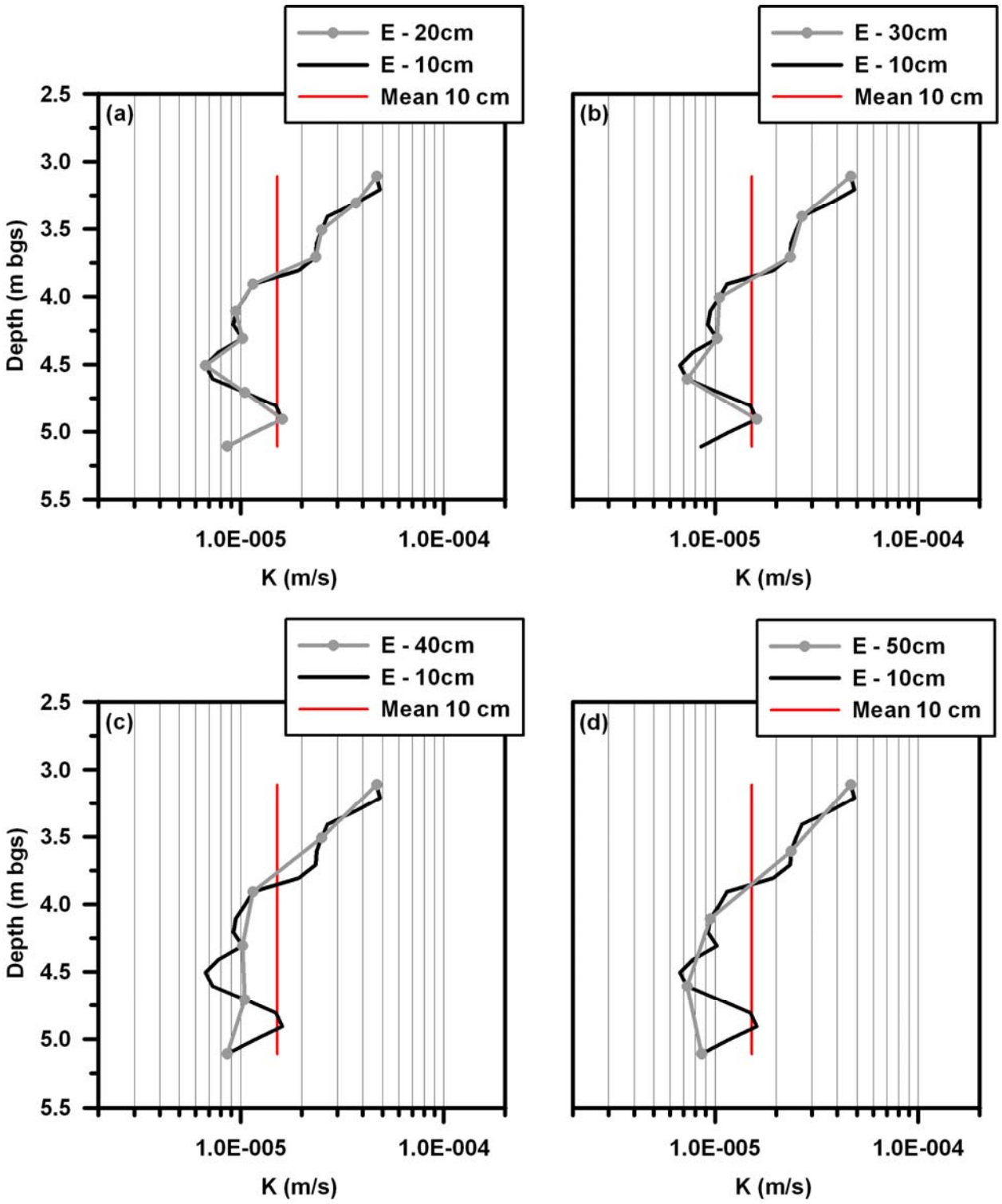

Figure A.4. DFT K_r^E estimates for monitoring well MW-8 from DFTs completed at 0.20 m (a), 0.30 m (b), 0.40 m (c), and 0.50 m (d) intervals. DFT K_r^E estimates at 0.10 m intervals shown as gray line and mean K_r^E for well shown in red.

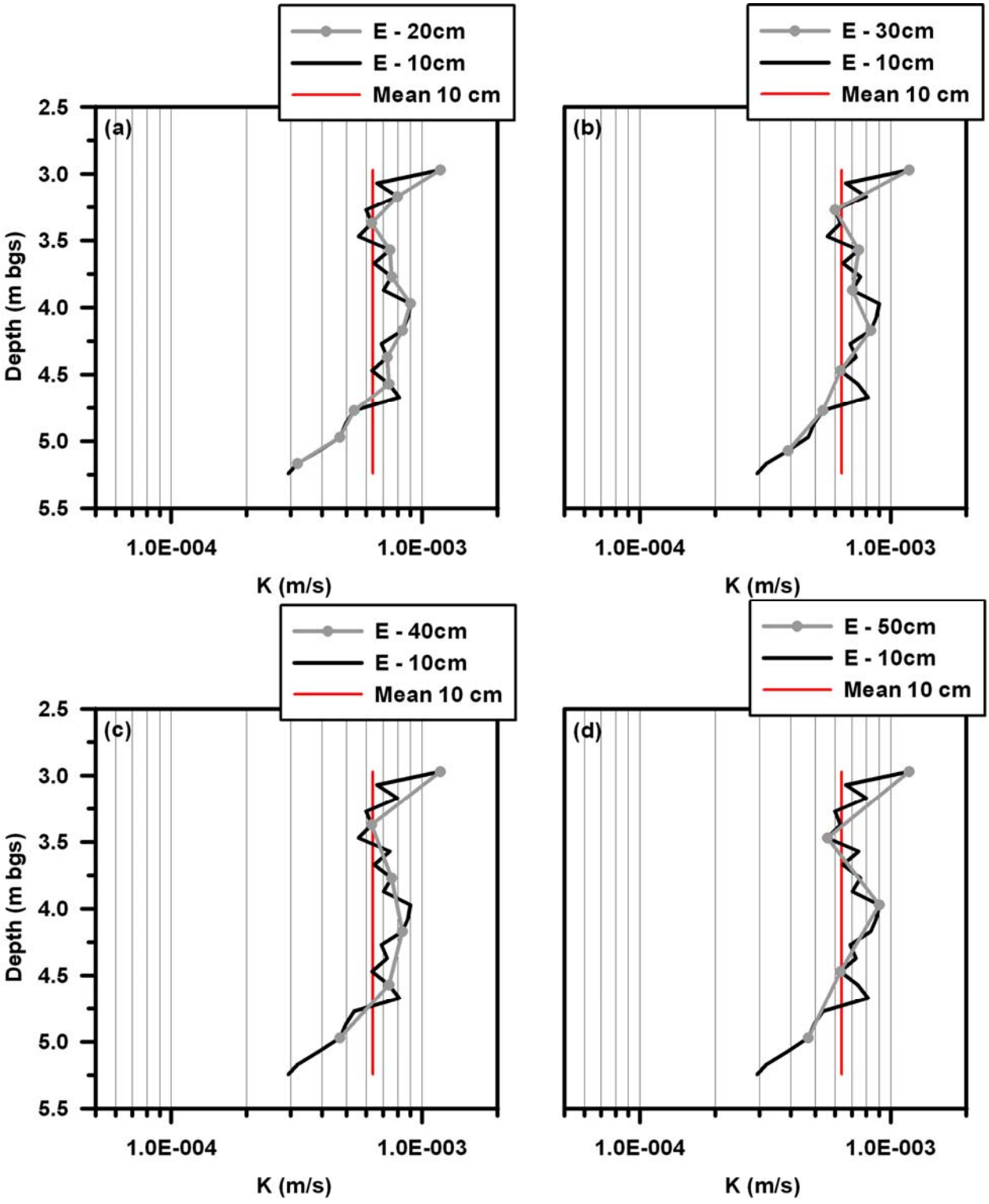

Figure A.5. DFT K_r^E estimates for monitoring well MW-4 from DFTs completed at 0.20 m (a), 0.30 m (b), 0.40 m (c), and 0.50 m (d) intervals. DFT K_r^E estimates at 0.10 m intervals shown as gray line and mean K_r^E for well shown in red.

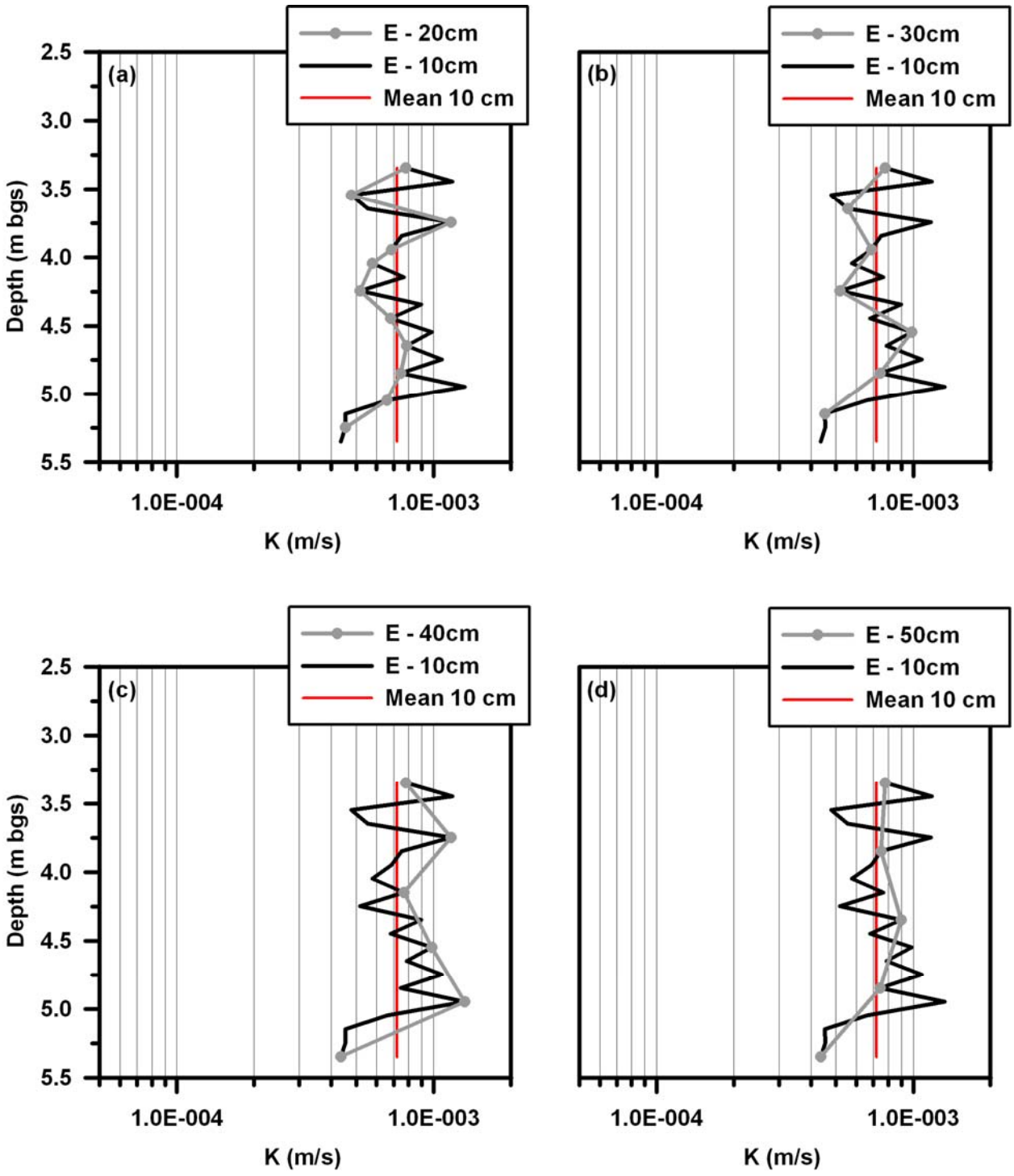

Figure A.6. DFT K_r^E estimates for monitoring well MW-7 from DFTs completed at 0.20 m (a), 0.30 m (b), 0.40 m (c), and 0.50 m (d) intervals. DFT K_r^E estimates at 0.10 m intervals shown as gray line and mean K_r^E for well shown in red.

Appendix B – Dipole Flow and Tracer Test (DFTT) Data

Appendix B contains plots of all the BTCs for the DFTTs completed in the monitoring wells at CFB Borden (Figure B.1 to Figure B.44). Data collected from the probes (pH, EC, DO, and Eh) during the DFTTs are also shown on the figures. DFTT setup and some properties of the BTCs are summarized in Tables B.1 – B.3.

Table B.1. Field setup parameters for the DFTTs completed at CFB Borden.

Test ID	Date	L/Δ	Q (mL/min)	t_c (min)	R	s_I (cm)	s_E (cm)	$s_I + s_E$ (cm)	K_r (m/s)
3-2.9-A	20-Jun-07	S	320	7.42	Y	22.8	56.4	79.3	2.0E-05
3-3.2-A	20-Jun-07	S	320	7.42	Y	15.1	17.4	32.5	4.8E-05
3-3.2-B	22-Jun-07	S	560	4.24	Y	35.0	26.6	61.6	4.4E-05
3-3.2-C	9-Jul-08	W	392	6.05	Y	22.3	16.7	39.0	4.5E-05
3-3.2-D	21-Aug-08	W	386	6.15	N	22.4	22.1	44.5	3.9E-05
3-3.7-A	21-Nov-07	W	550	4.31	Y	3.9	23.4	27.3	9.2E-05
3-3.8-A	22-Jun-07	S	560	4.24	Y	26.7	10.3	37.0	7.4E-05
3-3.8-B	25-Jun-07	S	515	4.61	Y	29.7	14.9	44.5	6.1E-05
3-3.8-C	28-Jun-07	S	540	4.39	Y	19.1	20.5	39.6	6.9E-05
3-3.8-D	13-Aug-08	W	543	4.37	Y	16.1	28.2	44.3	5.5E-05
3-4.3-A	6-Dec-07	W	550	4.24	Y	19.0	15.7	34.7	7.3E-05
3-4.9-A	27-Nov-07	W	550	4.31	Y	9.8	19.5	29.3	8.5E-05
3-4.9-B	4-Jun-08	W	706	3.36	Y	22.6	31.4	53.9	5.9E-05
3-4.9-C	24-Jul-08	W	359	6.60	Y	10.2	16.1	26.3	6.2E-05
3-4.9-D	11-Aug-08	W	553	4.29	Y	20.2	20.0	40.2	6.2E-05
3-4.9-E	21-Aug-08	W	551	4.30	N	22.4	23.8	46.2	5.4E-05
3-4.9-F	1-Oct-08	W	553	4.29	Y	7.8	9.7	17.4	1.4E-04
4-3.2-A	23-Jun-07	S	560	4.24	Y	1.8	2.2	4.0	6.9E-04
4-3.2-B	26-Jun-07	S	1860	1.28	Y	14.4	1.2	15.5	3.3E-04
4-3.6-A	7-Dec-07	W	546	4.35	Y	1.1	2.1	3.2	7.6E-04
4-4.9-A	10-Oct-08	W	650	3.65	Y	4.4	6.2	10.6	2.8E-04
4-4.9-B	10-Oct-08	W	650	3.65	N	8.9	0.9	9.8	3.0E-04
6-2.9-A	23-Jun-07	S	560	4.24	Y	111.6	69.7	181.3	1.5E-05
6-2.9-B	27-Jun-07	S	1840	1.29	Y	13.6	118.6	132.2	6.9E-05
6-3.1-A	21-Jun-07	S	560	4.24	Y	103.6	31.9	135.6	2.0E-05
6-3.3-A	26-Jun-07	S	1040	2.28	Y	137.7	151.6	289.3	1.8E-05
6-3.3-B	29-Nov-07	W	589	4.03	Y	39.9	76.2	116.1	2.3E-05
6-3.3-C	24-Jul-08	W	398	5.97	Y	32.6	52.6	85.2	2.1E-05
6-3.3-D	7-Aug-08	W	591	4.02	Y	51.4	81.6	133.0	2.0E-05
6-3.3-E	11-Aug-08	W	589	4.03	Y	48.4	91.1	139.5	1.9E-05
6-3.3-F	17-Sep-08	W	592	4.01	Y	26.6	51.1	77.7	3.4E-05
6-3.3-G	6-Oct-08	W	422	5.62	Y	40.8	49.6	90.4	2.1E-05
6-3.3-H	15-Oct-08	W	800	2.97	Y	22.4	84.8	107.2	3.4E-05
6-4.3-A	5-Dec-07	W	754	3.15	Y	42.0	85.9	127.9	2.7E-05
6-4.3-B	23-May-08	W	494	4.81	Y	42.7	48.4	91.1	2.4E-05
6-4.3-C	26-Aug-08	W	1354	1.75	Y	106.3	99.2	205.5	3.0E-05
6-4.9-A	13-Dec-07	W	516	4.60	Y	82.2	41.3	123.6	1.9E-05
6-4.9-B	19-Aug-08	W	751	3.16	N	134.6	38.4	173.0	2.0E-05
8-2.8-A	27-Jun-07	S	1860	1.28	Y	1.5	38.7	40.2	2.3E-04
8-3.2-A	18-Jun-08	W	383	6.25	Y	39.0	17.1	56.1	3.0E-05
8-3.8-A	27-Jun-07	S	1860	1.28	Y	162.4	189.8	352.1	2.6E-05
8-4.6-A	18-Jun-08	W	386	6.14	Y	59.1	76.0	135.1	1.3E-05
8-4.9-A	12-Dec-07	W	590	4.02	Y	153.8	88.3	242.1	1.1E-05
8-4.9-B	26-Aug-08	W	589	4.03	N	166.7	133.4	300.1	8.8E-06
8-4.9-C	8-Oct-08	W	590	4.02	N	155.1	136.7	291.8	9.1E-06
8-4.9-D	20-Oct-08	W	592	4.01	Y	117.9	119.4	237.3	1.1E-05

Table B.2. Summary of tracer injection parameters for the DFTTs completed at CFB Borden.

Test ID	Q_{inj} (mL/min)	% tracer injection to flow	RWT (mg/L)	SRB (mg/L)	Bromide (mg/L)	Acetate (mg/L)	Toluene (mg/L)	Tracer volume (mL)	t_{inj} (min)
3-2.9-A	10	3.1%	1	-	6,500	-	-	50	5.0
3-3.2-A	10	3.1%	1	-	6,500	-	-	50	5.0
3-3.2-B	5	0.9%	50	-	6,500	-	-	50	10.0
3-3.2-C	5	1.3%	75	-	20,000	20,000	-	50	10.0
3-3.2-D	5	1.3%	-	50	15,000	-	-	50	10.0
3-3.7-A	5	0.9%	50	-	1,000	-	-	50	10.0
3-3.8-A	27	4.8%	50	-	6,500	-	-	250	9.3
3-3.8-B	27	5.2%	-	-	10,000	10,000	-	250	9.3
3-3.8-C	30	5.6%	~50	-	-	-	500	300	10.0
3-3.8-D	25	5.6%	-	50	15,000	-	-	50	2.0
3-4.3-A	25	4.5%	75	-	20,000	~10,000	-	50	2.0
3-4.9-A	25	4.5%	50	-	1,000	-	-	50	2.0
3-4.9-B	25	3.5%	50	-	10,000	-	-	50	2.0
3-4.9-C	25	7.0%	-	50	20,000	20,000	-	50	2.0
3-4.9-D	25	4.5%	-	50	15,000	-	-	50	2.0
3-4.9-E	25	4.5%	-	50	15,000	-	-	50	2.0
3-4.9-F	5	0.9%	-	50	15,000	-	-	50	10.0
4-3.2-A	27	4.8%	50	-	6,500	-	-	250	9.3
4-3.2-B	100	5.4%	-	-	10,000	10,000	-	500	5.0
4-3.6-A	25	4.6%	75	-	20,000	~10,000	-	50	2.0
4-4.9-A	10	1.5%	-	50	15,000	-	-	10	1.0
4-4.9-B	10	1.5%	-	50	15,000	-	-	10	1.0
6-2.9-A	27.5	4.9%	50	-	6,500	-	-	250	9.1
6-2.9-B	103	5.6%	~50	-	10,000	10,000	-	500	4.9
6-3.1-A	5	0.9%	50	-	6,500	-	-	50	10.0
6-3.3-A	50	4.8%	-	-	10,000	10,000	-	500	10.0
6-3.3-B	25	4.2%	50	-	1,500	-	-	52	2.1
6-3.3-C	5	1.3%	-	50	20,000	20,000	-	50	10.0
6-3.3-D	25	4.2%	-	50	20,000	20,000	-	50	2.0
6-3.3-E	25	4.2%	-	50	15,000	-	-	50	2.0
6-3.3-F	25	4.2%	-	50	15,000	-	-	50	2.0
6-3.3-G	25	5.9%	-	50	15,000		-	50	2.0
6-3.3-H	25	3.1%	-	50	15,000		-	50	2.0
6-4.3-A	25	3.3%	75	-	20,000	-	-	50	2.0
6-4.3-B	25	5.1%	50	-	10,000	-	-	25	1.0
6-4.3-C	25	1.8%	-	50	15,000	-	-	50	2.0
6-4.9-A	25	4.8%	75	-	20,000	20,000	-	50	2.0
6-4.9-B	25	3.3%	-	50	15,000	-	-	50	2.0
8-2.8-A	100	5.4%	50	-	6,500	-	-	500	5.0
8-3.2-A	5	1.3%	50	-	10,000	~7500	-	50	10.0
8-3.8-A	100	5.4%	50	-	6,500	-	-	500	5.0
8-4.6-A	5	1.3%	50	-	10,000	~7500	-	25.5	5.1
8-4.9-A	25	4.2%	75	-	20,000	20,000	-	50	2.0
8-4.9-B	25	4.2%	-	50	15,000	-	-	50	2.0
8-4.9-C	25	4.2%	-	50	15,000	-	-	50	2.0
8-4.9-D	25	4.2%	-	50	15,000	-	-	50	2.0

Table B.3. Selected BTC properties for the DFTTs completed at CFB Borden.

Test ID	Time to skin (min)	Time to front (min)	Time to peak (min)	Time to return (min)	max M/Mo	Time to skin	Time to front	Time to peak	Time to return	Time to max M/Mo	Type
3-2.9-A	-	-	-	-	-	-	-	-	-	-	-
3-3.2-A	-	-	-	-	-	-	-	-	-	-	-
3-3.2-B	15.0		15.0	>240	0.53	3.5	-	3.5	>56	57	3
3-3.2-C	18.9	-	71.6	>1740	1.34	3.1	-	11.8	>288	288	3
3-3.2-D	17.0	-	66.9	> 240	0.16	2.8	-	10.9	> 39	39	3
3-3.7-A	22.7	57.0	98.9	>210	0.17	5.3	13.2	22.9	>49	49	1
3-3.8-A	-	15.0	35.0	>230	1.24	-	3.5	8.3	>54	54	1
3-3.8-B	5.0	16.5	35.0	>170	1.03	1.1	3.6	7.6	>37	37	1
3-3.8-C	5.0	15.0	30.0	>220	-	1.1	3.4	6.8	>50	50	1
3-3.8-D	10.2	42.7	62.4	>300	0.94	2.3	9.8	14.3	>69	69	1
3-4.3-A	12.5		47.0	>280	0.20	2.9	-	11.1	>67	67	-
3-4.9-A	22.1	40.6	57.1	>156	0.19	5.1	9.4	13.2	36.2	>36	1
3-4.9-B	14.3	32.3	44.6	>420	1.14	4.3	9.6	13.3	>125	125	1
3-4.9-C	21.7	58.7	79.8	>300	0.61	3.3	8.9	12.1	>45	45	1
3-4.9-D	11.4	40.2	51.1	>300	0.75	2.7	9.4	11.9	>70	70	1
3-4.9-E	15.0	41.3	57.9	>240	0.51	3.5	9.6	13.5	>57	57	1
3-4.9-F	17.4	44.5	58.3	>300	0.73	4.0	10.4	13.6	>70	70	1
4-3.2-A	10.0	3.0	10.0	56	2.11	2.4	0.7	2.4	13.2	33	2
4-3.2-B	6.0	1.0	6.0	21	2.51	4.7	0.8	4.7	16.5	180	2
4-3.6-A	8.0	4.3	8.0	269	3.02	1.8	1.0	1.8	61.9	69	2
4-4.9-A	5.5	4.1	5.5	47	4.20	1.5	1.1	1.5	13.0	34	2
4-4.9-B	5.5	3.5	5.5	11	1.09	1.5	1.0	1.5	2.9	16	2
6-2.9-A	12.5	-	12.5	>200	0.55	2.9	-	2.9	>47	47	4
6-2.9-B	6.0	-	6.0	>90	1.37	4.7	-	4.7	>70	70	4
6-3.1-A	-	-	-	-	-	-	-	-	-	-	-
6-3.3-A	10.0	-	10.0	>145	0.15	4.4	-	4.4	>64	64	2
6-3.3-B	7.6	-	7.6	> 180	0.14	1.9	-	1.9	>45	45	2
6-3.3-C	14.5	-	14.5	50	0.19	2.4	-	2.4	8.4	30	2
6-3.3-D	6.8	-	6.8	21	0.21	1.7	-	1.7	5.2	75	2
6-3.3-E	6.0	-	6.0	21	0.21	1.5	-	1.5	5.3	75	2
6-3.3-F	5.5	-	5.5	15	0.26	1.4	-	1.4	3.8	60	2
6-3.3-G	11.0	-	11.0	37	0.35	2.0	-	2.0	6.6	49	2
6-3.3-H	5.0	-	5.0	14	0.25	1.7	-	1.7	4.7	81	2
6-4.3-A	8.8	20.1	40.0	>301	0.62	2.8	6.4	12.7	>96	96	1
6-4.3-B	-	-	-	-	-		-		-	-	1
6-4.3-C	4.9	10.6	20.1	171	0.71	2.8	6.0	11.5	97.6	137	1
6-4.9-A	7.7	-	52.4	> 300	0.60	1.7	-	11.4	>65	65	3
6-4.9-B	5.8	-	43.3	>240	0.67	1.8	-	13.7	>76	76	3
8-2.8-A	10.0	-	30.0	80	0.44	7.8	-	23.5	62.7	94	-
8-3.2-A	20.7	-	20.7	>400	0.43	3.3	-	3.3	>64	64	3
8-3.8-A	5.0	-	5.0	>90	0.53	3.9	-	3.9	>71	71	2
8-4.6-A	13.0	-	13.0	37	0.14	2.1	-	2.1	6.0	13.3	2
8-4.9-A	6.0	-	38.3	> 211	0.60	1.5	-	9.5	>53	53	4
8-4.9-B	5.2	-	29.3	>240	0.49	1.3	-	7.3	>60	60	3
8-4.9-C	6.0	-	35.6	>240	0.48	1.5	-	8.8	>60	60.0	3
8-4.9-D	5.3	-	33.1	>240	0.60	1.3	-	8.2	>60	60.0	3

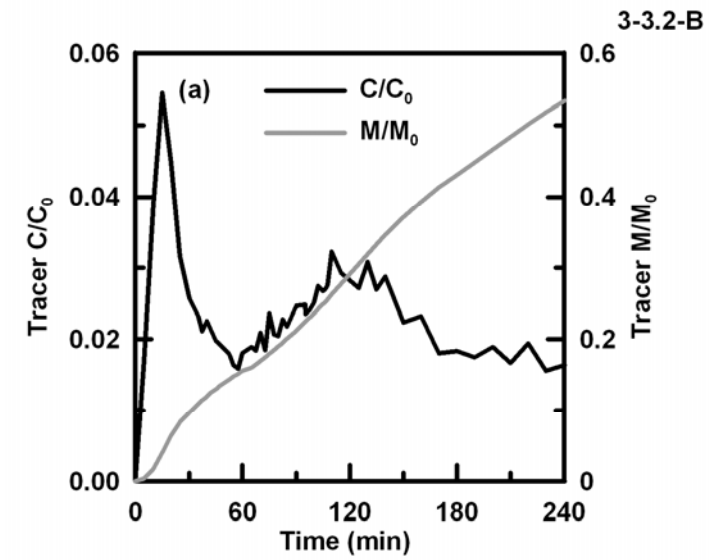

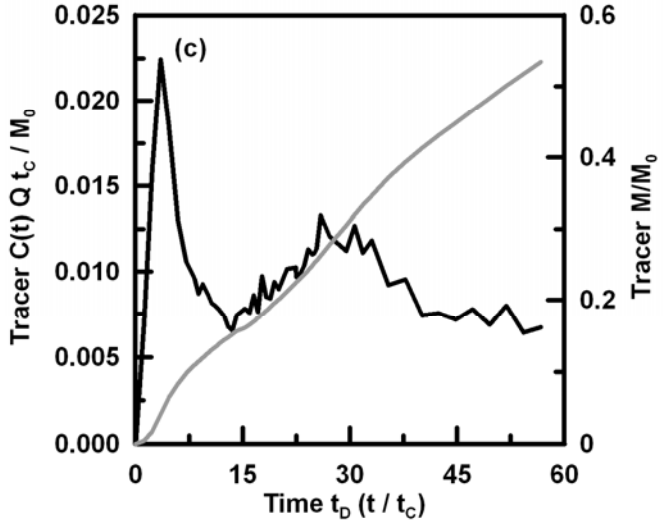

Figure B.1. BTCs for DFTT 3-3.2-B.

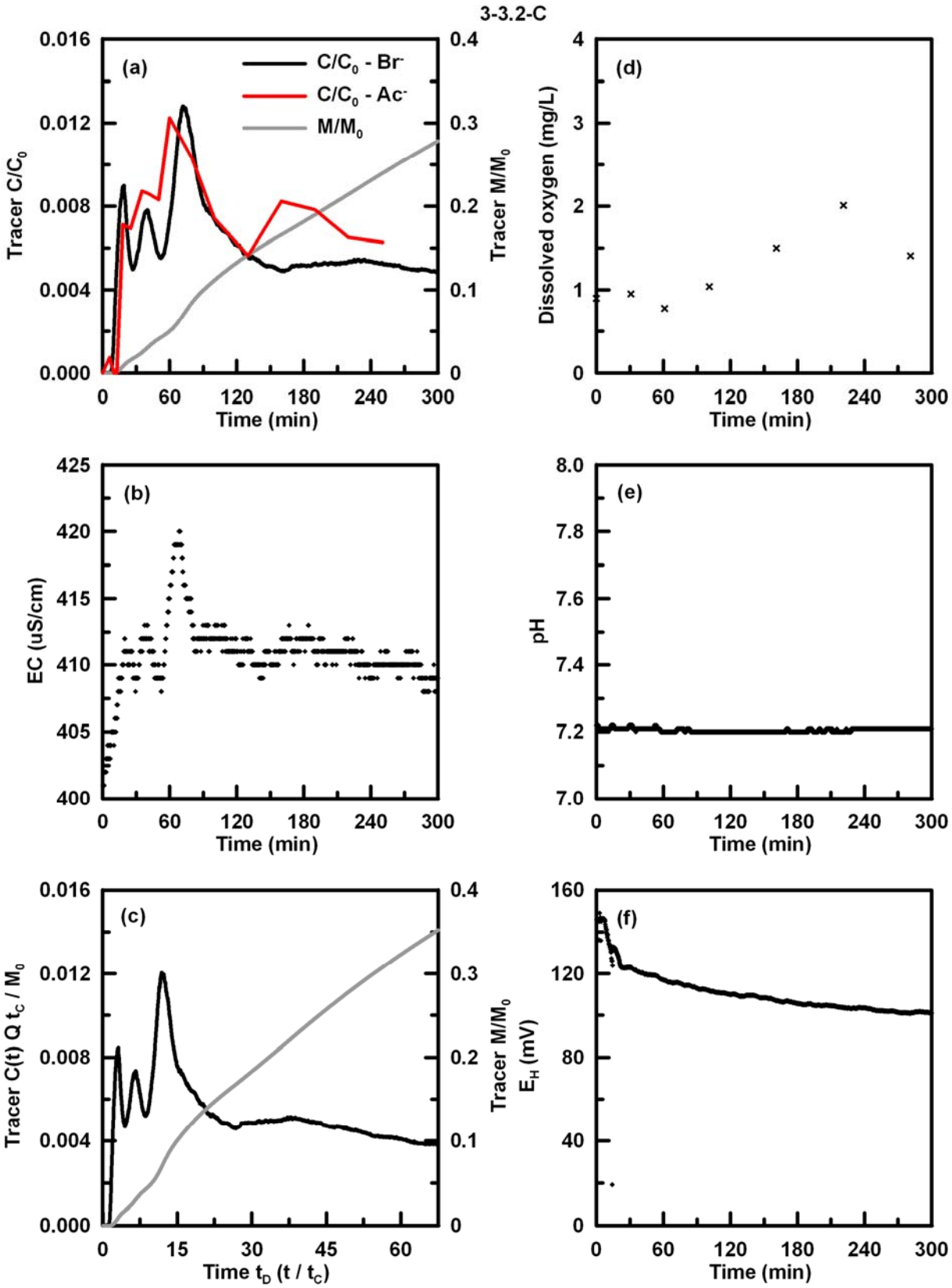

Figure B.2. BTCs and monitoring data for first 300 min of DFTT 3-3.2-C.

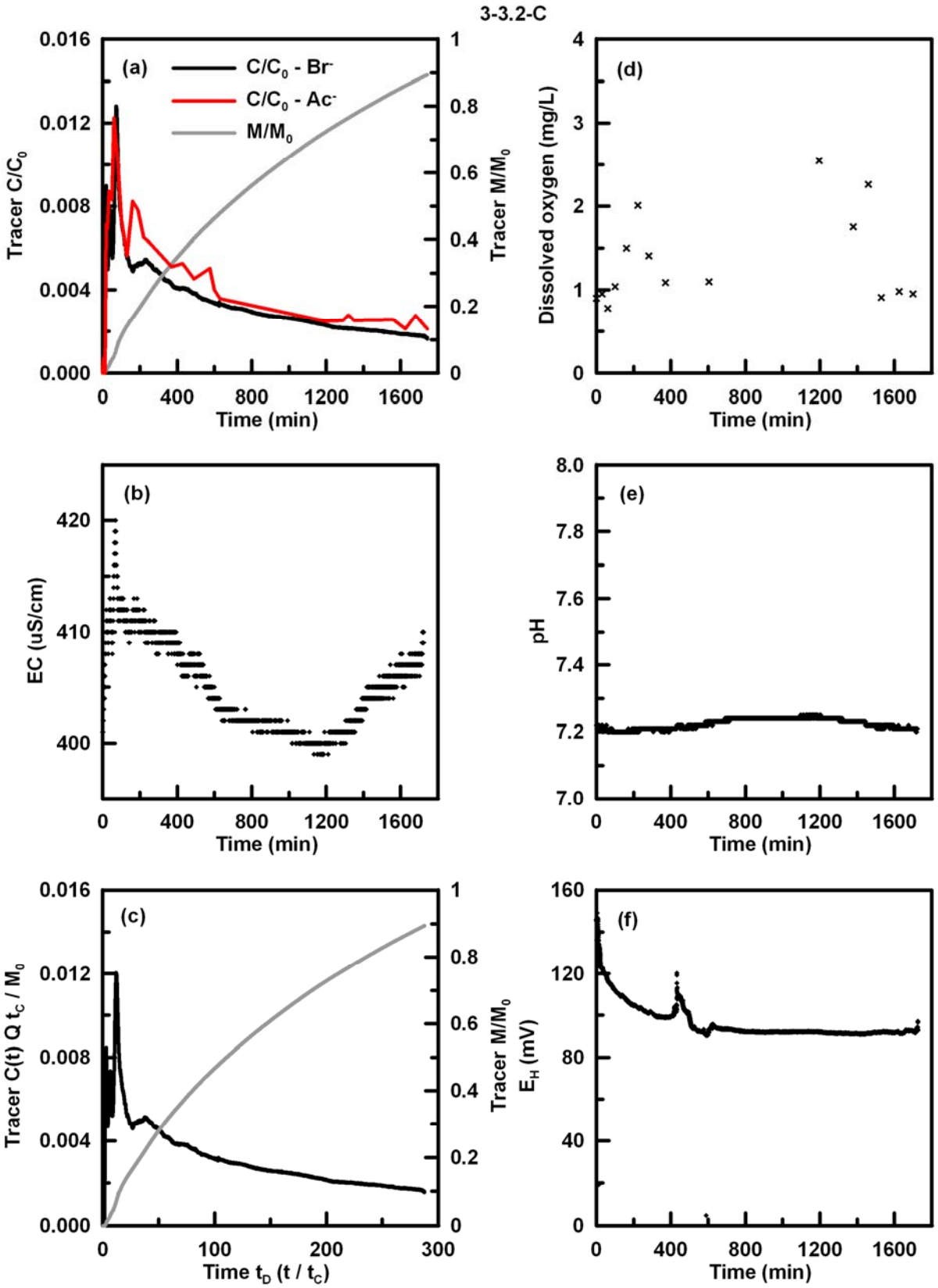

Figure B.3. BTCs and monitoring data for complete 1800 min of DFTT 3-3.2-C.

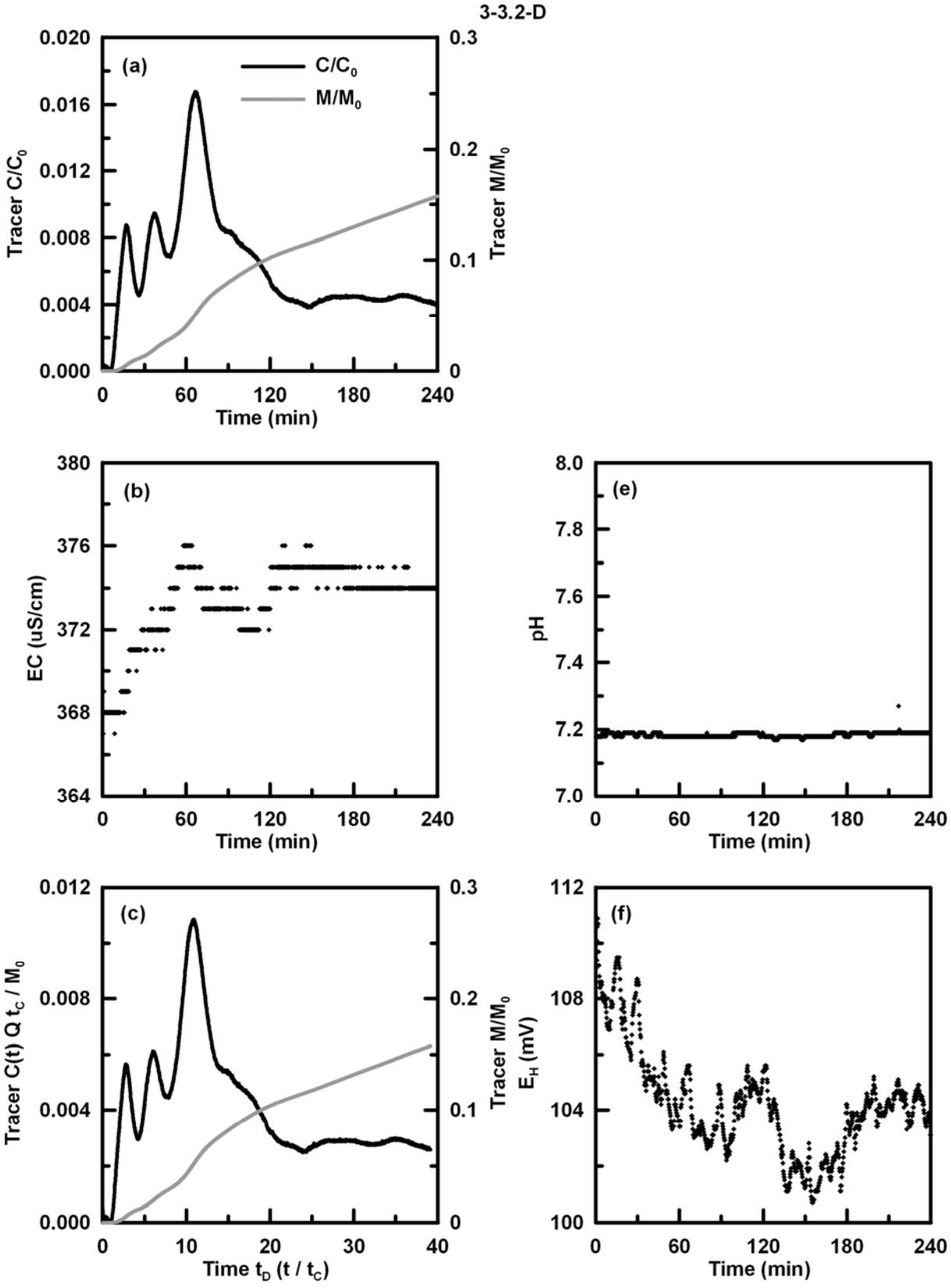

Figure B.4. BTCs and monitoring data for DFTT 3-3.2-D.

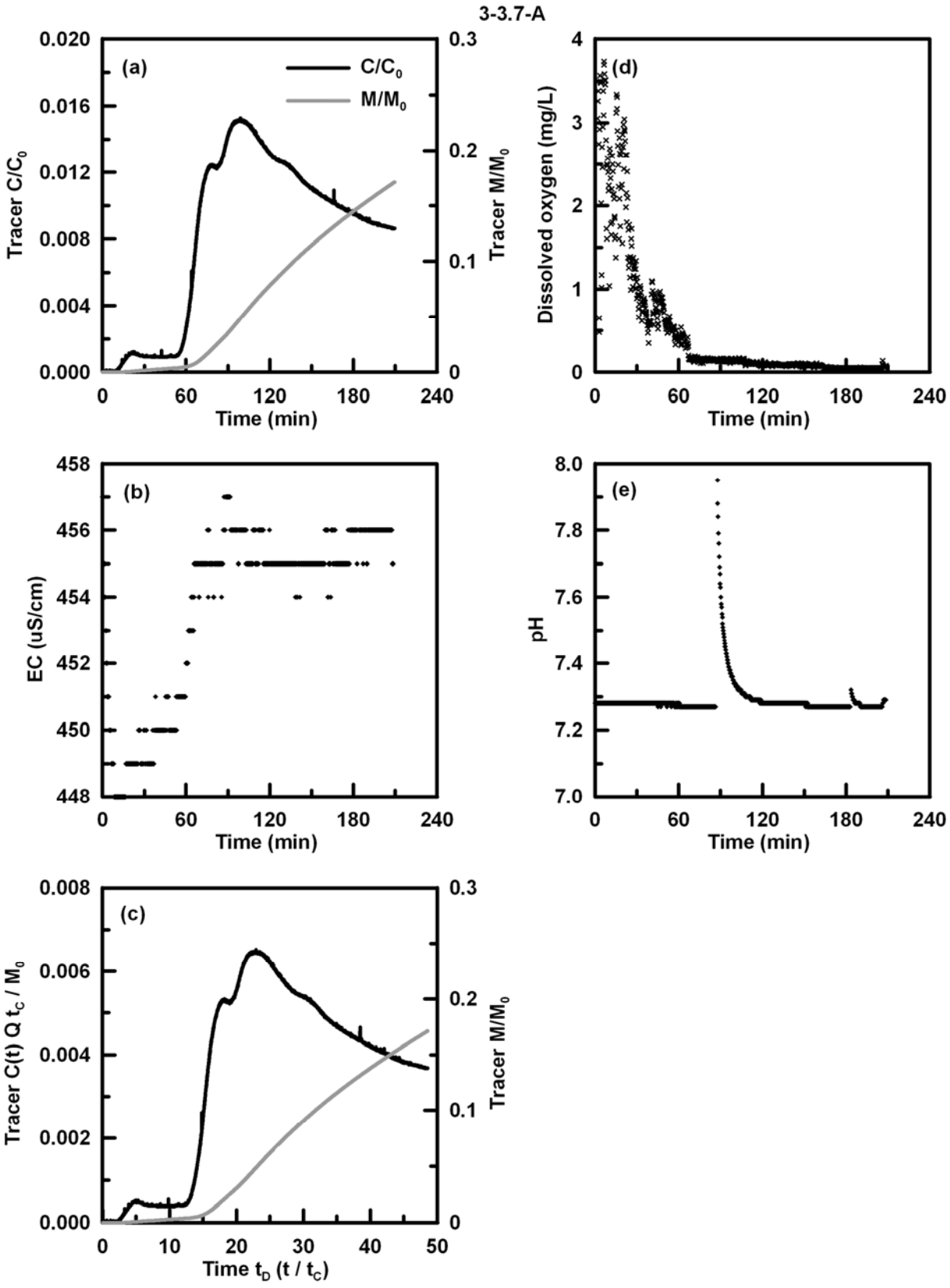

Figure B.5. BTCs and monitoring data for DFTT 3-3.7-A.

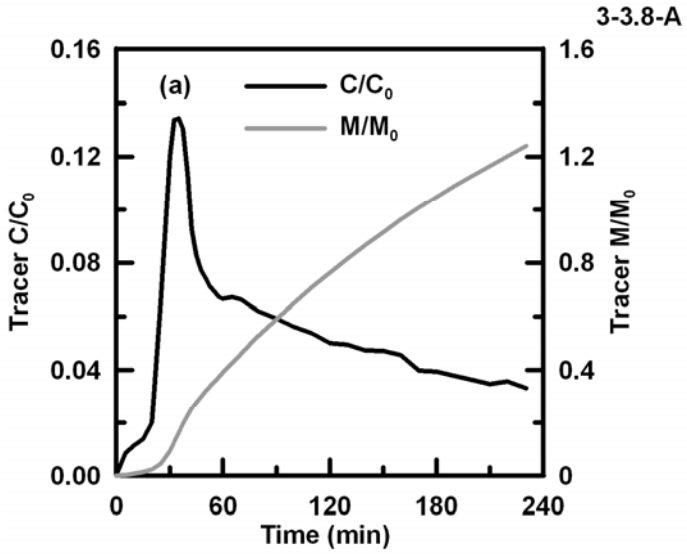

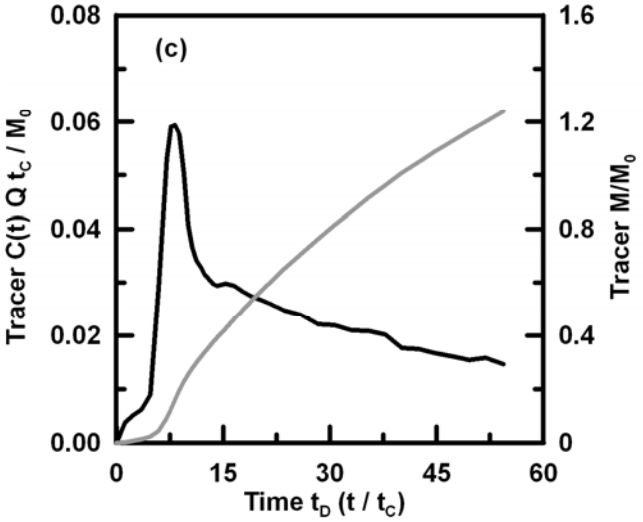

Figure B.6. BTCs for DFTT 3-3.8-A.

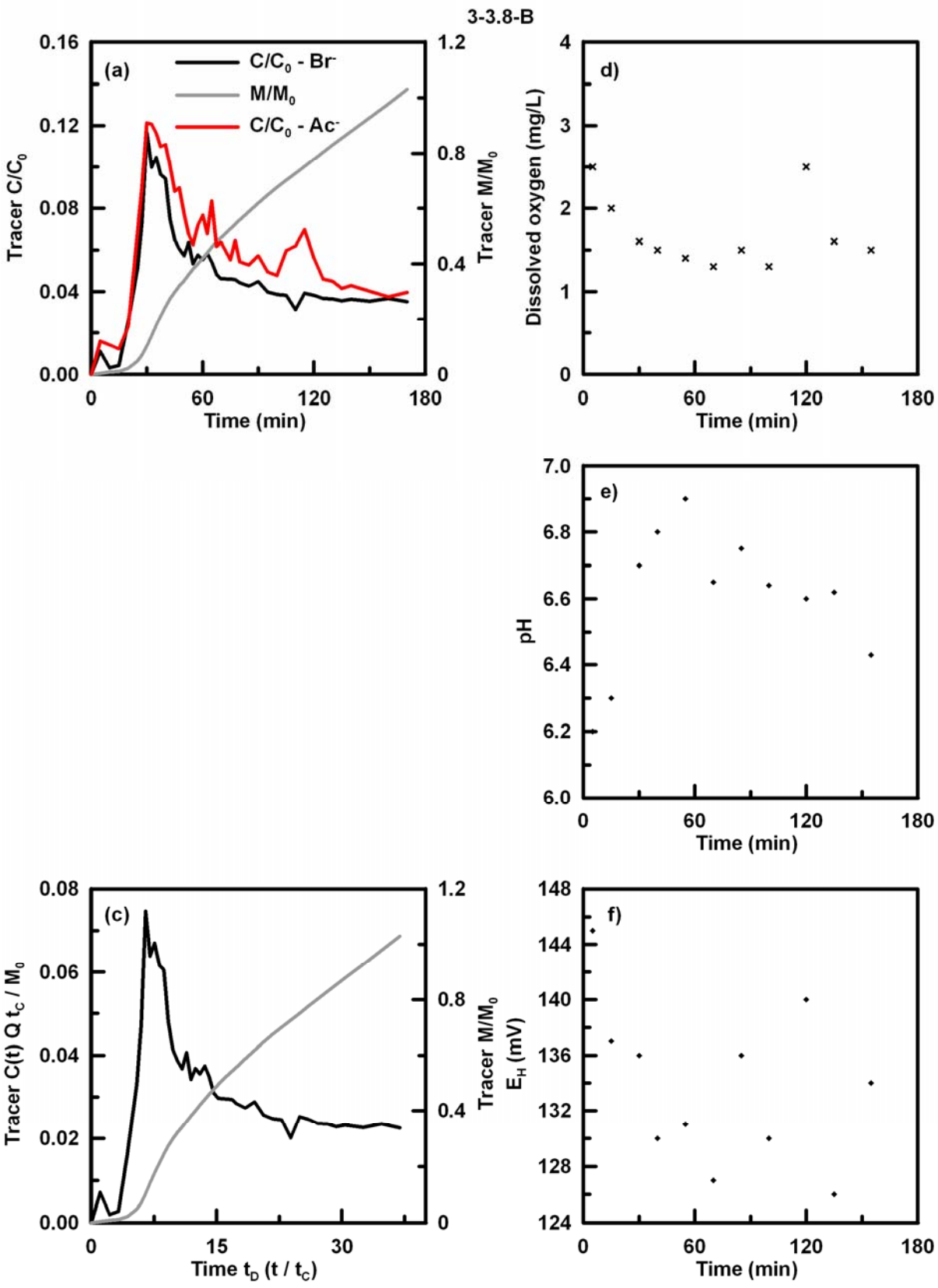

Figure B.7. BTCs and monitoring data for DFTT 3-3.8-B.

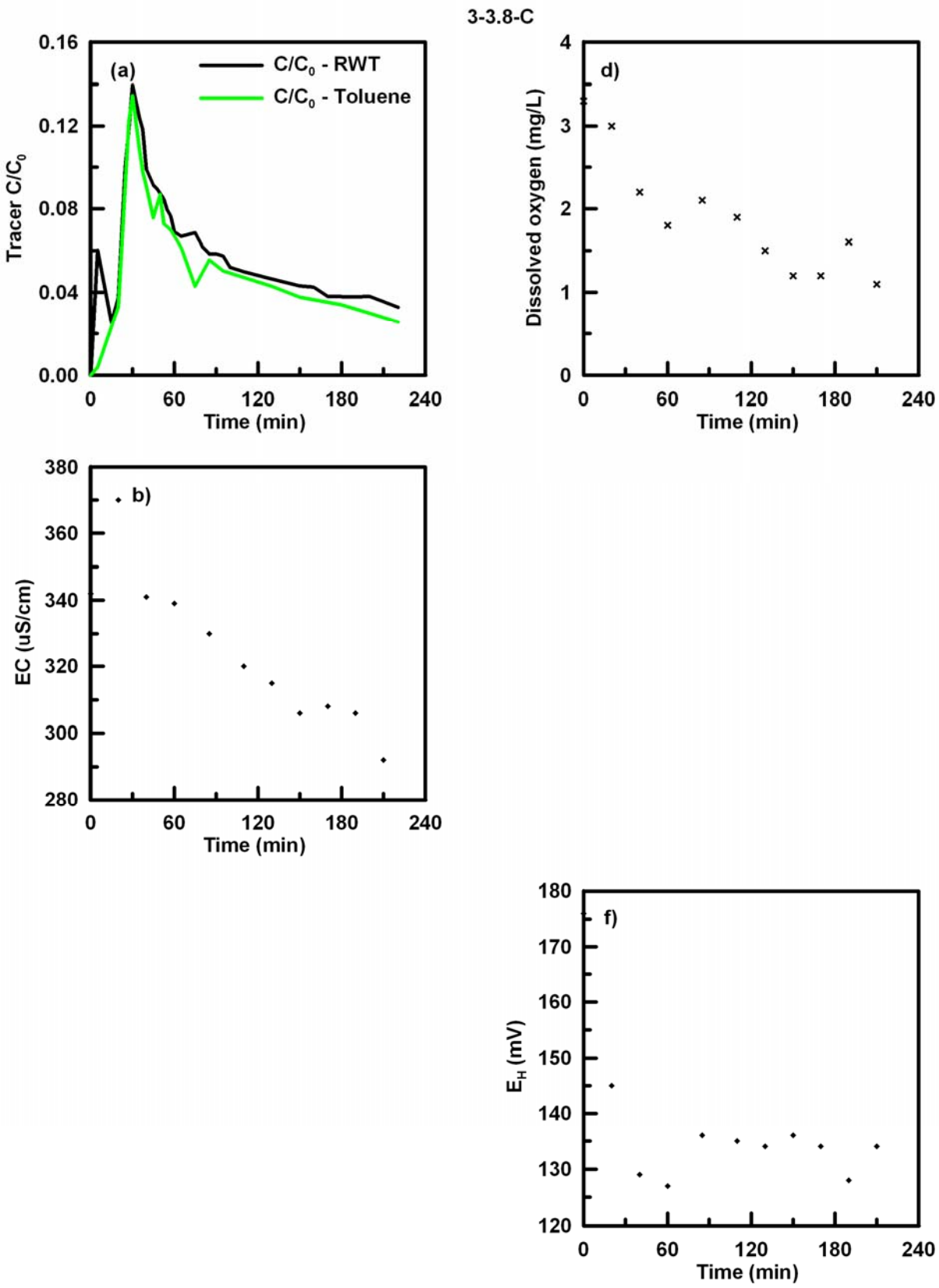

Figure B.8. BTCs and monitoring data for DFTT 3-3.8-C.

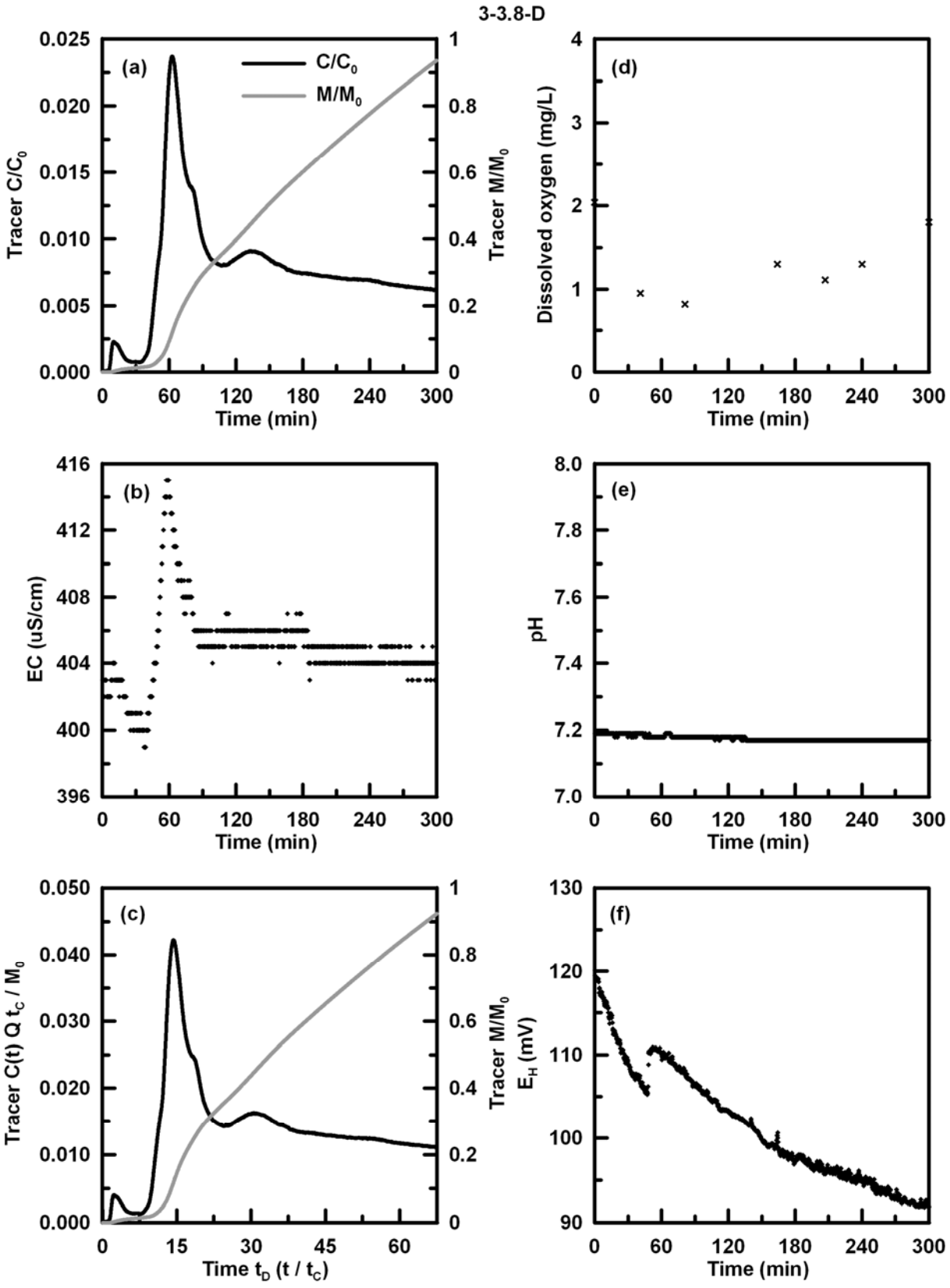

Figure B.9. BTCs and monitoring data for DFTT 3-3.8-D.

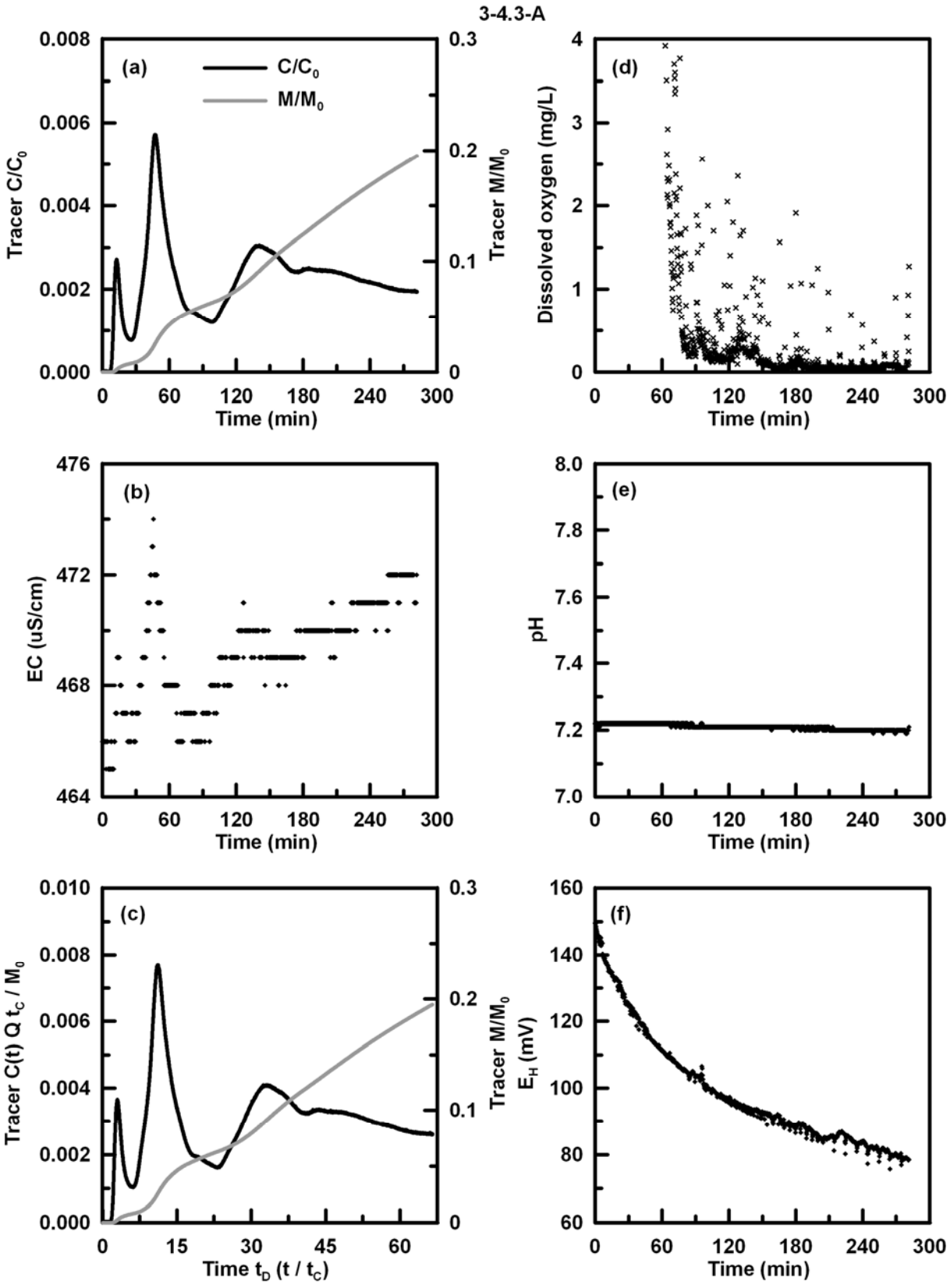

Figure B.10. BTCs and monitoring data for DFTT 3-4.3-A.

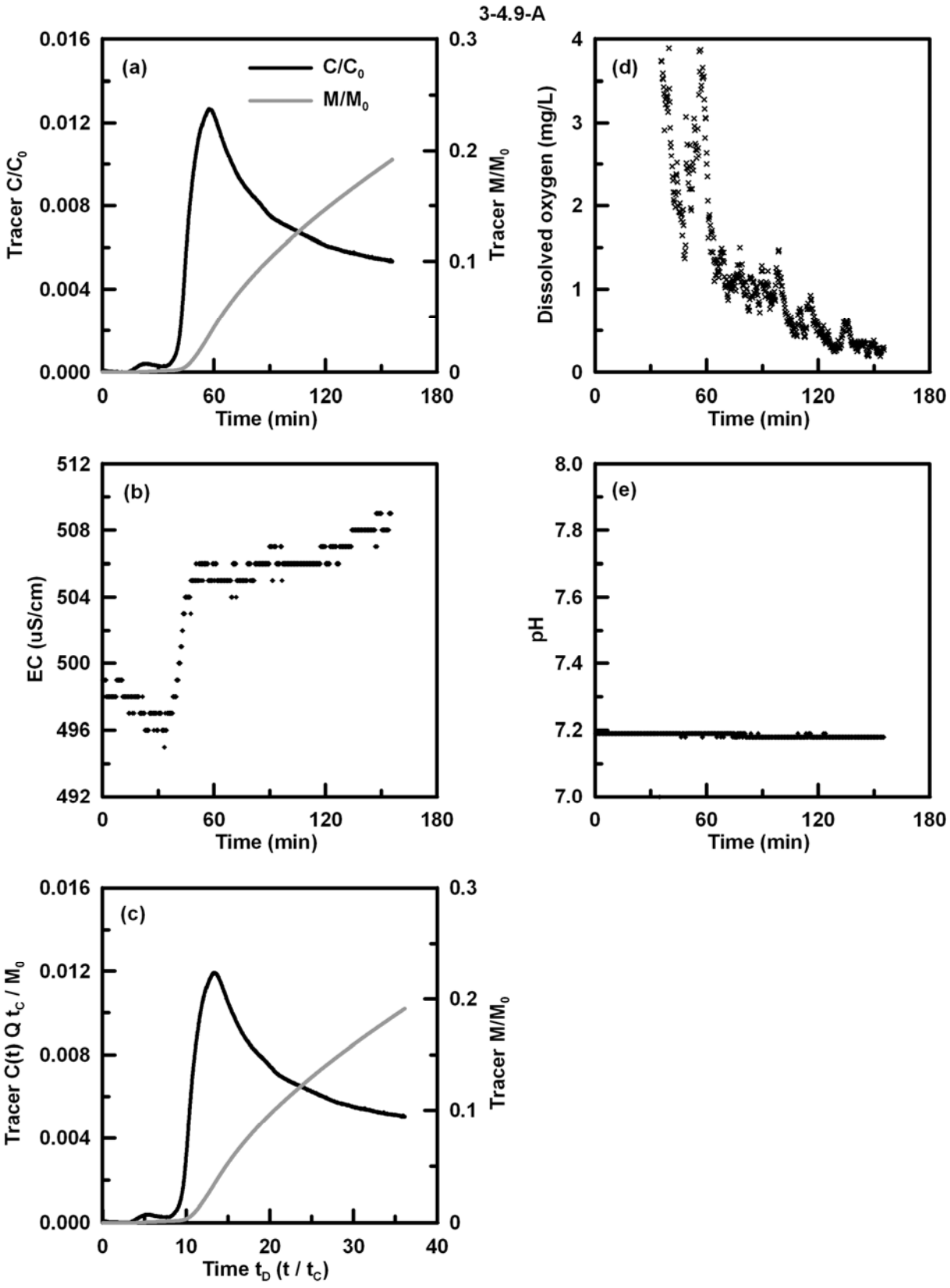

Figure B.11. BTCs and monitoring data for DFTT 3-4.9-A.

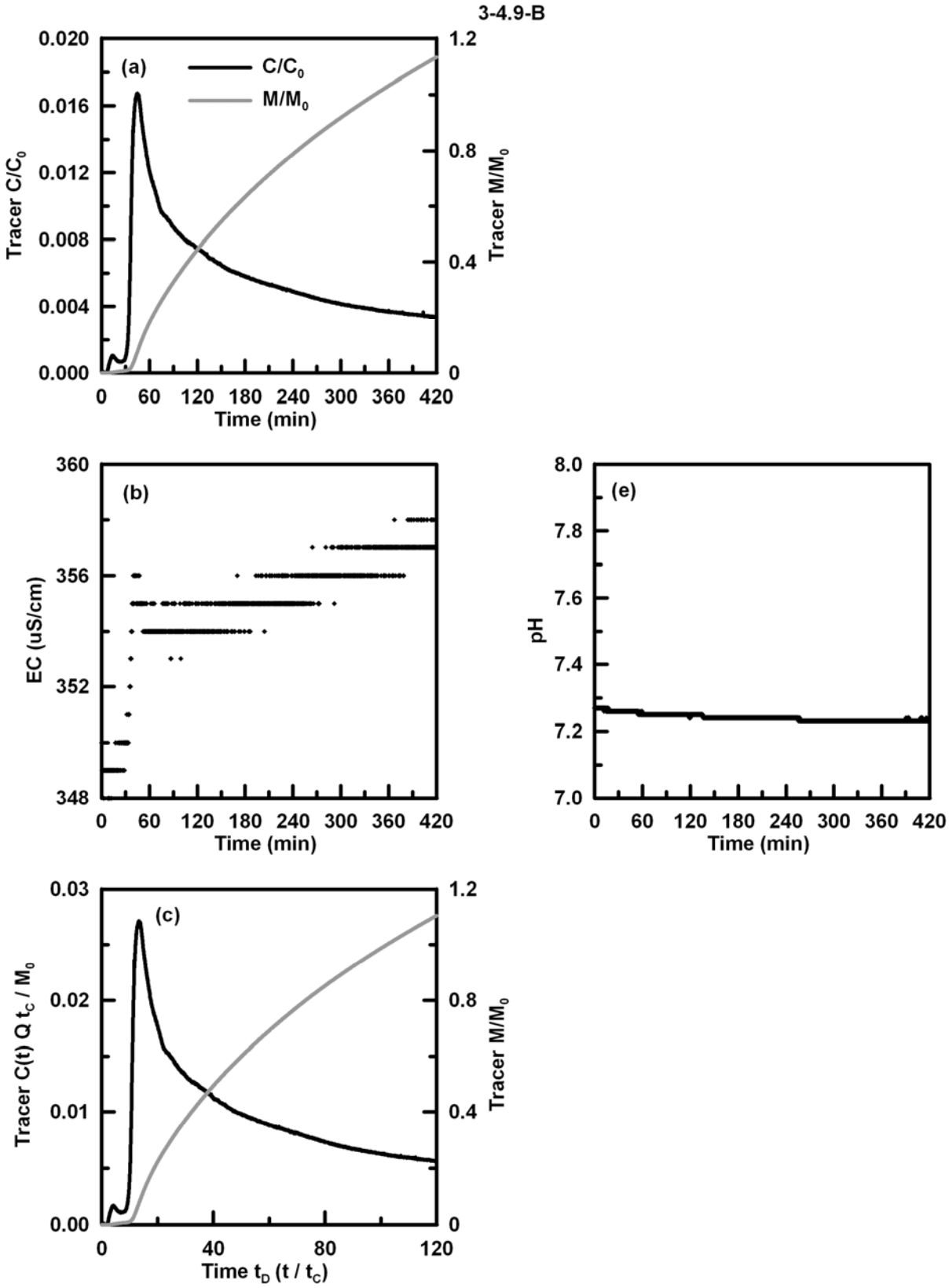

Figure B.12. BTCs and monitoring data for DFTT 3-4.9-B.

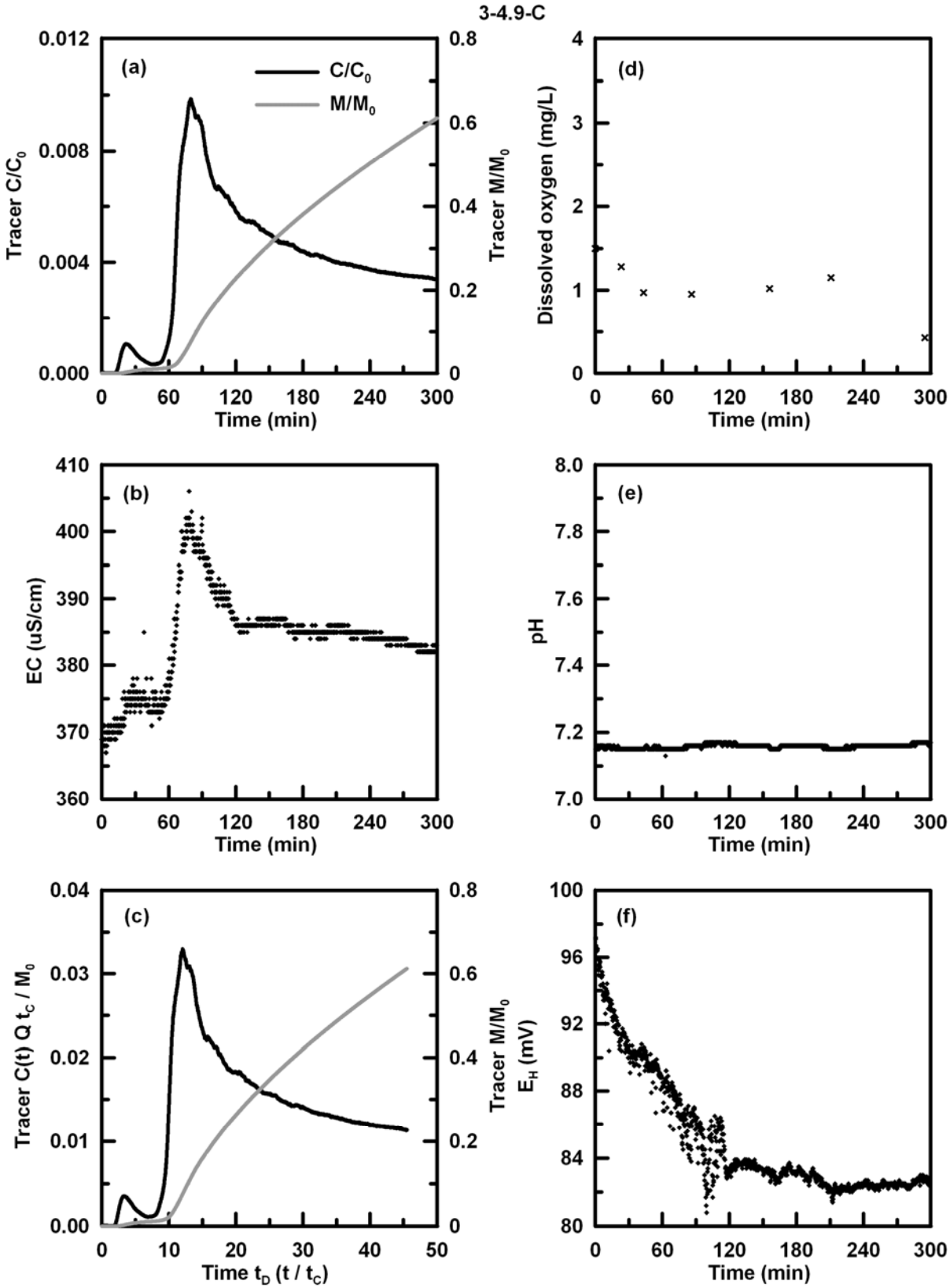

Figure B.13. BTCs and monitoring data for DFTT 3-4.9-C.

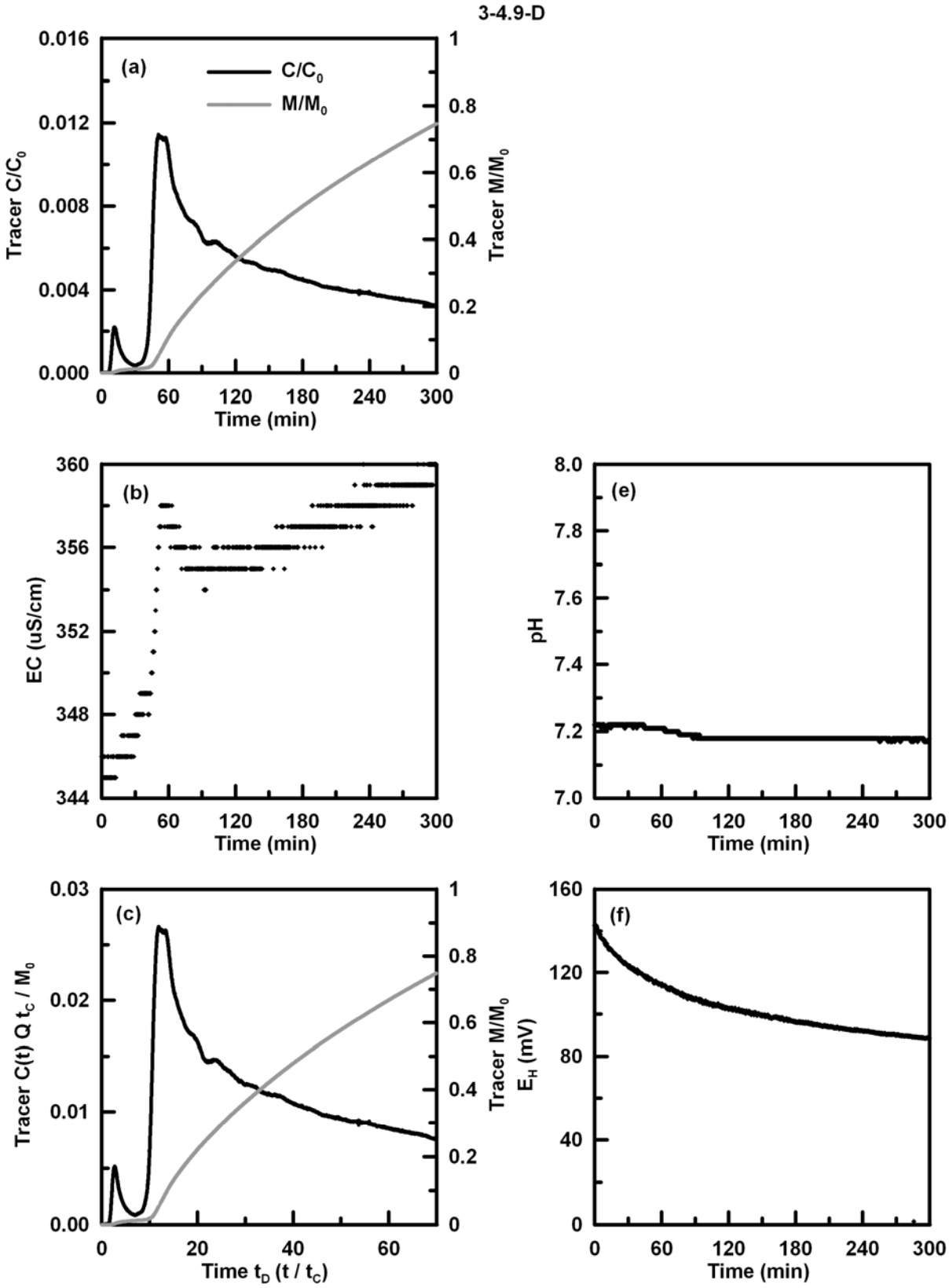

Figure B.14. BTCs and monitoring data for DFTT 3-4.9-D.

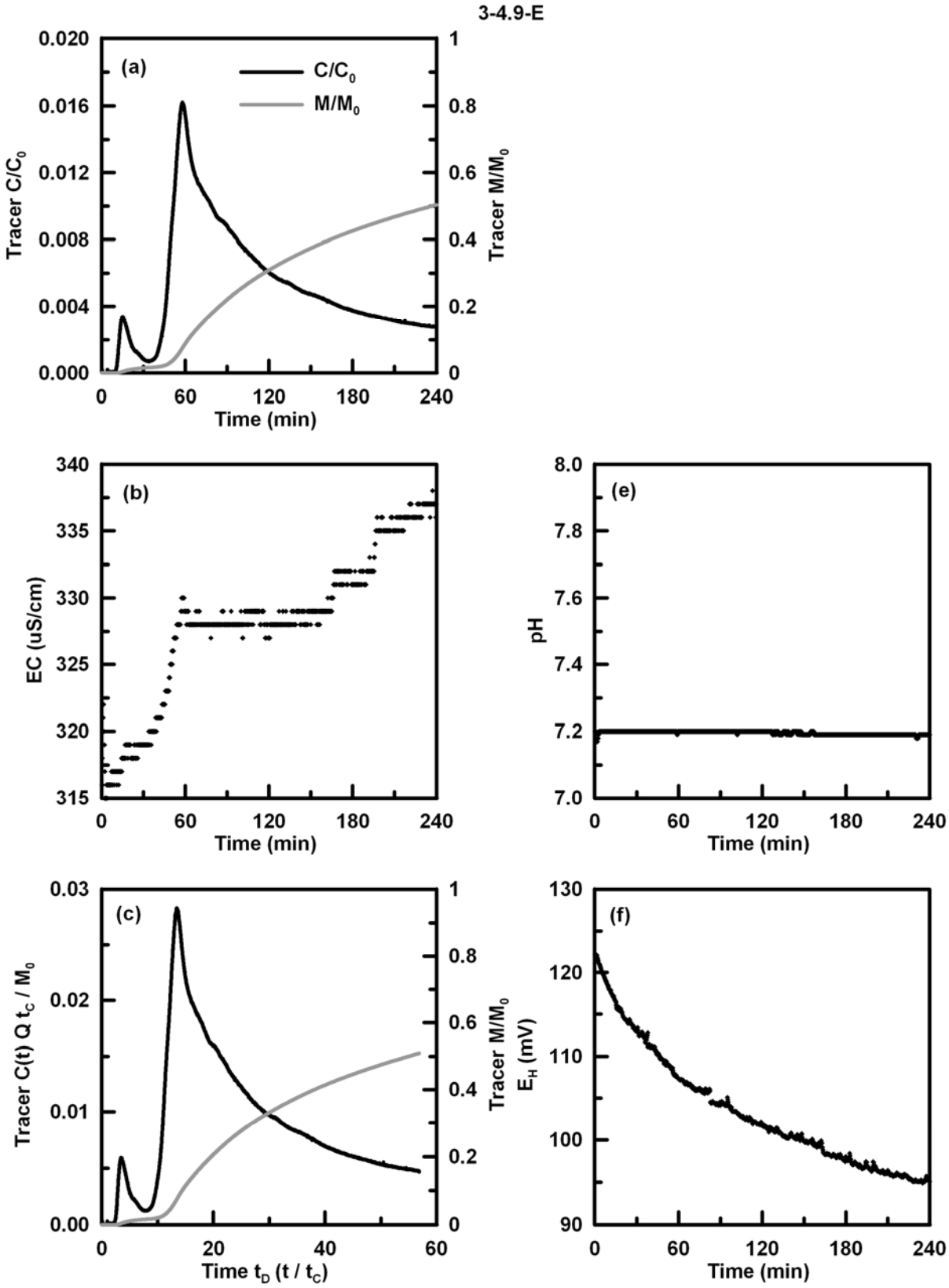

Figure B.15. BTCs and monitoring data for DFTT 3-4.9-E.

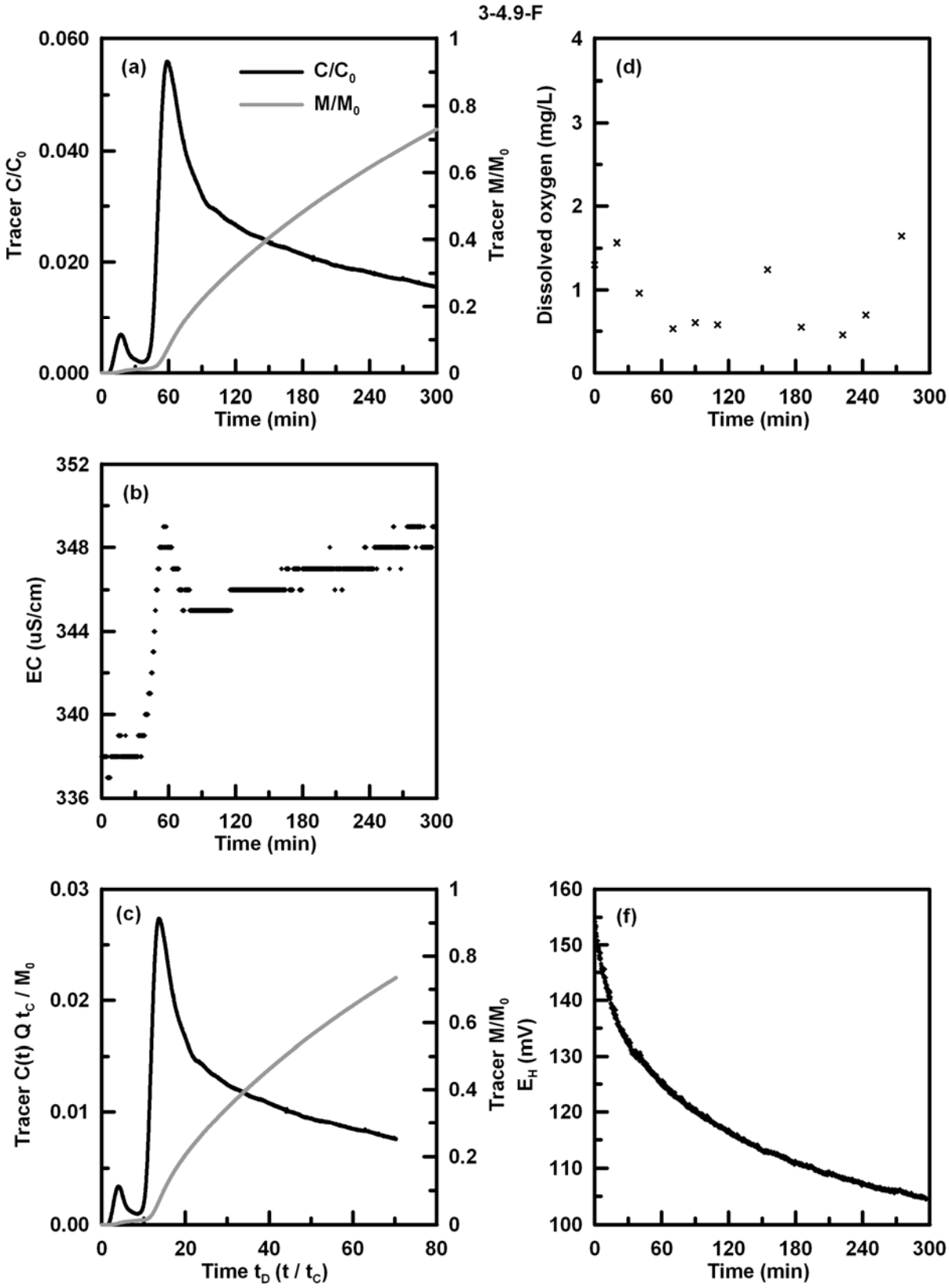

Figure B.16. BTCs and monitoring data for DFTT 3-4.9-F.

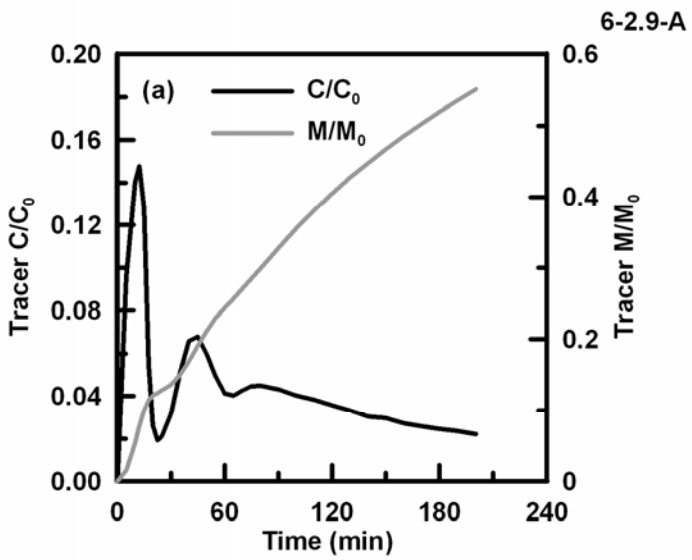

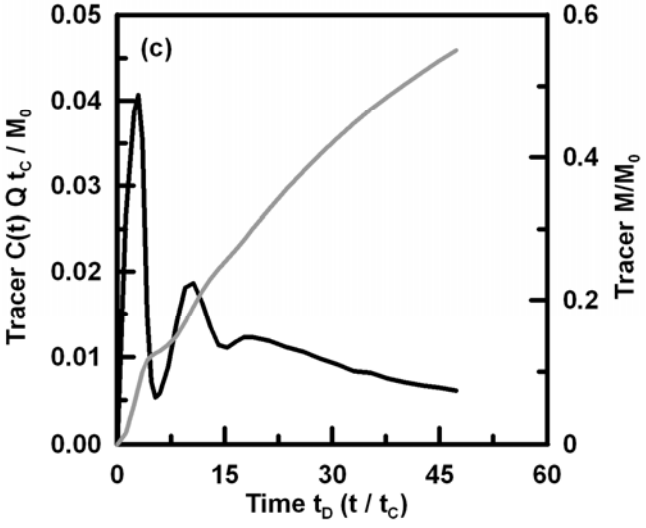

Figure B.17. BTCs for DFTT 6-2.9-A.

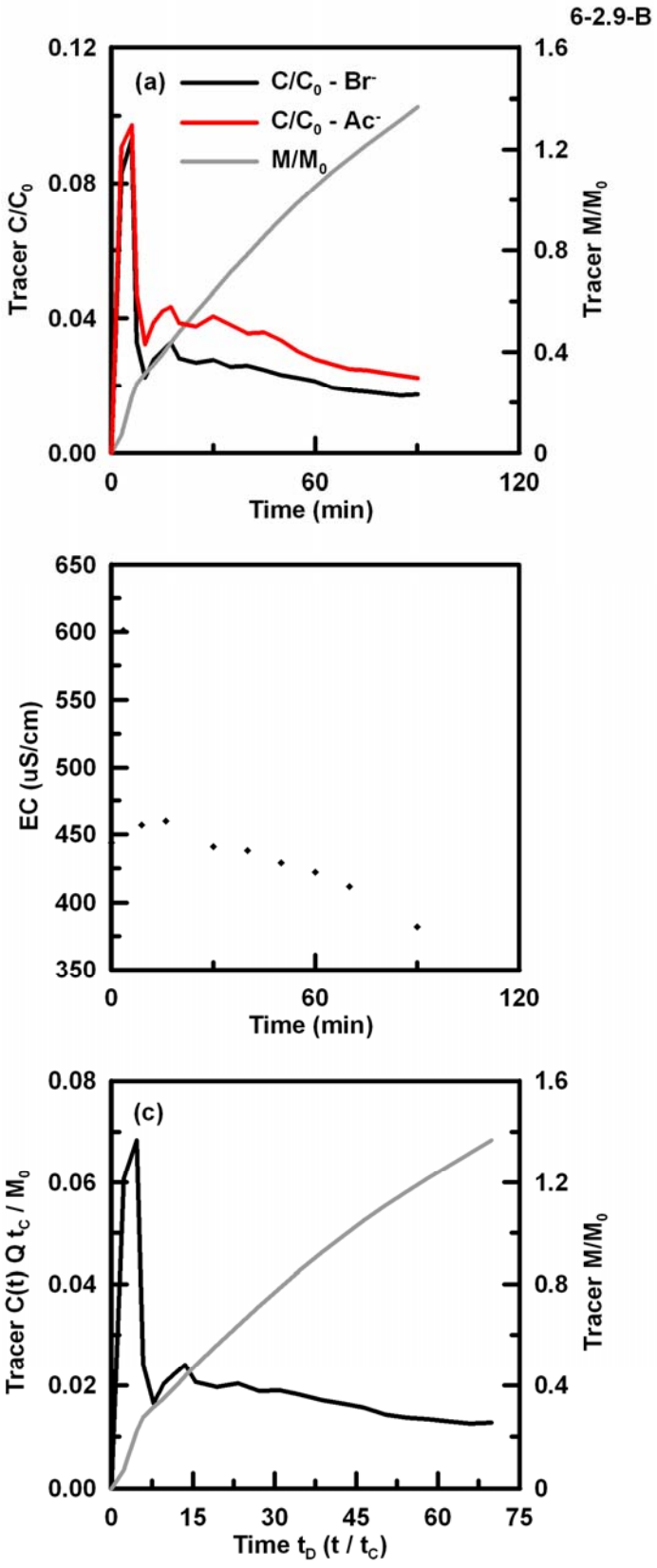

Figure B.18. BTCs and monitoring data for DFTT 6-2.9-B.

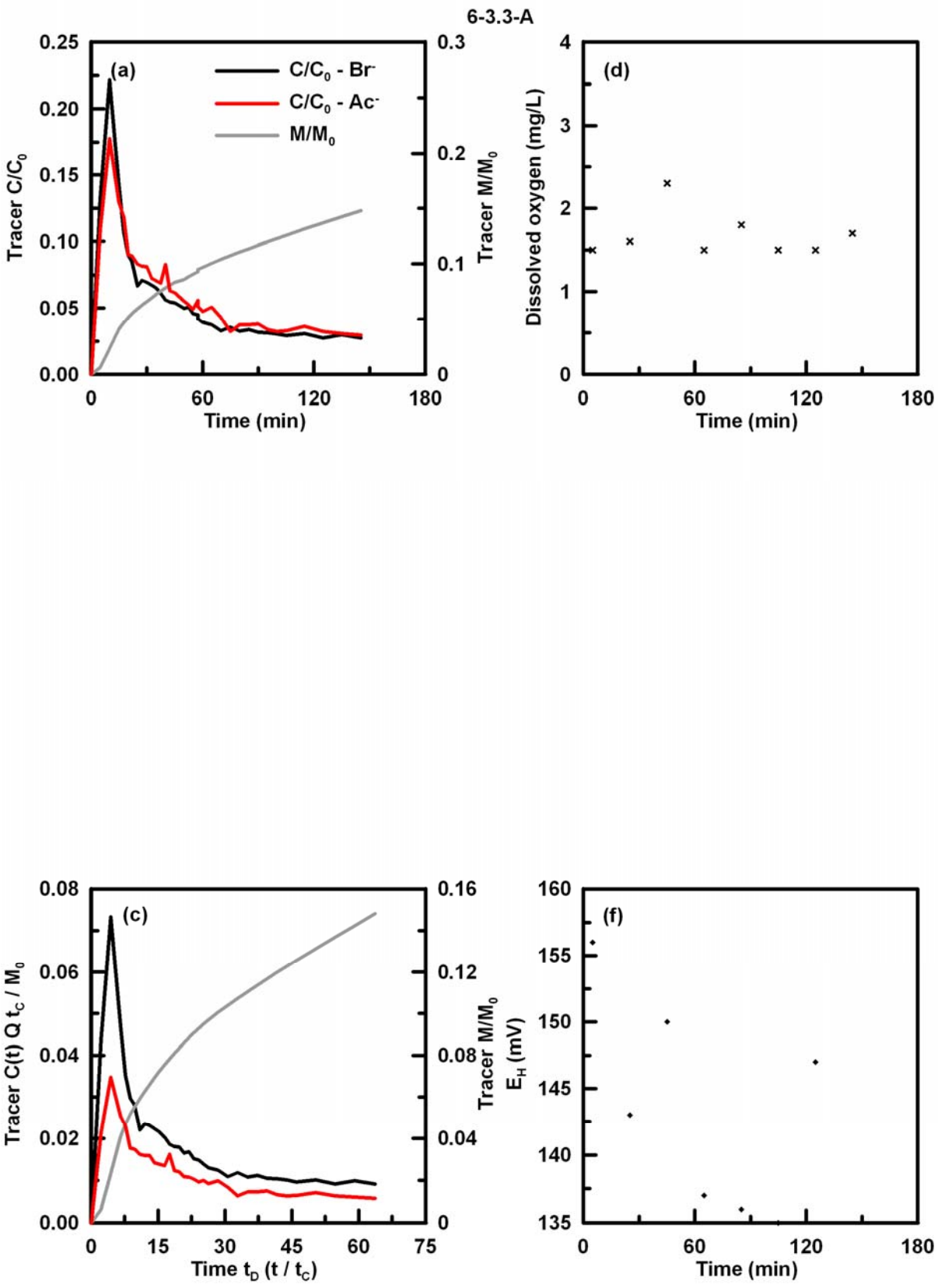

Figure B.19. BTCs and monitoring data for DFTT 6-3.3-A.

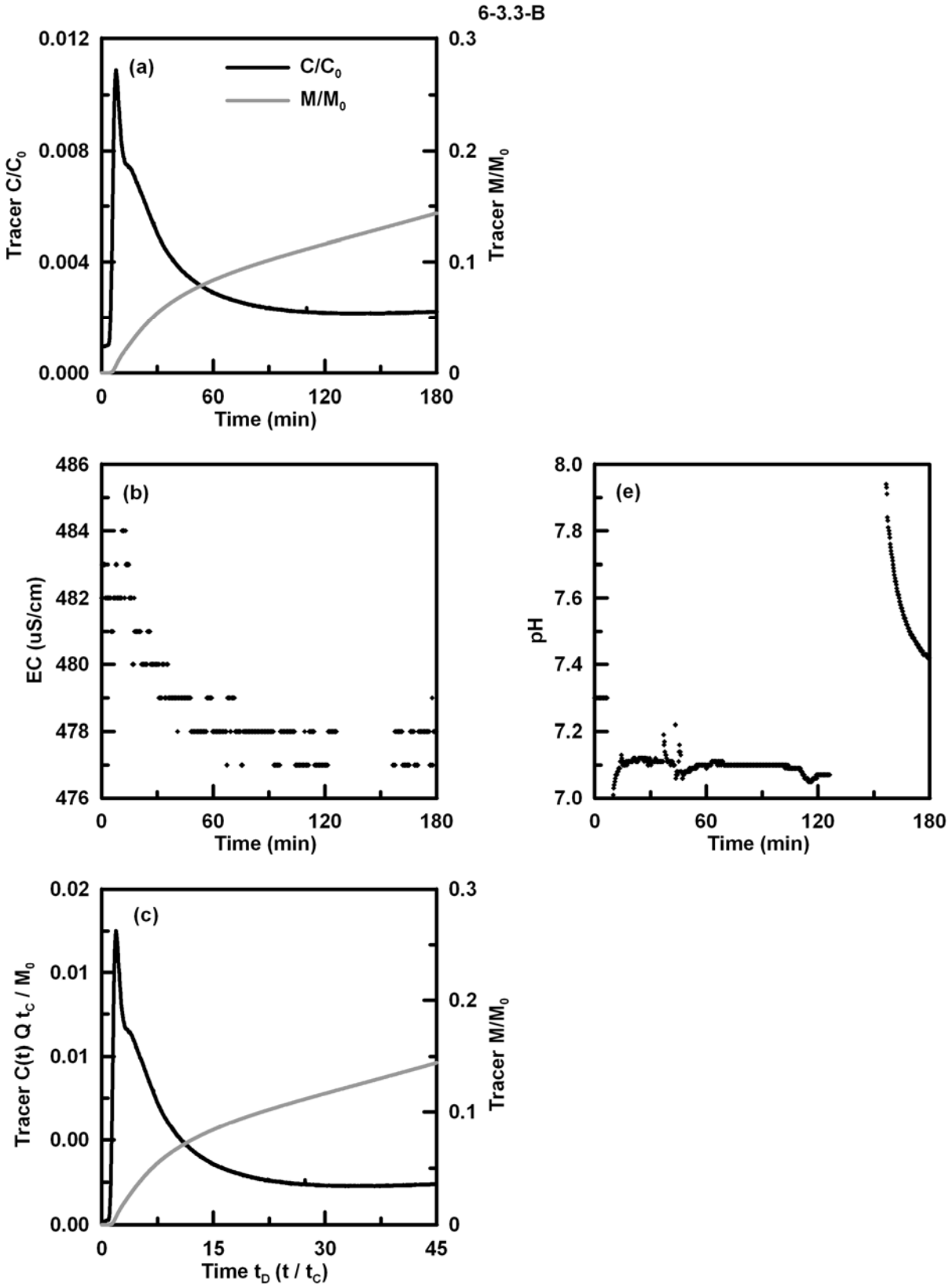

Figure B.20. BTCs and monitoring data for DFTT 6-3.3-B.

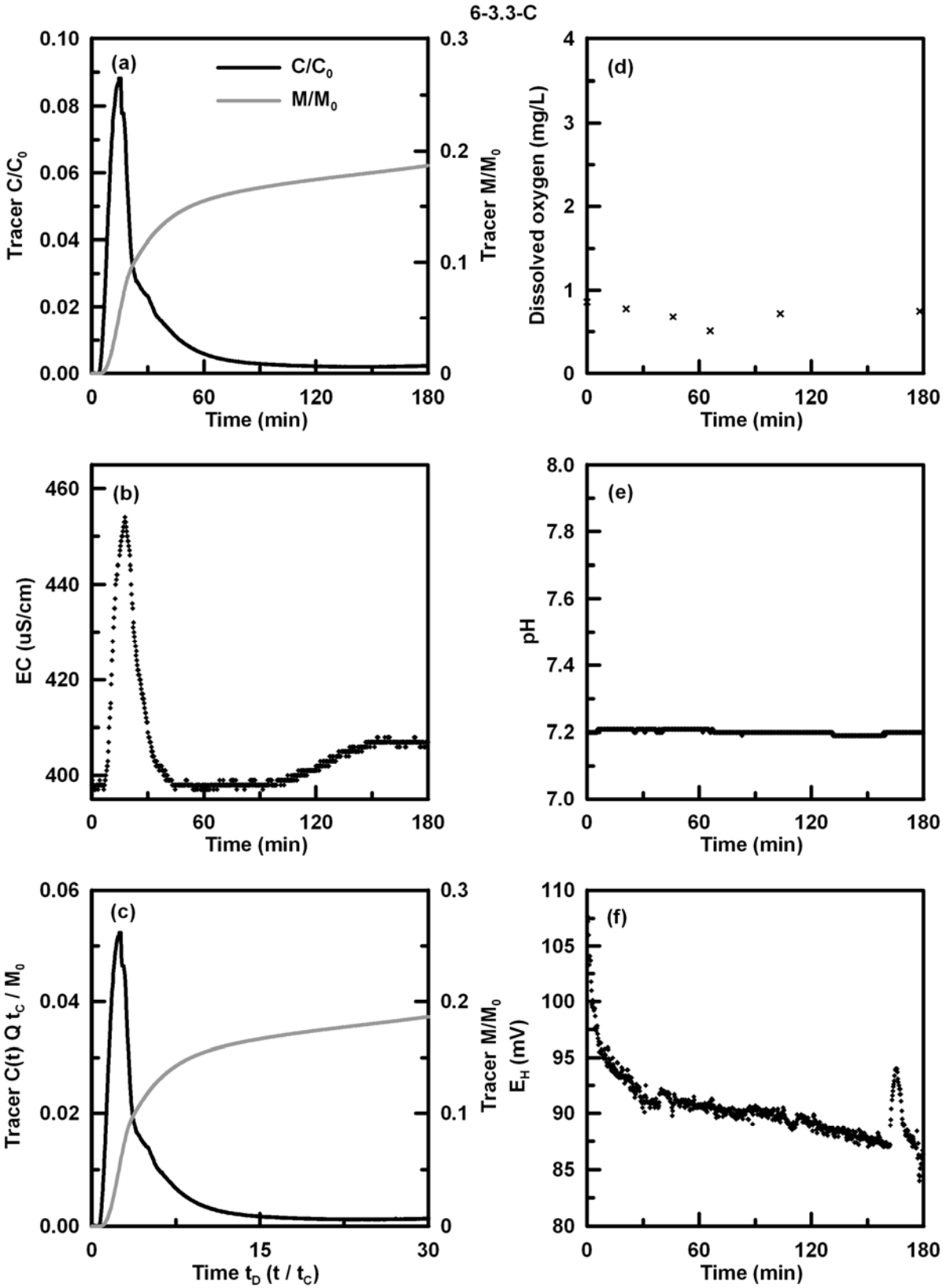

Figure B.21. BTCs and monitoring data for DFTT 6-3.3-C.

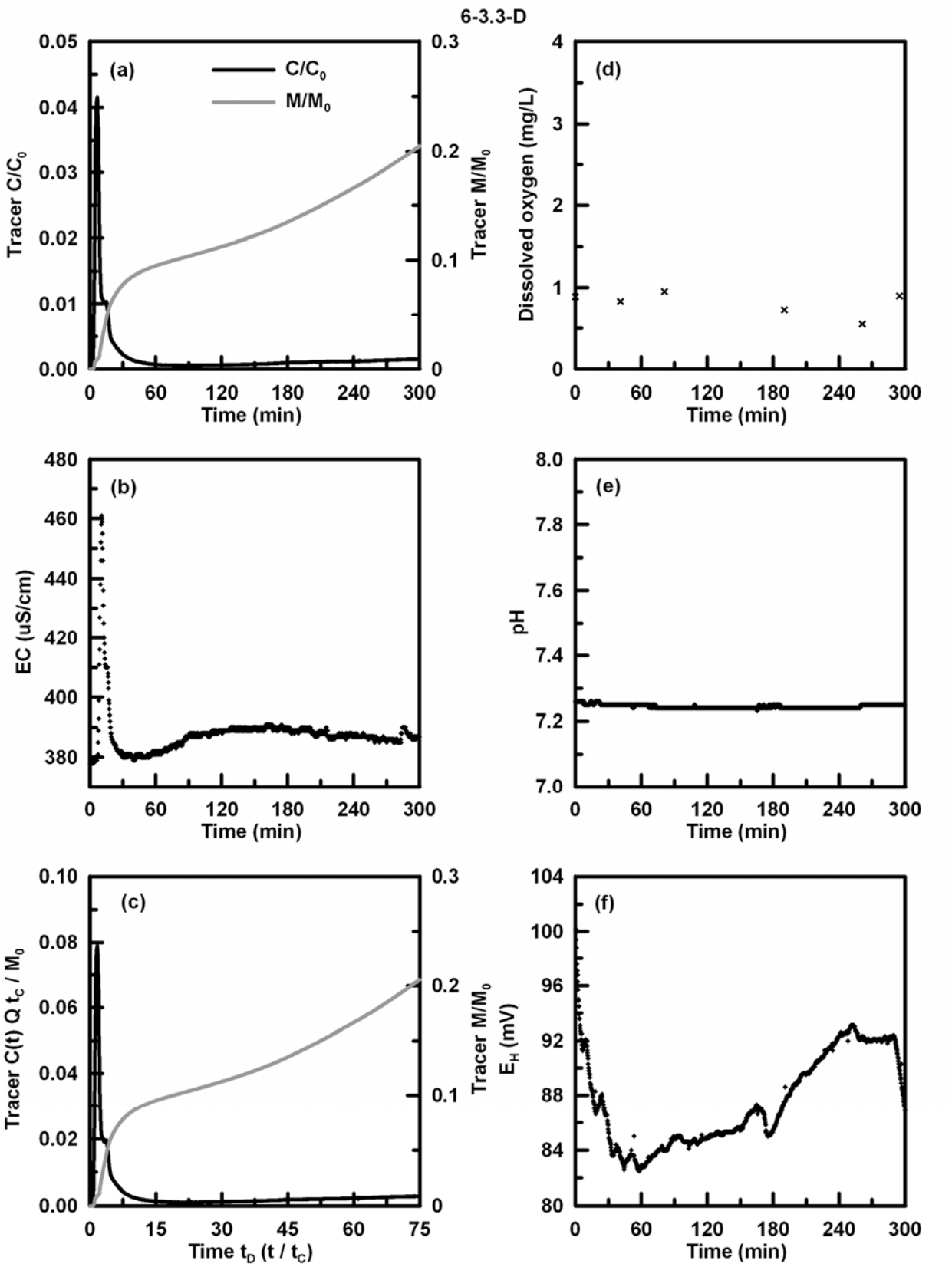

Figure B.22. BTCs and monitoring data for DFTT 6-3.3-D.

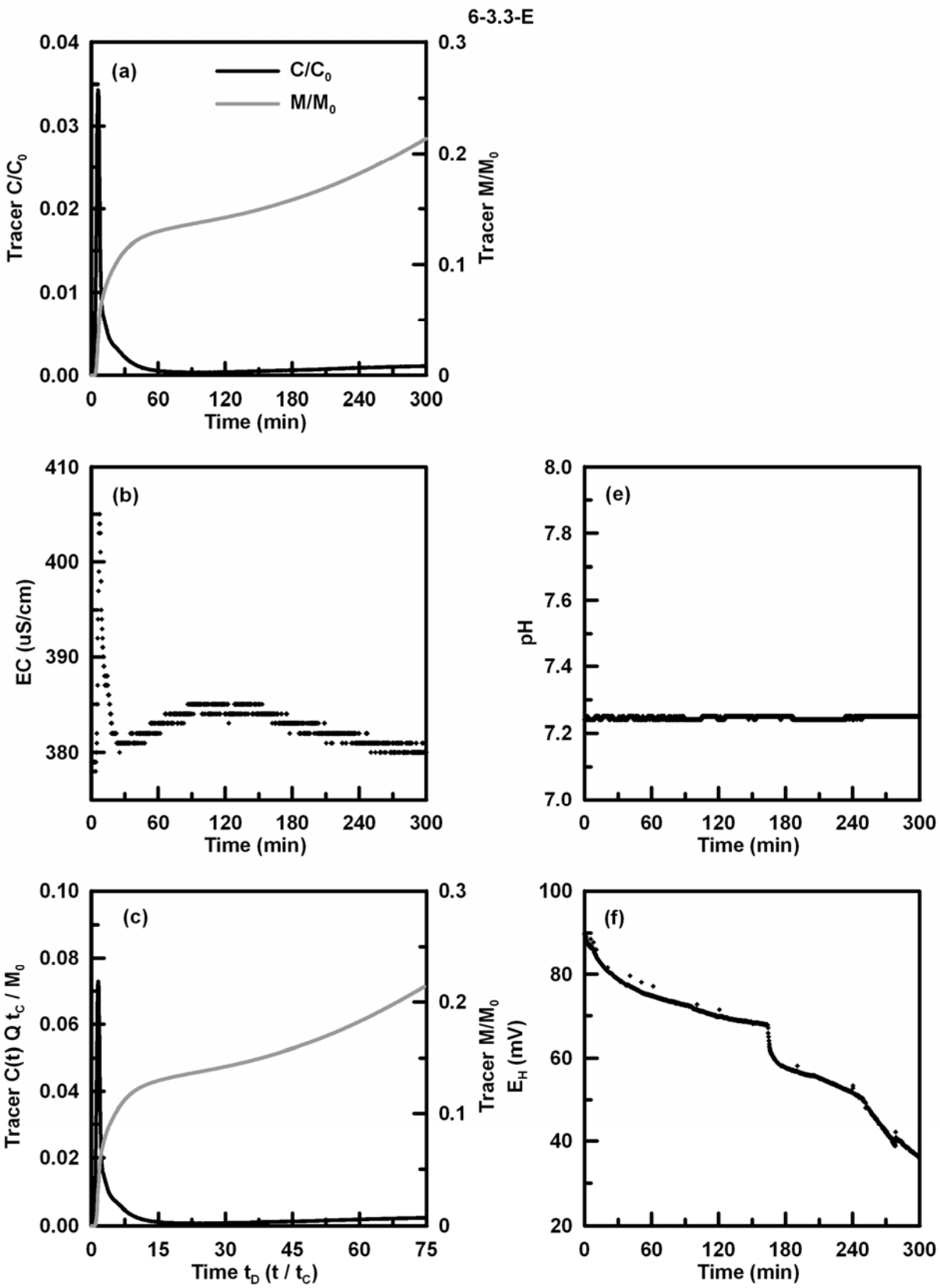

Figure B.23. BTCs and monitoring data for DFTT 6-3.3-E.

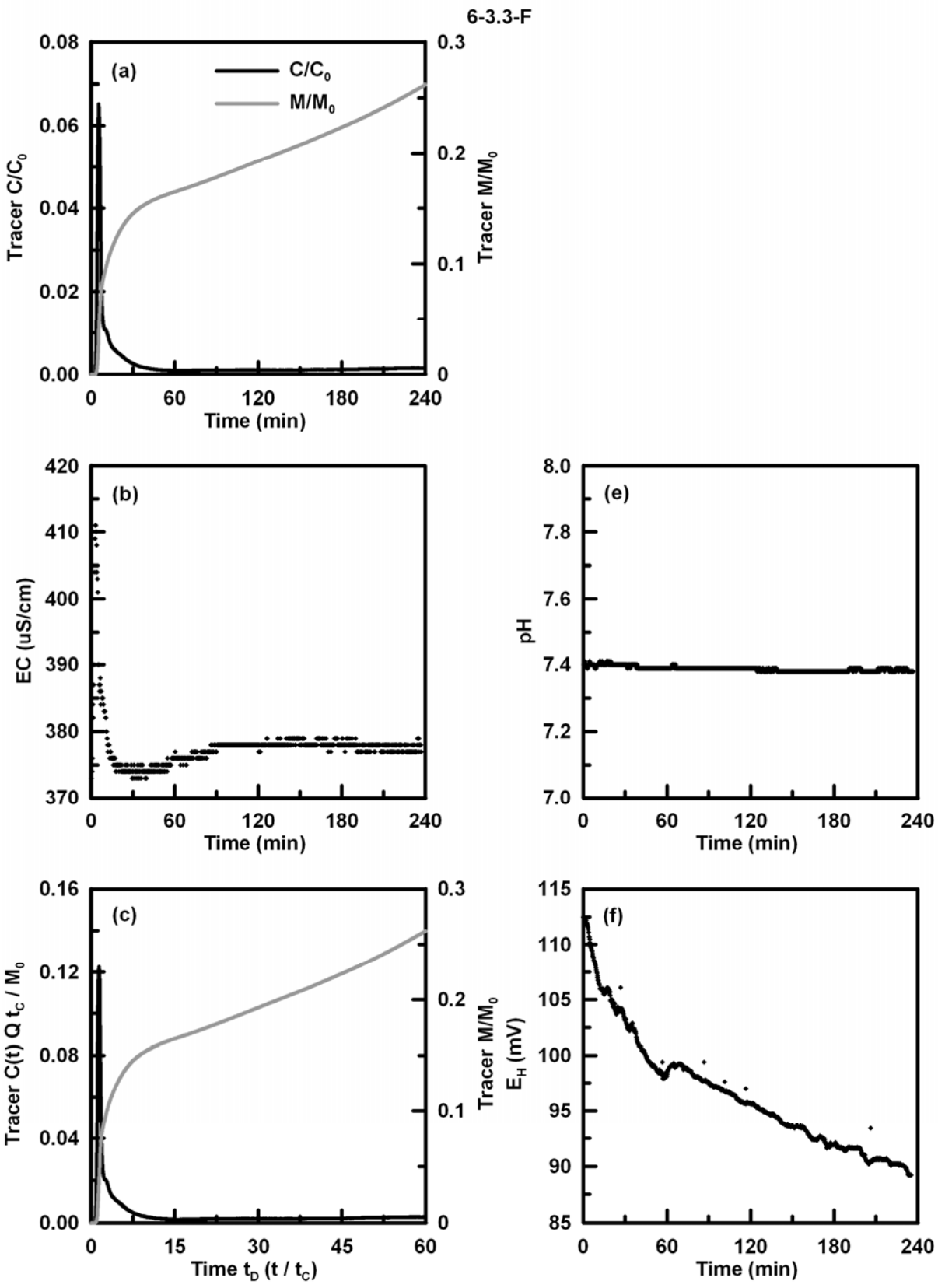

Figure B.24. BTCs and monitoring data for DFTT 6-3.3-F.

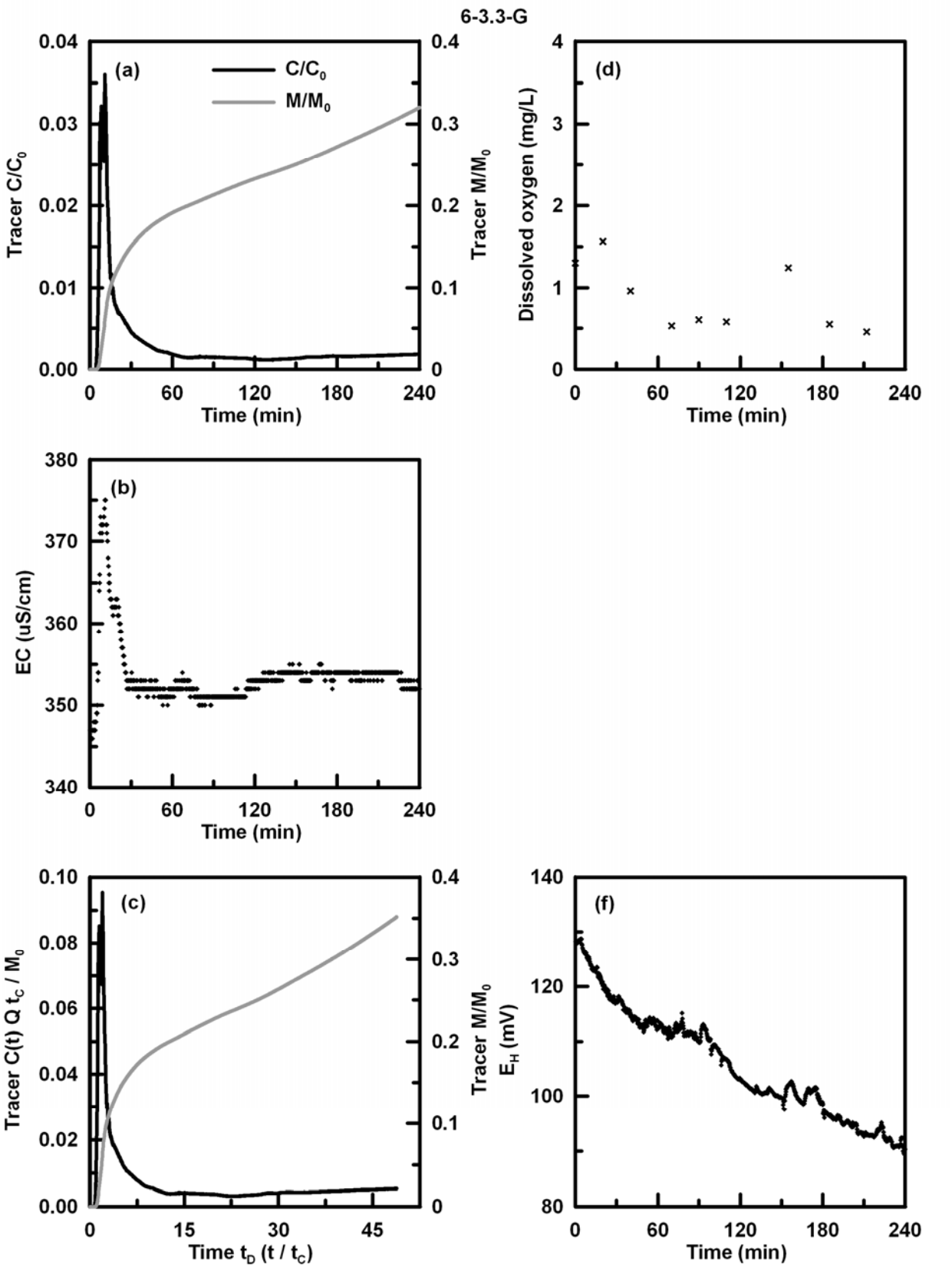

Figure B.25. BTCs and monitoring data for DFTT 6-3.3-G.

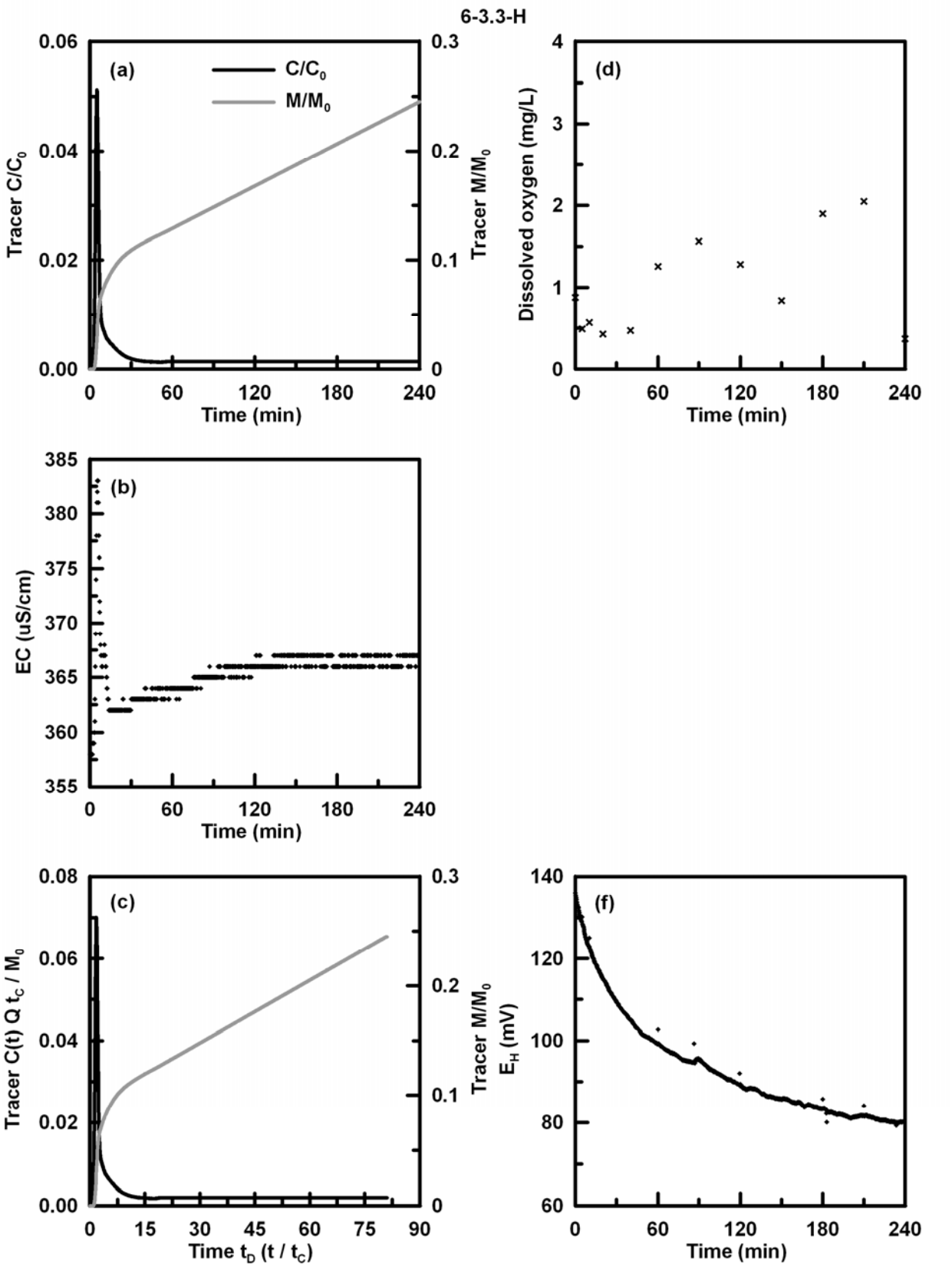

Figure B.26. BTCs and monitoring data for DFTT 6-3.3-H.

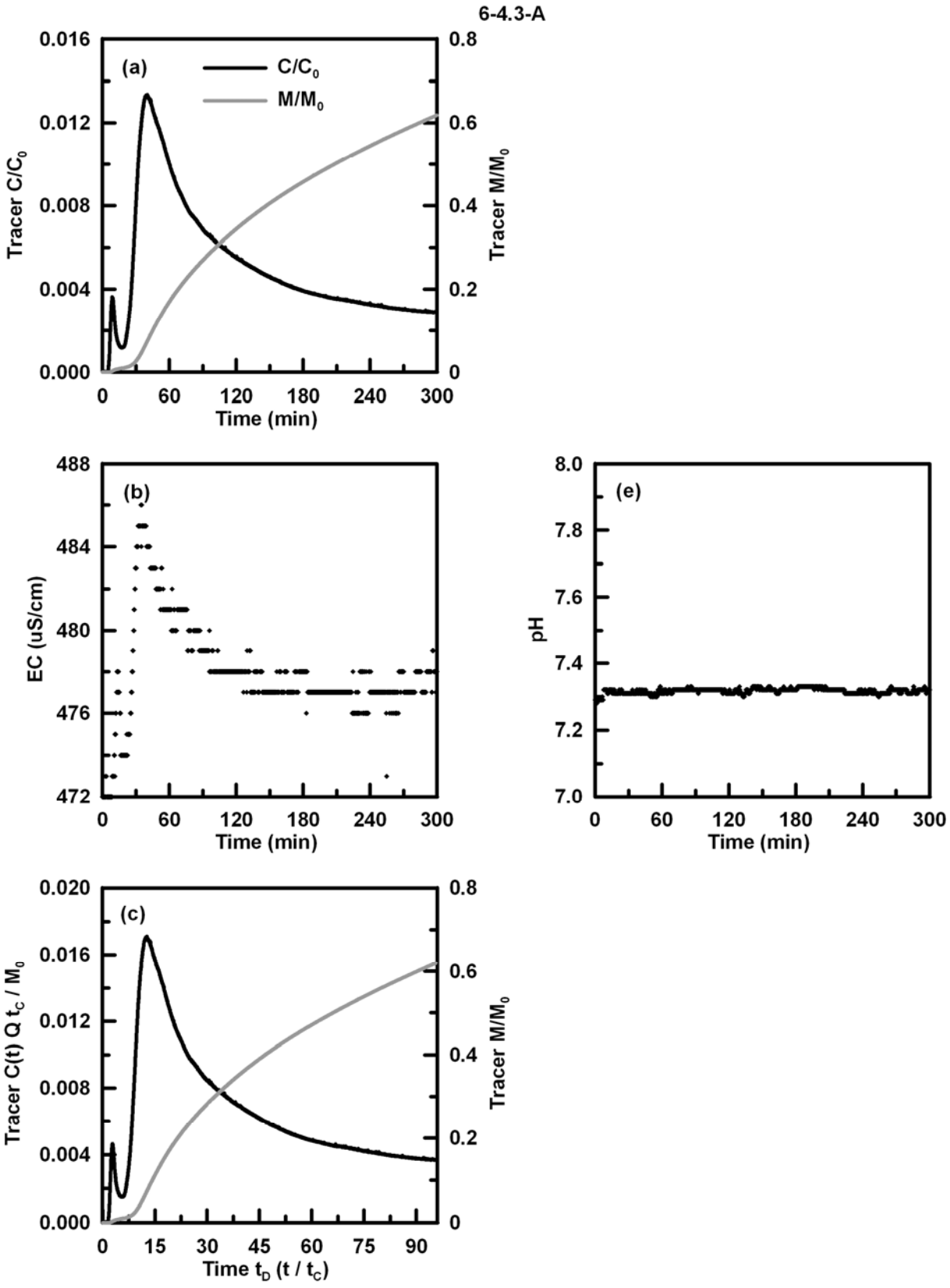

Figure B.27. BTCs and monitoring data for DFTT 6-4.3-A.

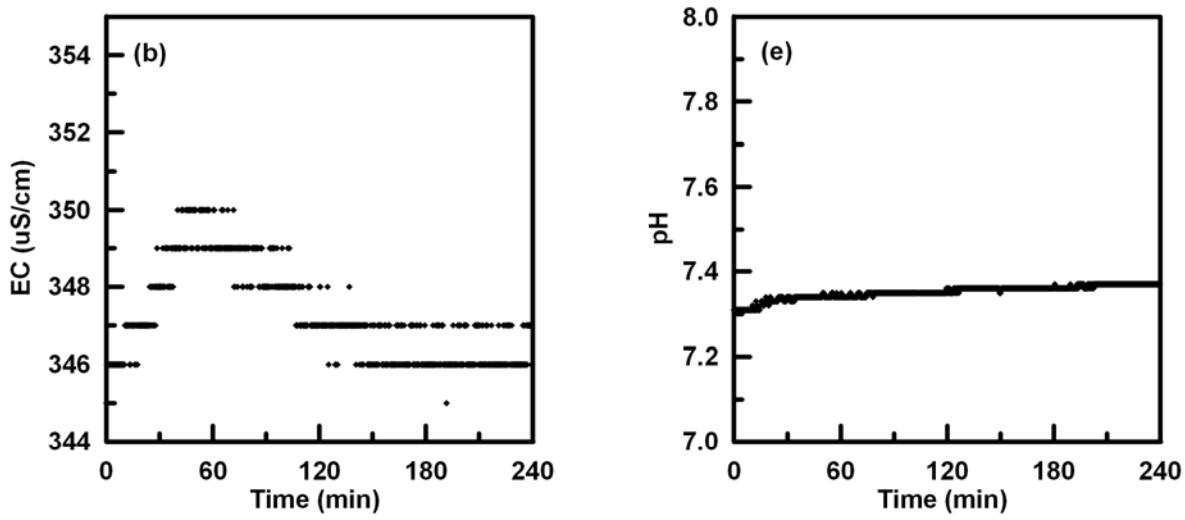

Figure B.28. BTCs and monitoring data for DFTT 6-4.3-B.

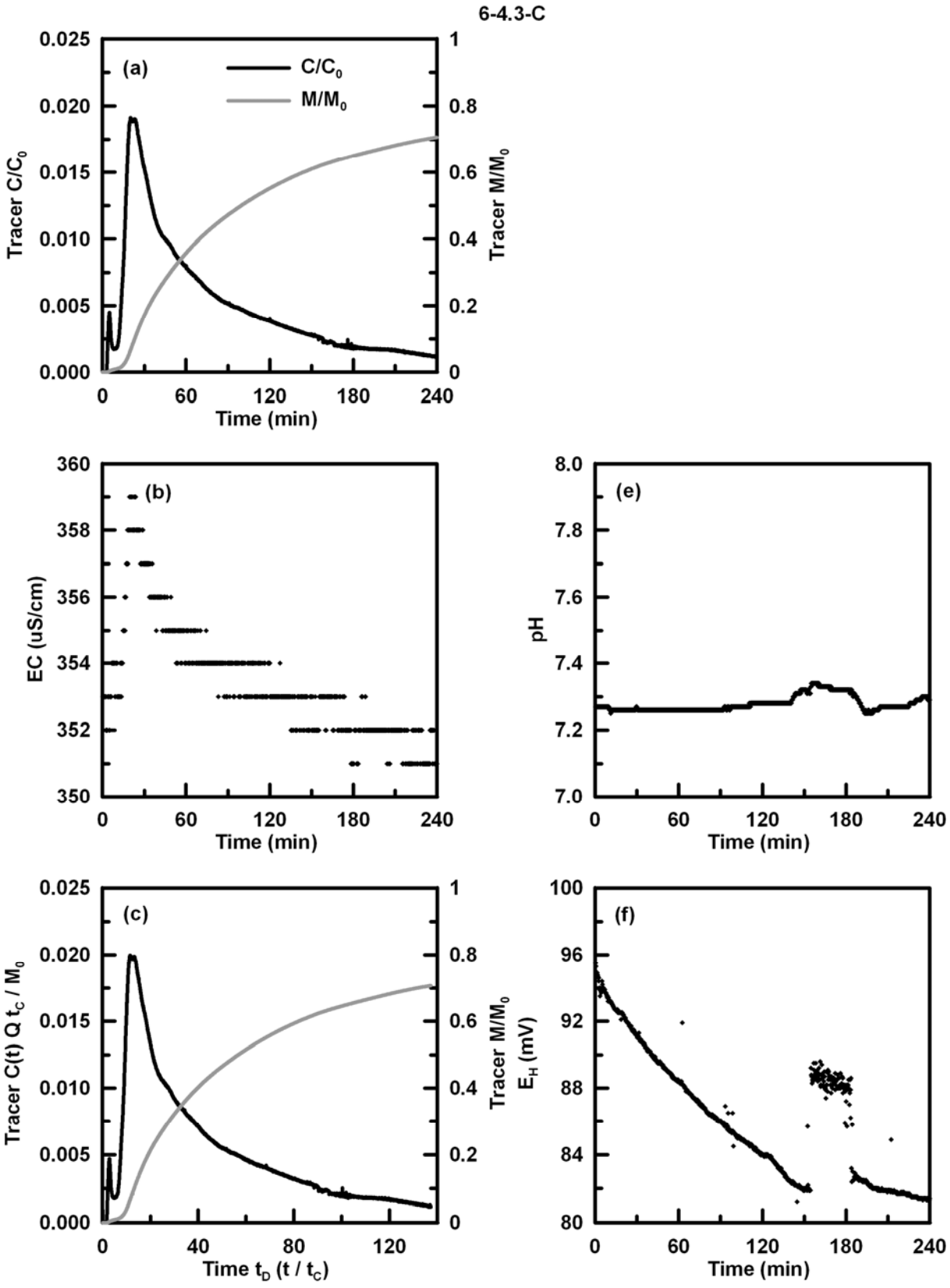

Figure B.29. BTCs and monitoring data for DFTT 6-4.3-C.

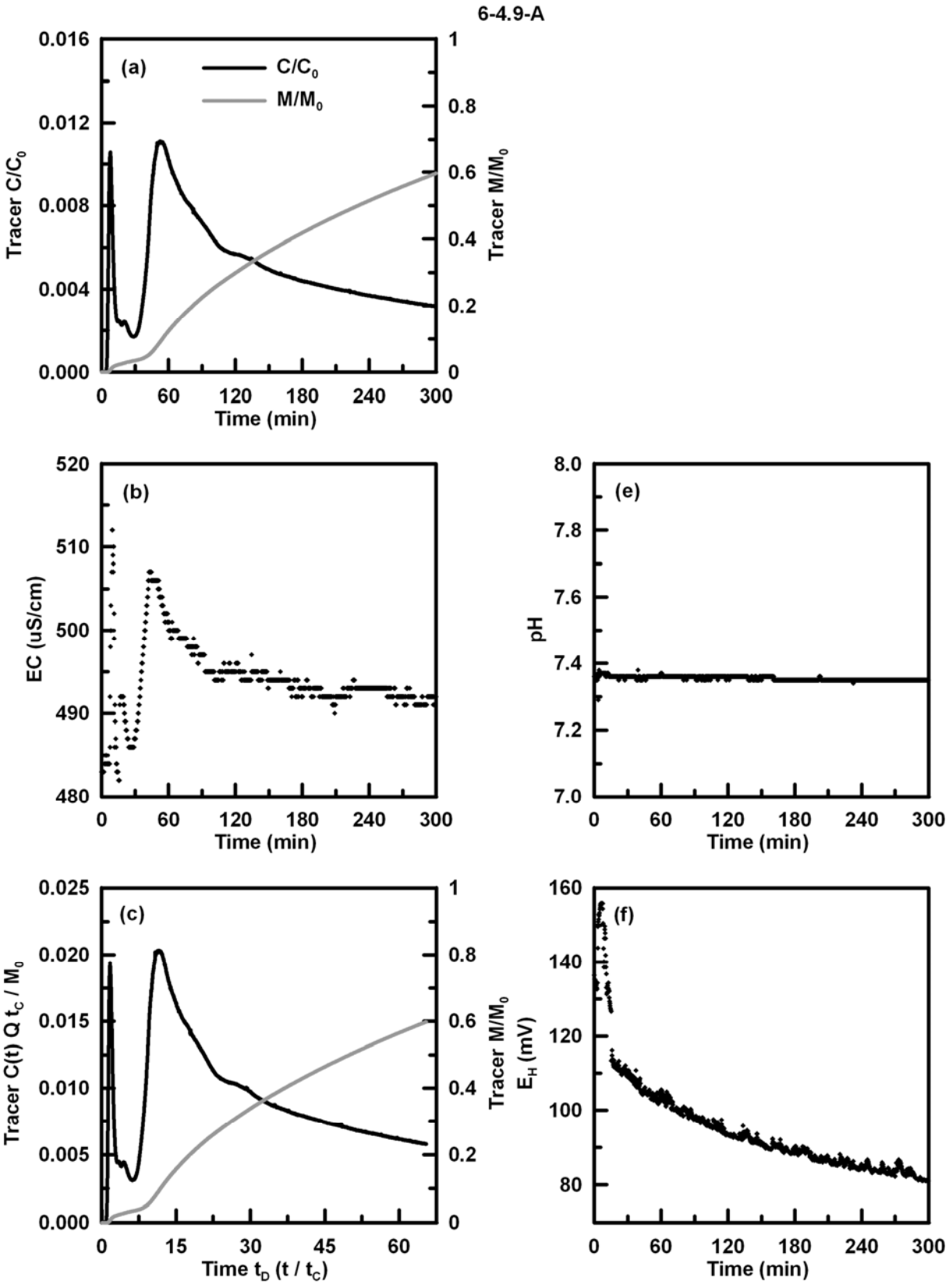

Figure B.30. BTCs and monitoring data for DFTT 6-4.9-A.

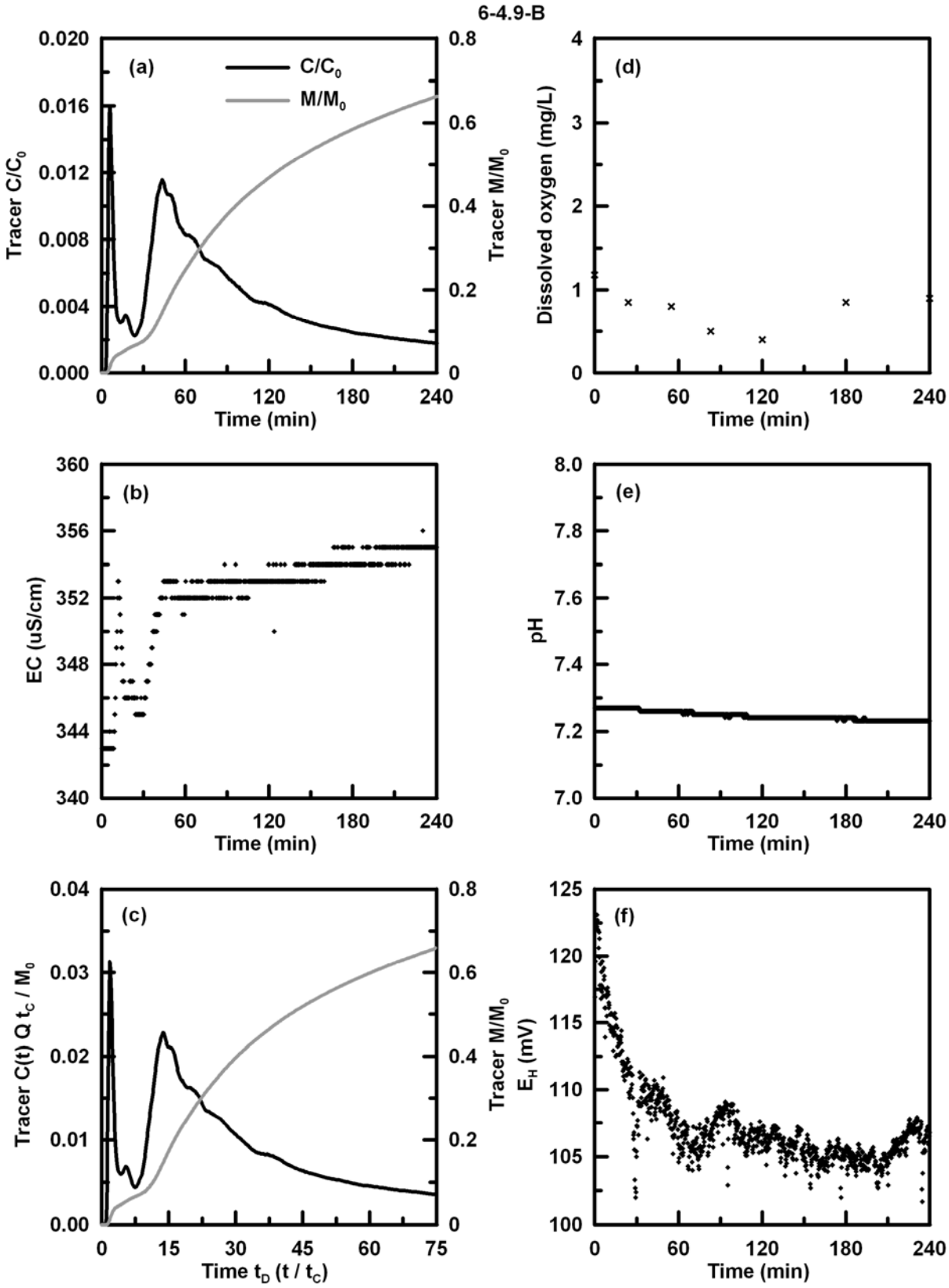

Figure B.31. BTCs and monitoring data for DFTT 6-4.9-B.

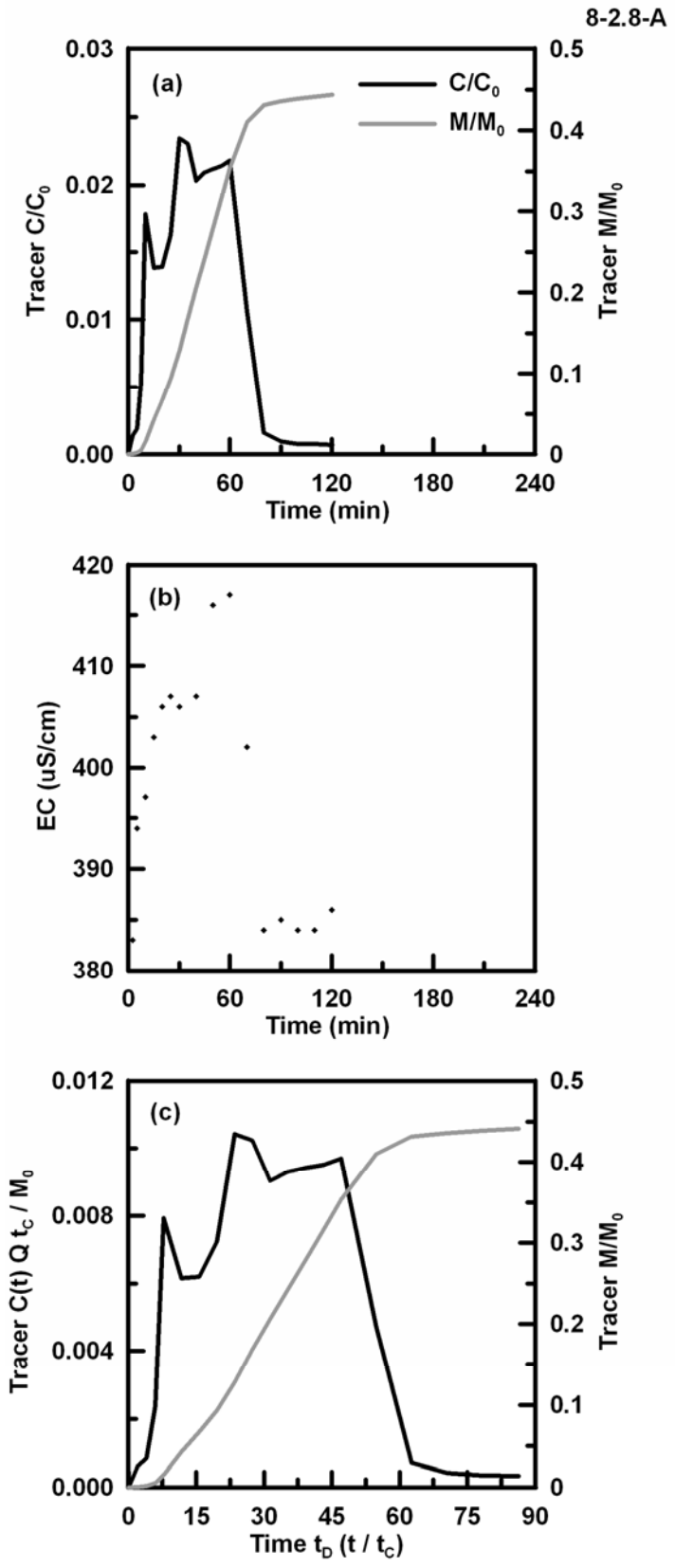

Figure B.32. BTCs and monitoring data for DFTT 8-2.8-A.

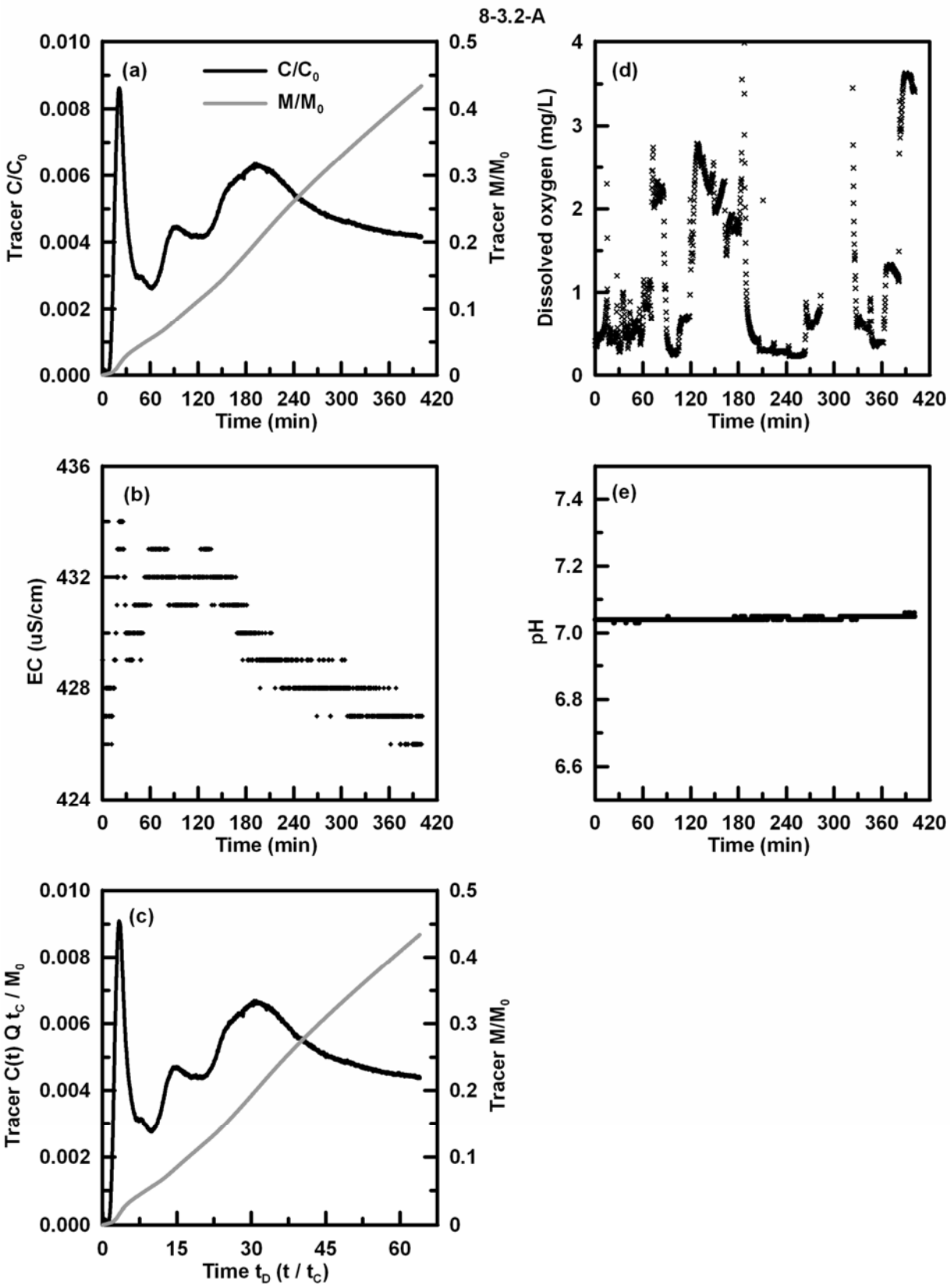

Figure B.33. BTCs and monitoring data for DFTT 8-3.2-A.

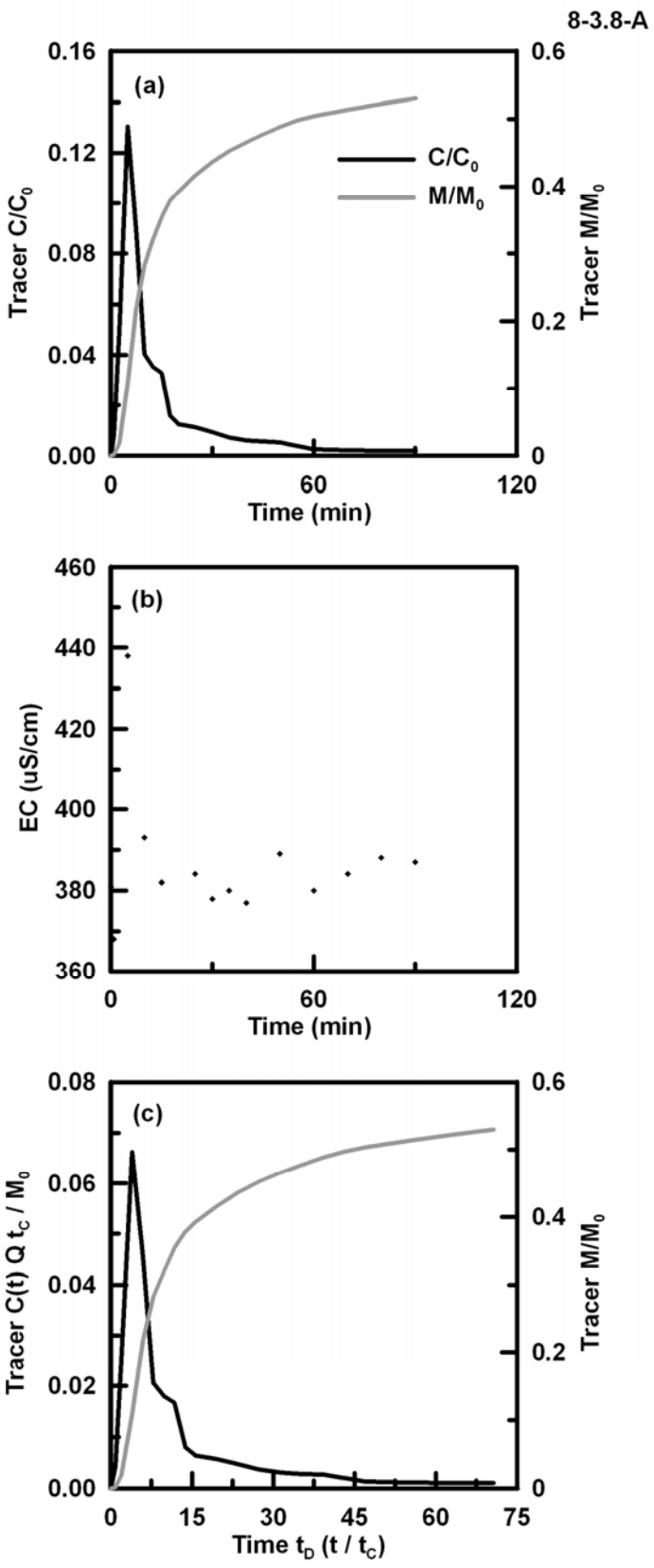

Figure B.34. BTCs and monitoring data for DFTT 8-3.8-A.

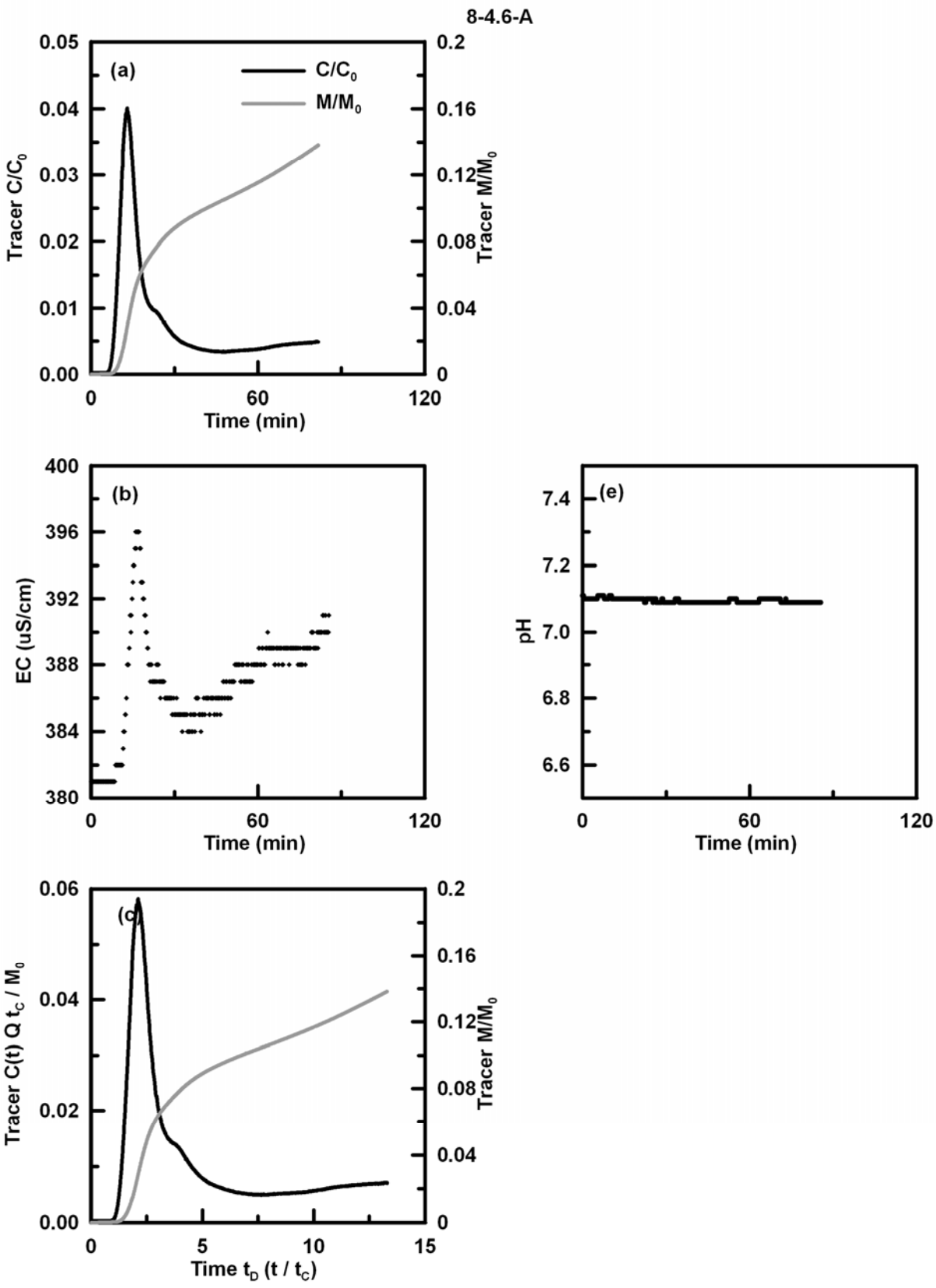

Figure B.35. BTCs and monitoring data for DFTT 8-4.6-A.

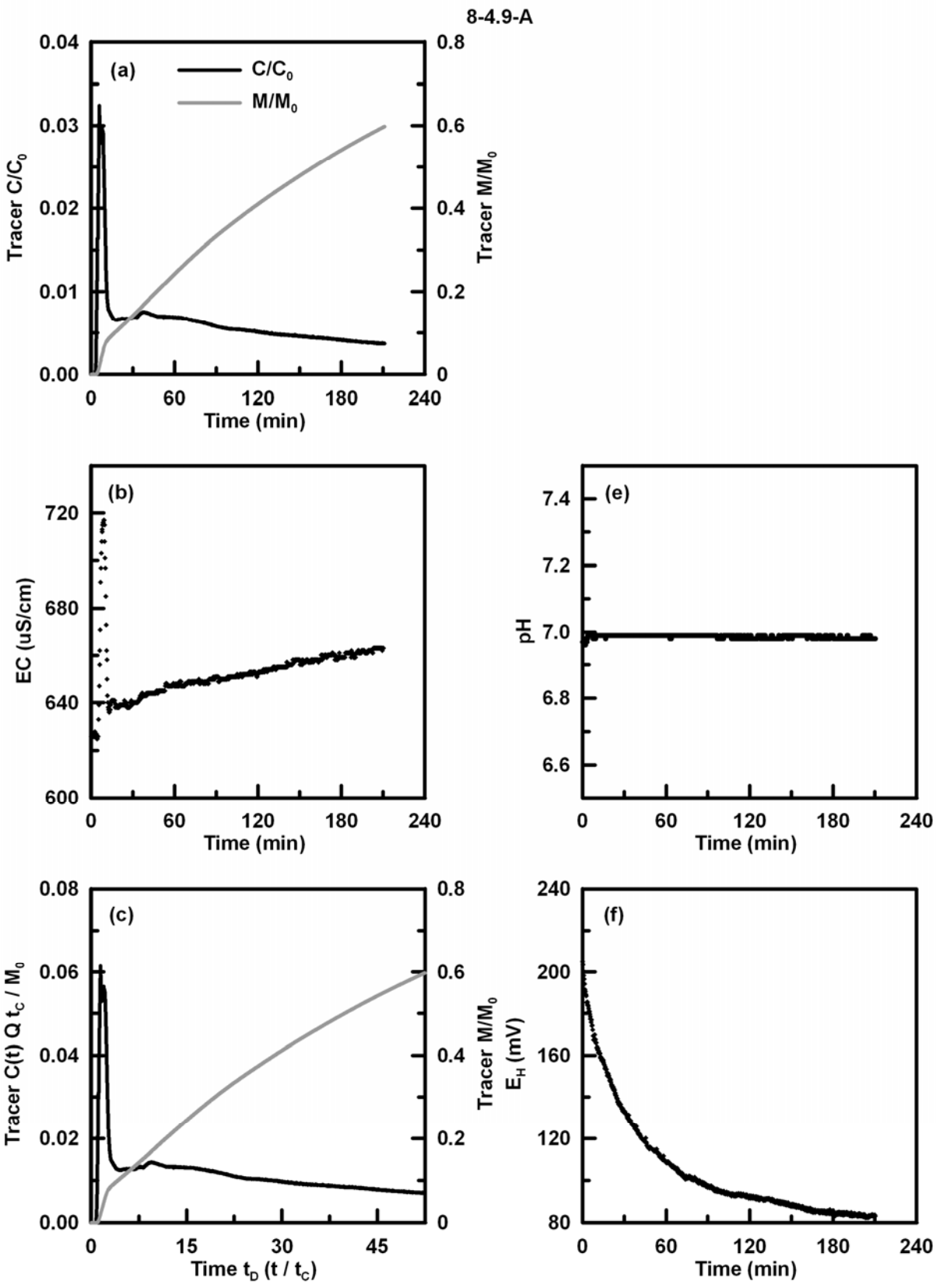

Figure B.36. BTCs and monitoring data for DFTT 8-4.9-A.

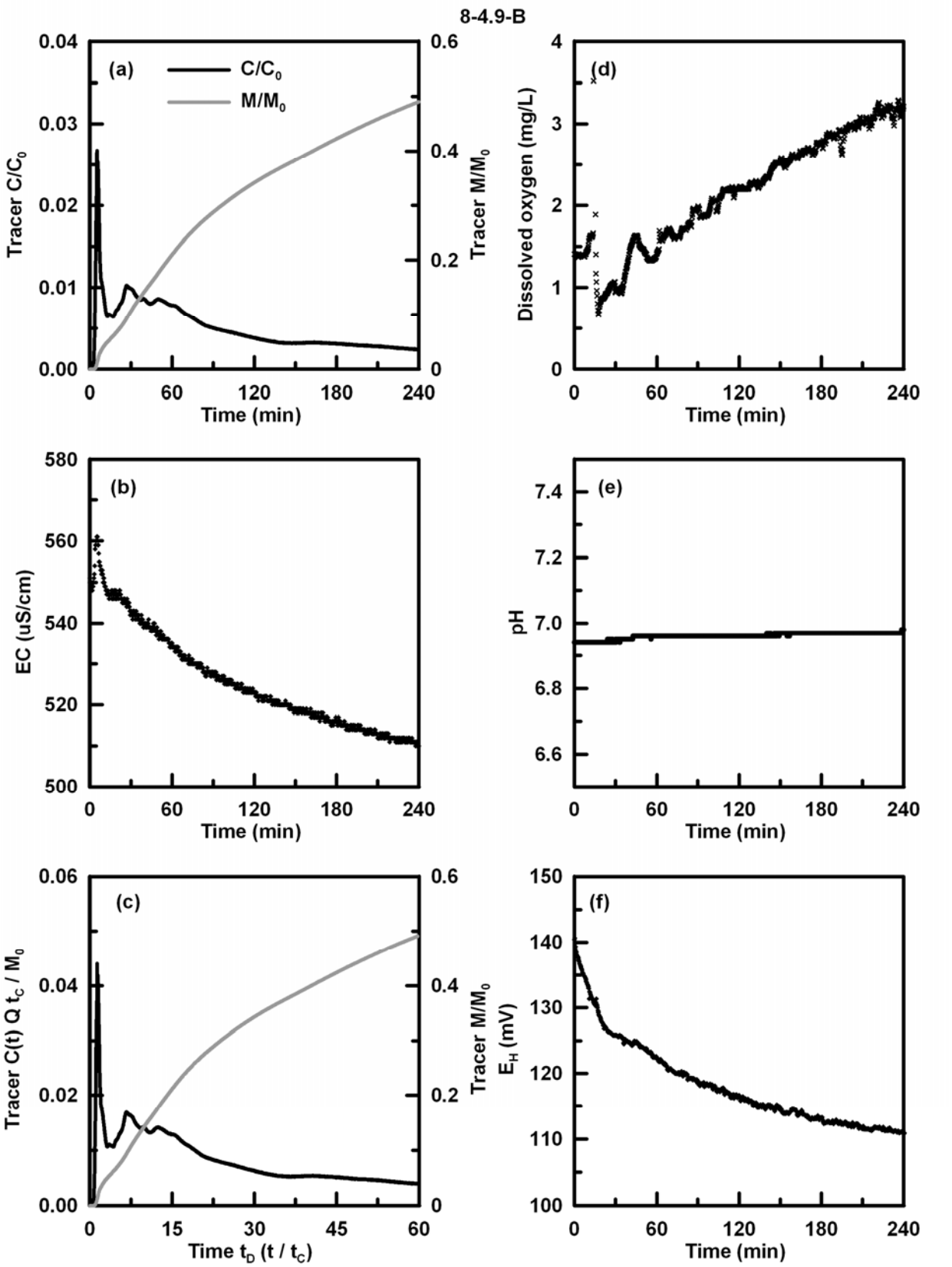

Figure B.37. BTCs and monitoring data for DFTT 8-3.8-B.

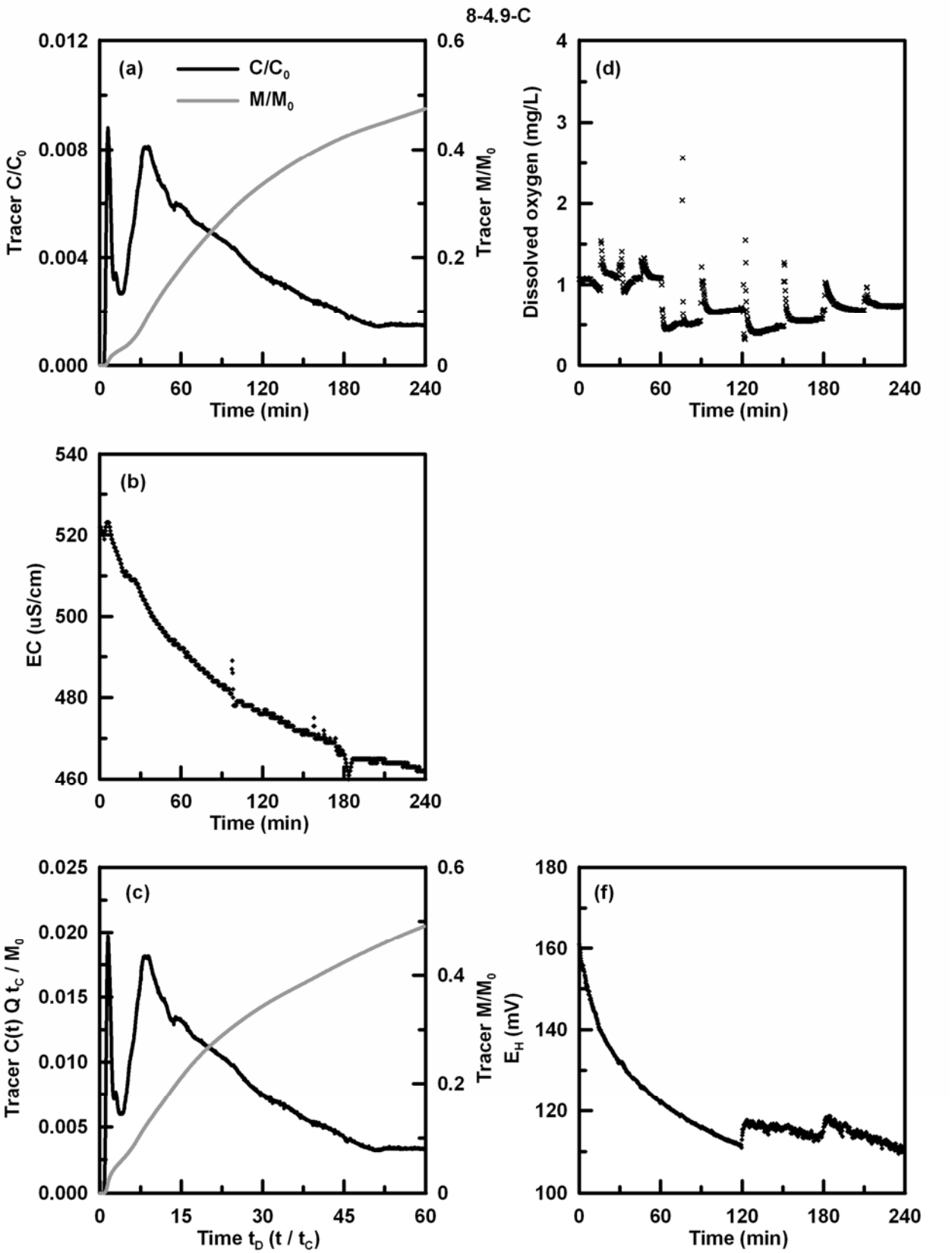

Figure B.38. BTCs and monitoring data for DFTT 8-3.8-C.

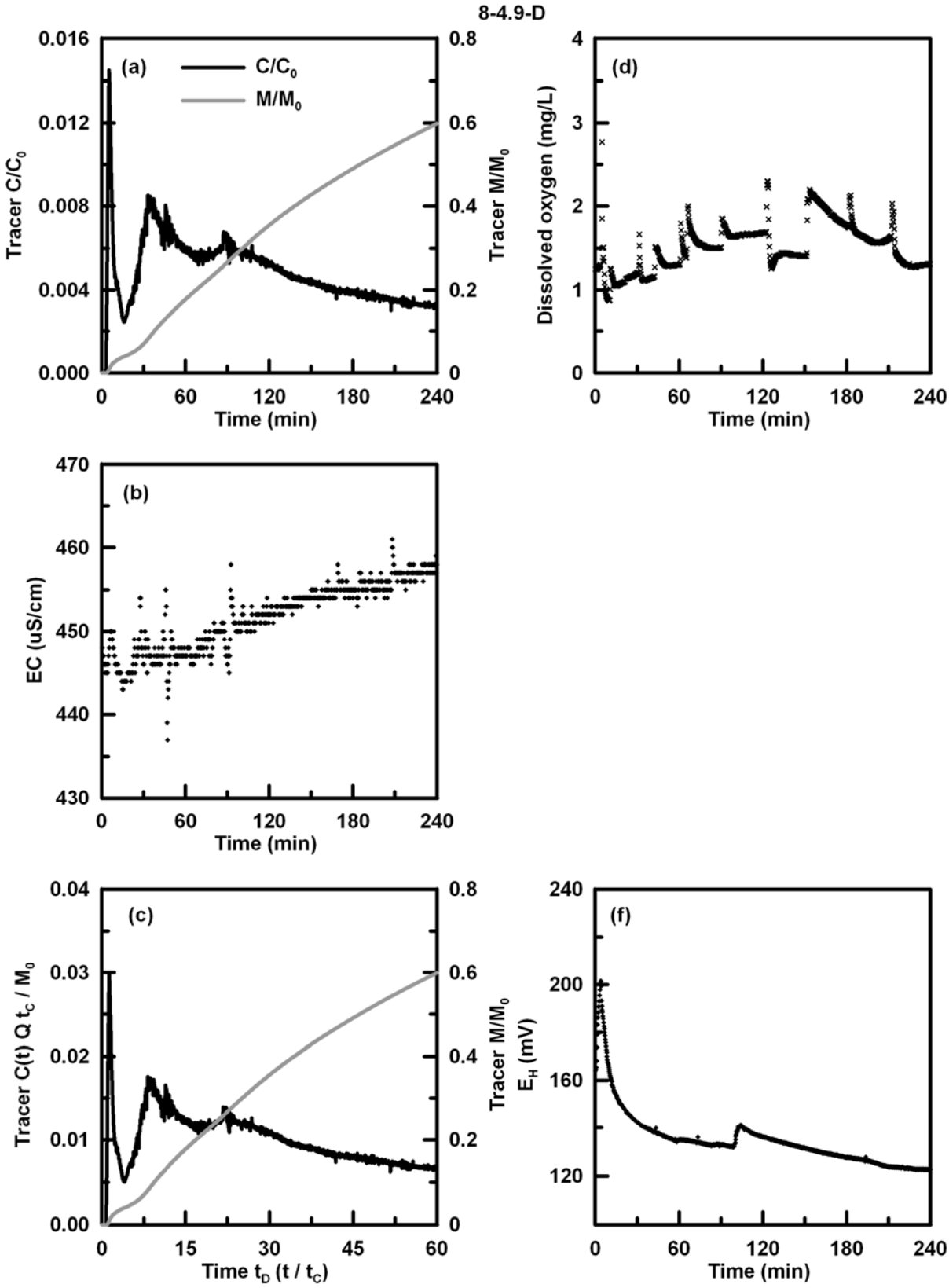

Figure B.39. BTCs and monitoring data for DFTT 8-3.8-D.

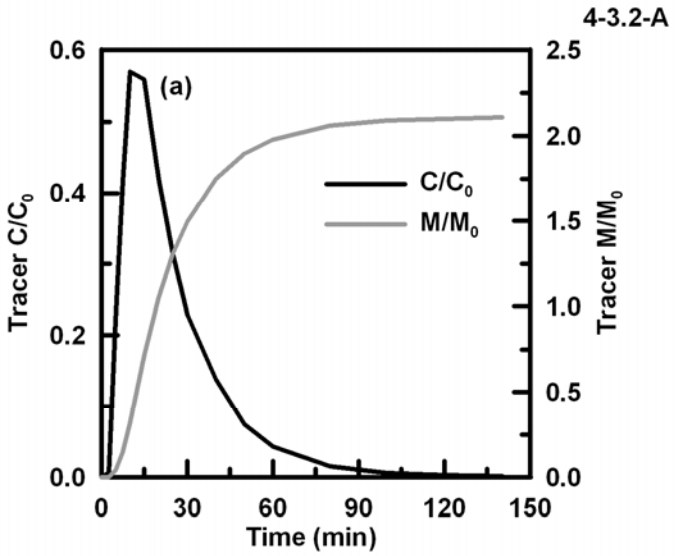

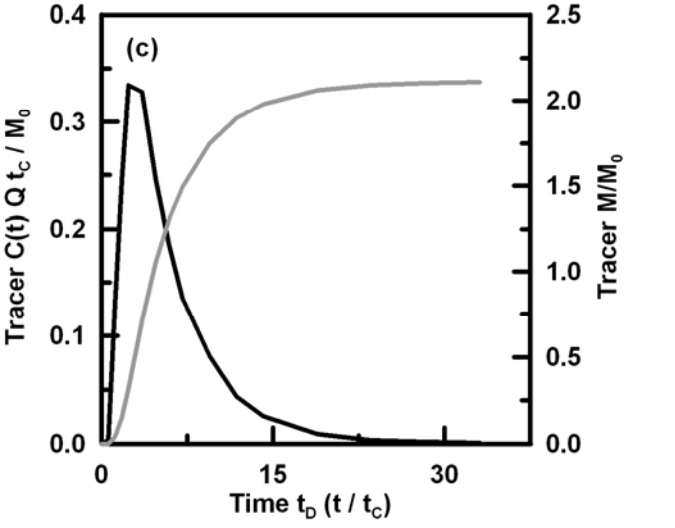

Figure B.40. BTCs for DFTT 4-3.2-A.

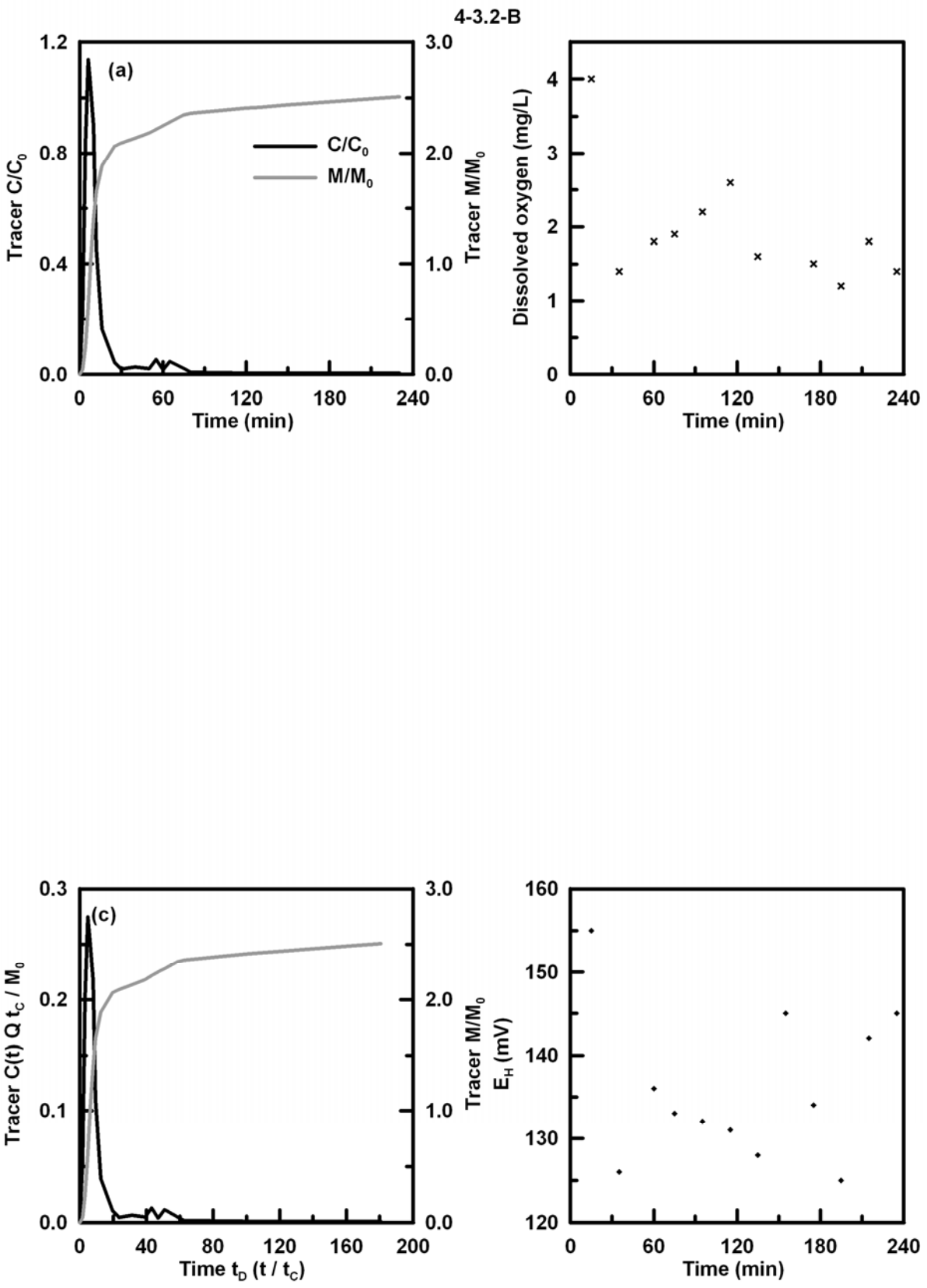

Figure B.41. BTCs and monitoring data for DFTT 4-3.2-B.

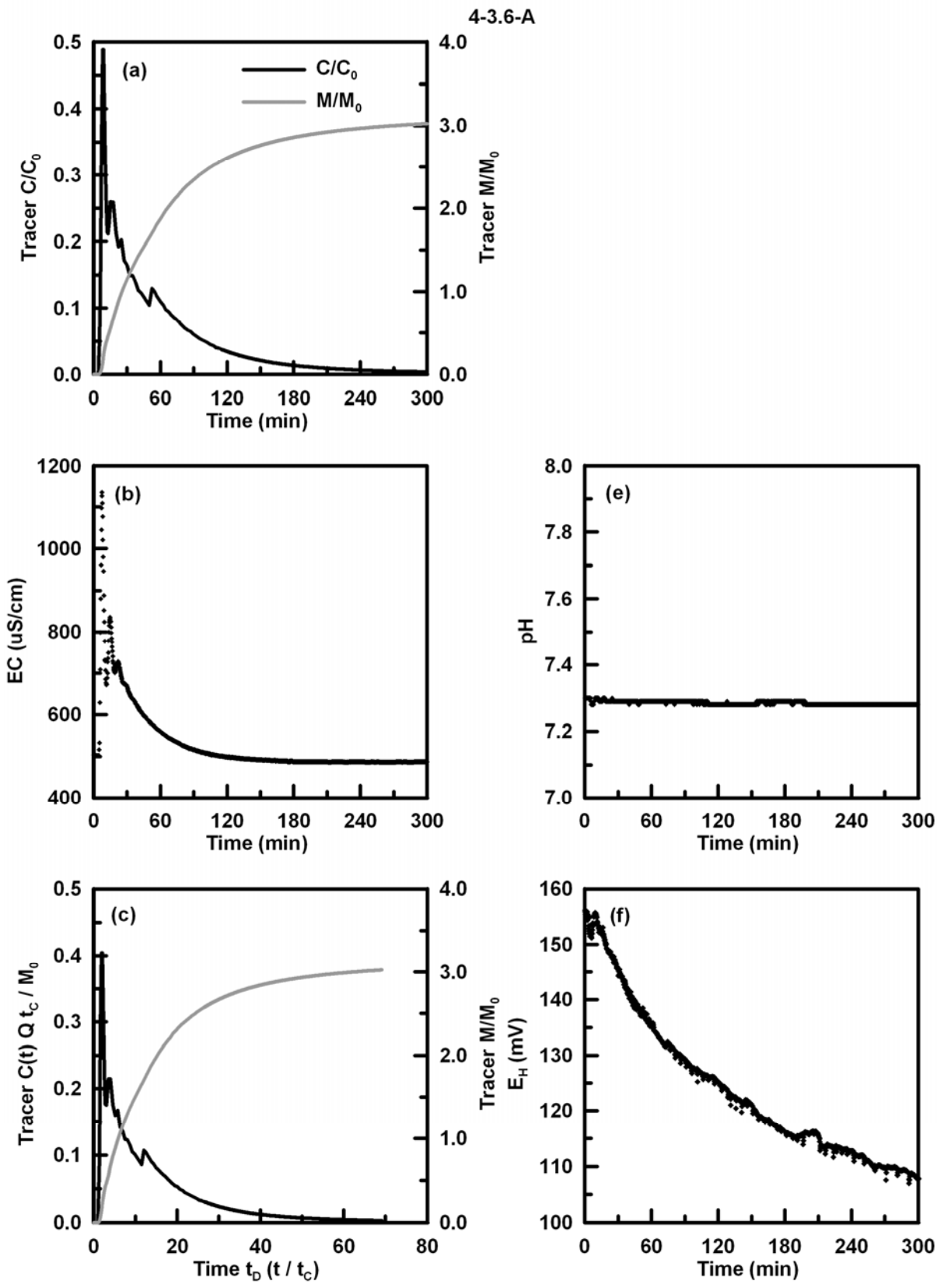

Figure B.42. BTCs and monitoring data for DFTT 4-3.6-A.

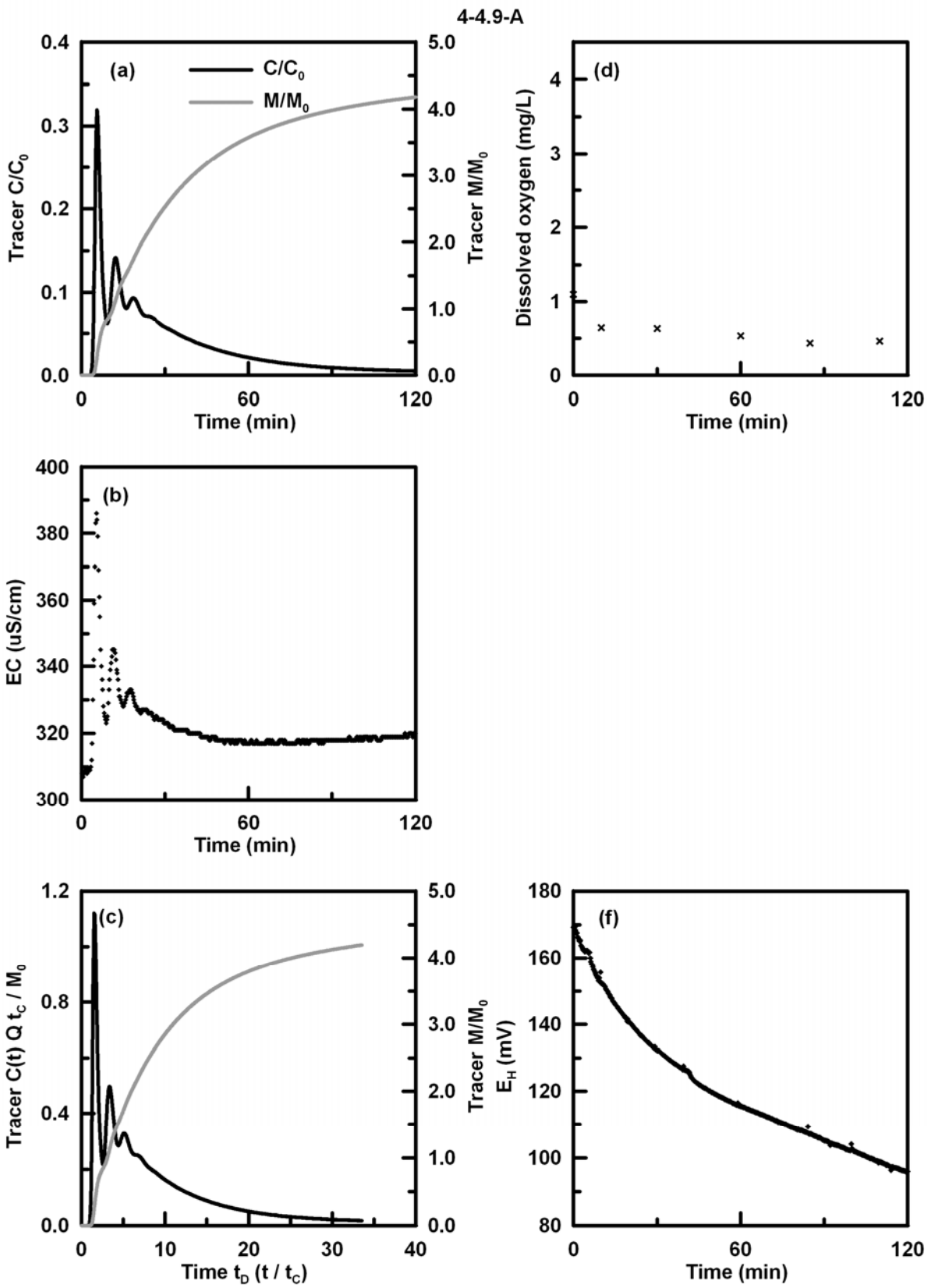

Figure B.43. BTCs and monitoring data for DFTT 4-4.9-A.

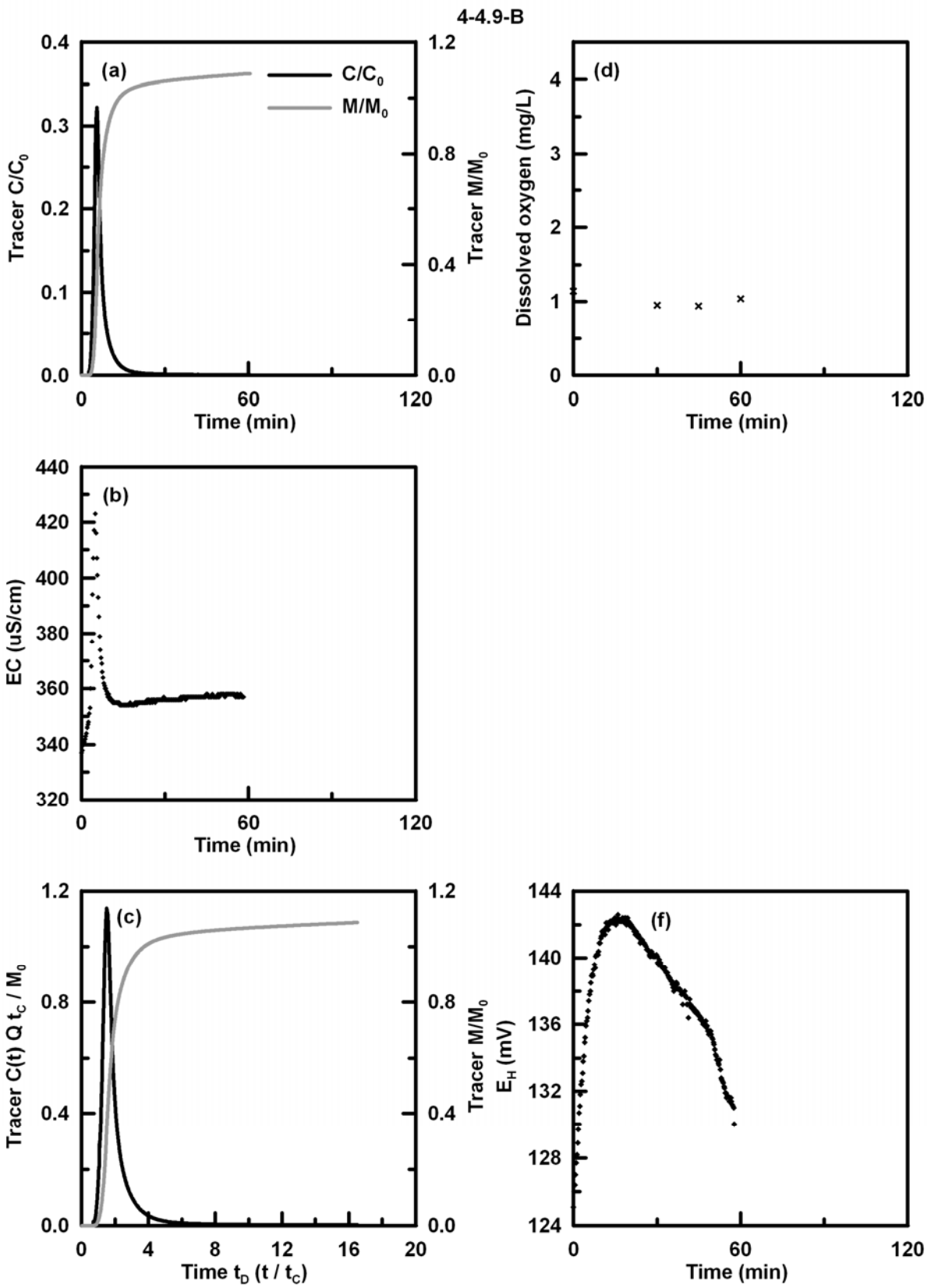

Figure B.44. BTCs and monitoring data for DFTT 4-4.9-B.

Appendix C – Preliminary Work with the Dipole Flow and Reactive Tracer Test (DFRTT)

C.1 Reactive tracer selection

The acetate ion [CH3COO]- has been used during in situ remediation projects as a carbon source (e.g., Anderson et al., 2003). It is one of the lower molecular weight organic acid intermediary degradation products which may be present in natural ground waters. Therefore if acetate is introduced as a tracer, the rate of degradation may be representative of the existing microbial population (Kleikemper et al., 2002). Under denitrifying conditions in an unconfined glaciofluvial outwash deposit in Switzerland, the first-order rate coefficient for acetate was estimated to be 0.70 ± 0.05 day-1 via a push-pull test (Pombo et al., 2002). Similar estimates for the acetate first-order rate coefficient (0.60 ± 0.06 day-1) were obtained in the same aquifer under sulfate-reducing conditions (Kleikemper et al., 2002).

Toluene [$C_6H_5CH_3$] is a colourless liquid denser than water (density 0.8669 g/mL at 20°C) (ATSDR, 2000). The solubility of toluene in water is limited to 534.8 mg/L at 25°C (ATSDR, 2000) which has implications for the concentration of the tracer stock to be injected in a DFRTT. Laboratory experiments report log K_{ow} 2.72 for toluene (ATSDR, 2000). Reported retardation coefficients have ranged from 1.4 in a column experiment (MacQuarrie et al., 1990) to 1.6 at a field site (Mackay et al., 2006). Mackay et al. (2006) estimated the pseudo-first order degradation rate for toluene to be 1.03 day^{-1}.

C.2 Results - dipole flow and tracer test with biodegrading tracer

A biodegrading tracer BTC is expected to have a lower concentration tail than the conservative tracer BTC (Reiha, 2006). The DFRTT model would then interpret the BTCs and provide an estimate for the biodegradation rate of acetate at that location in the aquifer. Short DFRTTs (~4 hours) show no acetate degradation but show acetate agrees well with conservative bromide tracer (data not shown). As noted in section C.1, using a push-pull test the first-order rate coefficient for acetate was estimated to be 0.70 ± 0.05 day^{-1} under denitrifying conditions (Pombo et al., 2002).

To provide enough time for microbial assimilation of acetate, a 30 h DFRTT (3-3.2-C) was completed to estimate the biodegradation rate. Conservative tracers rhodamine WT and bromide were injected simultaneously with acetate to provide a basis for comparison as well as to provide a field indicator for tracer breakthrough. The conservative BTC of DFRTT 3-3.4-A is characterized by a series of three high concentration peaks (t_D 3, 7, and 12) followed by a long tail (Figure C.1(a)). The acetate BTC shows no evidence of biodegradation when compared to the conservative tracer BTCs. The CMCs for acetate and rhodamine WT are similar (Figure C.1(b)) which also provides evidence for the lack of biodegradation. Possible reasons for this lack of biodegradation are insufficient acclimation to the acetate substrate by the microbial population. The dissolved oxygen levels (Figure C.1(a)) in the vicinity of the DFRTT may not have been high enough to support rapid acetate assimilation.

C.3 Results - dipole flow and tracer test with sorbing tracer

The peak concentration of sorbing tracer is expected to be delayed compared to a conservative tracer (Reiha, 2006). The DFRTT model would then interpret the conservative and sorbing BTCs and provide an estimate for the sorptive properties of the aquifer (e.g., fraction of organic carbon) at that location.

A sorbing DFRTT (3-3.8-C) was completed in monitoring well MW-3 using toluene and rhodamine WT as sorbing and conservative tracers, respectively. The rhodamine WT and toluene BTCs have similar times to peak concentration and similar peak concentrations (Figure C.2). This indicates limited sorption occurred during the DFRTT. The only potential indicator of sorption may be the different slopes of the tail of the BTC (RWT -2.12×10^{-4} ; toluene -2.20×10^{-4}) however the differences between the tails of the two BTCs could also be accounted for by aquifer heterogeneity. The limited sorption in the Borden aquifer is not unexpected as the fraction of organic carbon is low (0.2 mg/g) (Mackay et al., 1986). Although it seems unlikely due to the short duration of the DFRTT, it is possible some of the toluene may have been biodegraded aerobically. During the DFRTT, the dissolved oxygen concentration dropped from 3.5 mg/L to 1.0 mg/L which may be the result of aerobic biodegradation; however, as acetate was not readily biodegraded during a longer DFTT (section C.2), it is unlikely toluene

would be degraded during this short tracer test. The decrease in dissolved oxygen concentrations is then attributed to variability in the aquifer and instrumentation.

Due to the nature of the materials used in the construction of the dipole apparatus, some sorption of toluene was expected to occur with the pump tubing, the extraction and injection lines and the packer rubber. This sorption was not visible in the toluene BTC. As a DFRTT with toluene as a sorptive tracer would not receive regulatory approval, a search for a suitable organic sorbing tracer is underway. Once a potential tracer has been found, an additional dipole apparatus will be constructed with the use of less sorptive materials.

In selecting the flow rate for the DFRTT at 540 mL/min, it was assumed the flow rate was low enough not to have an effect on the shape of the BTC; however it is possible the flow rate may not have been low enough to allow enough contact time between the toluene tracer and the sorptive sites in the aquifer. In a column experiment, Weigand and Totsche (1998) found sorption of dissolved organic matter was affected by flow rate. At higher flow rates (1.87 mL/min), the reduced contact time between the dissolved organic matter and the soil reduced the amount of sorption and changed the shape of the BTC obtained at the lower flow rate (0.95 mL/min).

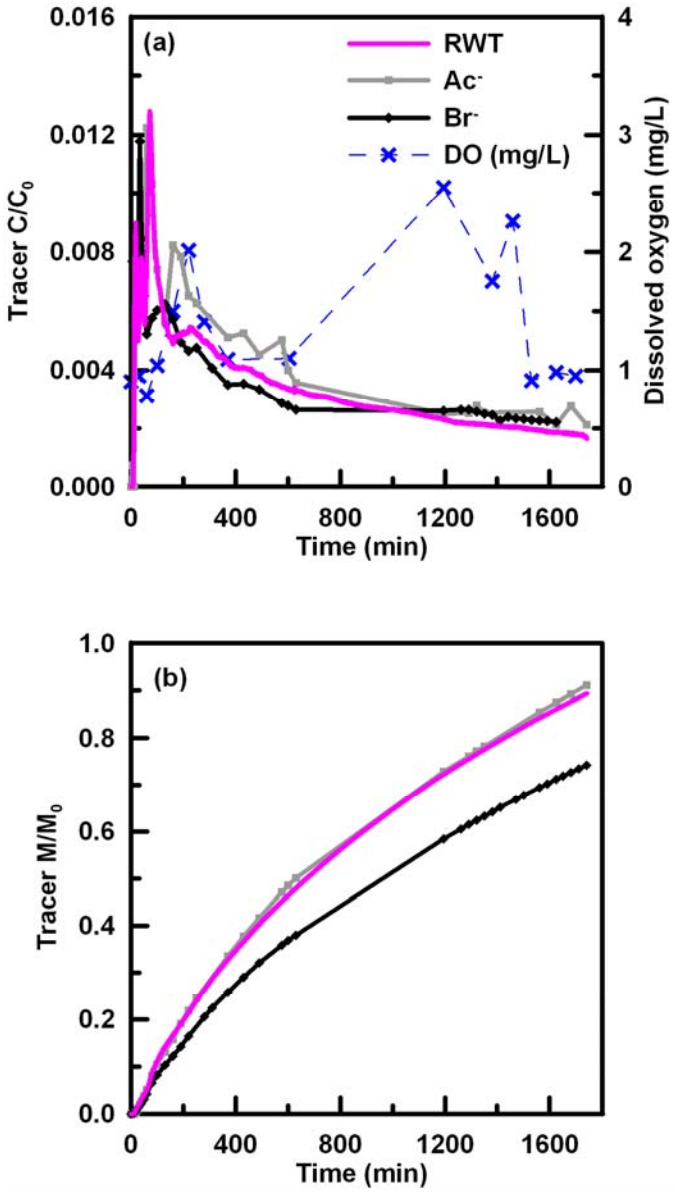

Figure C.1. Tracer BTCs (a) and CMCs (b) for DFRTT 3-3.2-C completed with acetate as a biodegrading tracer.

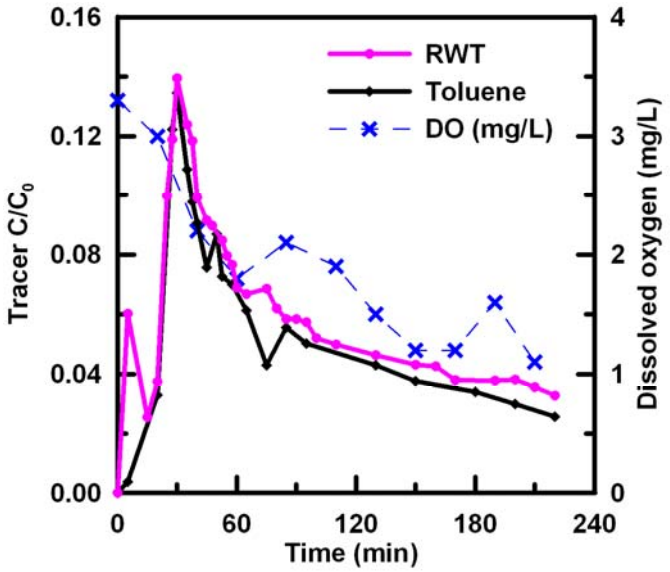

Figure C.2. Tracer BTCs for DFRTT 3-3.8-C completed with toluene as a sorbing tracer.